SPHINGOLIPID DYSREGULATION IN ERYTHROCYTES DURING SICKLE CELL DISEASE CONTRIBUTES TO PRO-INFLAMMATORY MICROPARTICLE GENERATION AND SUBSEQUENT INFLAMMATORY CELL ACTIVATION

A Dissertation
Presented to
The Academic Faculty

by

Anthony Olatokunboh Awojoodu

In Partial Fulfillment
of the Requirements for the Degree
Doctor of Philosophy in Biomedical Engineering in the
Wallace H. Coulter Department of Biomedical Engineering at Georgia Tech and Emory University

Georgia Institute of Technology
December 2014

SPHINGOLIPID DYSREGULATION IN ERYTHROCYTES DURING SICKLE CELL DISEASE CONTRIBUTES TO PRO-INFLAMMATORY MICROPARTICLE GENERATION AND SUBSEQUENT INFLAMMATORY CELL ACTIVATION

Approved by:

Dr. Edward Botchwey, Advisor
Wallace H. Coulter Department of Biomedical Engineering
Georgia Institute of Technology

Dr. Manu Platt
Wallace H. Coulter Department of Biomedical Engineering
Georgia Institute of Technology

Dr. Greg Gibson
Department of Biology
Georgia Institute of Technology

Dr. Gilda Barabino
Grove School of Engineering
The City College of New York

Dr. Shayn Peirce-Cottler
Department of Biomedical Engineering
The University of Virginia

Date Approved: October 31st, 2014

I would like to dedicate this dissertation to several people. First, and foremost, to my Lord and Savior, Jesus Christ, from whom all of my strength comes from. Second, to my mother, Florence Awojoodu, who has shown me unconditional love, resilience and the power of prayer throughout my life. Third, to my baby sister, Sola Awojoodu, who has lived 21+ years with Sickle Cell Disease and whose strength and spirit is a source of inspiration. Finally, I dedicate this to my beautiful fiancée and wife-to-be, Shewa, who has stood by my side as a consistent source of encouragement and love throughout this entire journey. I am blessed and thankful to have each of you in my life.

ACKNOWLEDGEMENTS

"Life is not a solo act. It's a huge collaboration, and we all need to assemble around us the people who care about us and support us in times of strife." – Tim Gunn

There is no way on earth I would have been able to accomplish this work without the support, guidance, motivation and inspiration of numerous people. Firstly, I'd like to thank my advisor, Dr. Edward A. Botchwey for helping to mold my scientific mind and guide the direction of my work from its inception. A commonality we share is having close family members with sickle cell disease and I am very fortunate to have received his support, and encouragement, to study a disease that means so much to me. I would especially like to thank Dr. Botchwey for believing in me despite my own personal doubts. He was pivotal in my decision to start [and finish] a PhD program and I am forever grateful for that. I would secondly like to thank my committee members, Dr. Manu Platt, Dr. Greg Gibson, Dr. Gilda Barabino and Dr. Shayn Peirce-Cottler for their invaluable insight in the areas of sickle cell disease pathogenesis, inflammatory cell activation, genetics and microvascular remodeling. All of your countless hours of reading, listening and communicating have greatly improved the quality of this work.

I would like to thank the members of the Botchwey laboratory, past and present, for making my graduate experience amazing. Dr. Lauren Anderson, Dr. Rebekah Neal Hensley, Uma Loganathan, Molly Dickinson, Daniel Bowers, Steven Lenz, Cynthia Huang, Nathan Chiappa, Claire Segar, Dr. Anusuya Das, Dr. Molly Ogle, Jada Selma, Jack Krieger, Cheryl Lau and Caitlin Powell, you have not only made me a better scientist through your input and collaboration but you have made this journey truly

enjoyable. I would also like to thank the numerous mentees I have had. Michael Tanes, Blair Hu, Carol Bampoe, Alicia Lane, Silvia Zhang, Jovanay Carter, Amadou Bah and Max Nguemeni, you have all helped me become a better leader and I am thankful for you. I would specifically like to thank my two undergraduate mentees for the past two years, Alicia and Silvia, who have dedicated long, tedious hours in lab studying sphingolipid metabolism in sickle cell disease. It has been beautiful seeing you two blossom and I thank you for all of your time and commitment.

I would like to thank my friends and family for all of their invaluable support and love through this process. There are too many of you all to name everyone but you each hold a very special place in my heart and have contributed to my journey. I would specifically like to thank Simpson Gregoire, Cynthia Huang, Riana Anderson and Lydia Abebe who kept me sane when graduate school had other plans. I would like to thank my brothers, Haroon Shaukat, Jiboy Ndubizu, Faisal Yayah, Ngozi Nwaneri, Victor Nwaneri, Ademola Sadik, Neil Samen, Akin Opesanmi, Kenneth Osei, Sheriff Muse-Ariyoh and Vyran George for always humbling me and reminding me of where I came from. I would also like to thank the many friends I have met through school, church, travel, etc. You have all impacted me greatly.

I would like to express my deepest gratitude to my family. You all are the reason I am who I am and are much of the reason I have made it through this process. I'd like to especially thank my mother, Florence Awojoodu, who I often call the strongest woman in the world. You inspire me, day after day, and I am forever grateful for how you raised me, nurtured me and prayed for me throughout my life. Thank you to my dad, Samson Awojoodu, for always being a calm voice of reason. Thank you to my sisters, Bola,

Joycee and Sola Awojoodu for putting up with your only brother and finding a way to love me despite my antics. Thank you to the Alades, Boasmanboons, Adekunbis and Mepaiyedas who have showered me with love and prayers throughout this journey. I could not have done this without you.

Finally to my fiancée, Shewa, I am truly the luckiest man in the world to have had you by my side through this journey and for the rest of my life. I know it hasn't been easy keeping our relationship as a central point of our lives with us both working on doctorates but I am so thankful for your efforts and dedication to me. Thank you for always believing in me and not just saying it, but truly believing. Thank you for listening to my highs, my downs and my long, rambling complaints about experiments that had no direct impact on your life. Most importantly, thank you for your love and your consistent support. Knowing that I always have a best friend to turn to in times of need has been a great motivating force in my life. You are the love of my life and I am blessed to call you mine.

TABLE OF CONTENTS

LIST OF TABLES

LIST OF FIGURES

but not phagocytosis

LIST OF SYMBOLS

α	alpha
β	beta
γ	gamma

LIST OF ABBREVIATIONS

Compound/Protein/Cell	Abbreviation	Description
Amitriptyline	Amit.	Acid sphingomyelinase inhibitor
Annexin A5	Annexin V	Marker for apoptotic cells and microparticles
Anti-inflammatory Monocytes/Macrophages	AM/M2 Macrophages	Tissue regeneration and angiogenesis
Ceramide	Cer	Sphingolipid precursor to sphingosine
CD11b	CD11b	Pan-myeloid marker
CD206	CD206	M2 marker
CD45	CD45	Pan-myeloid marker
CD68	CD68	Pan-macrophage marker
Ceramidase	CDase	Enzyme that converts ceramide to sphingosine
Ceramide	Cer	Sphingolipid at the hub of metabolism
Ceramide 1-phosphate	C1P	Bioactive phosphorylated ceramide
Colony Forming Unit	CFU	Colony of cells formed from one common stem cell
Compound 26	Cmpd26, C	$S1P_1$ agonist
CX3CR1	CX3CR1	AM marker
F4/80	F4/80	Pan-macrophage marker
FTY720	FTY, F	$S1P_1/S1P_3/S1P_4/S1P_5$ agonist
Glucosylceramide	GCer	Sphingolipid containing complex sugars on ceramide
Glycophorin A	GlycoA	Glycosylated protein on RBC membranes
Gr1	Gr1	IM marker
Granulocyte colony stimulating factor	G-CSF	Long term stem cell mobilizer
Hematopoietic Stem Cell	HSC	BM-derived hematopoietic lineage precursor stem cell
Inflammatory Monocytes/Macrophages	IM/M1 Macrophages	Phagocytose debris and clear bacteria
$Lineage^-/Sca1^+/c\text{-}kit^+$	LSK	Murine HSC
$Lineage^-/Sca1^+/c\text{-}kit^+/CD150^+/CD48^-$	LSK-SLAM	Putative long term Murine HSC
Ly6C	Ly6C	IM marker
MHC II	MHC II	M1 marker
Microparticles	MPs	Red blood cell derived lipid vesicles

Monocyte Chemoattractant Protein-1	MCP-1	Monocyte chemo-attractant
Non-SCD	AA	Samples from donors without SS
Plerixafor	AMD3100	Short term stem cell mobilizer
Poly(lactic-co-glycolic acid)	PLAGA, P	Polymer used to encapsulate and deliver S1P receptor compounds
Red Blood Cell	RBC	Oxygen-carrying cells that store S1P in blood
SEW2871	SEW, S	$S1P_1$ agonist
Sham	S	Backpack surgery with no implant
Sickle Cell Disease	SCD, SS	Samples from donors with Sickle Cell
Sphinganine	Sa	Dihydro- sphingosine
Sphinganine 1-phosphate	SaP	Dihydro sphingosine 1-phosphate
Sphingomyelin	SM	Most abundant sphingolipid in plasma membrane
Sphingomyelinase	SMase	Enzyme that converts sphingomyelin to ceramide
Sphingosine	So	Sphingolipid precursor to S1P
Sphingosine 1-phosphate	S1P	Bioactive signaling lipid with diverse biological functions through 5 GPCRs and metabolism
Sphingosine 1-phosphate Receptor 1	$S1P_1$	GPCR S1P receptor present on many cells
Sphingosine 1-phosphate Receptor 1	$S1P_3$	GPCR S1P receptor present on many cells
Sphingosine Kinase 1	SK1	Converts Sphingosine to S1P – intracellularly
Sphingosine Kinase 2	SK2	Converts Sphingosine to S1P – on membrane
Stromal Derived Factor-1	SDF-1	Stem cell chemo-attractant
VPC01091	VPC, V	$S1P_1/S1P_4/S1P_5$ agonist, $S1P_3$ antagonist

SUMMARY

Sickle cell disease (SCD) is a hereditary blood disorder caused by a point mutation in the gene encoding hemoglobin. This mutation causes hemoglobin molecules to polymerize during de-oxygenation of erythrocytes leading to rod-shaped polymers that bend and distort the red blood cell (RBC) membrane, making it more rigid and "sickled". This sickling causes red blood cells to lose their flexibility and become trapped in small capillaries and arteries leading to chronic inflammation and many complications such as peripheral artery disease, stroke, myocardial infarction, vasculitis and even death.

Red blood cell dysregulation is pathognomonic in sickle cell disease. Red blood cells have a normal lifespan of about 120 days. In SCD, however, this lifespan is significant reduced to around 10 days. The reversible sickling and un-sickling that the RBC membrane undergoes makes the cells prone to cell lysis. Additionally, loss of lipid asymmetry contributes to this decrease in RBC lifespan. Enzymes known as flippases, floppases and scrambleases maintain lipid asymmetry in normal cells by concentrating certain lipids on the inner (i.e. phosphatidyl serine, phosphatidylethanolamine) or outer (i.e. sphingomyelin, phosphoryl choline) membrane. When lipid asymmetry is lost, due to RBC sickling, phosphatidyl serine can be exposed on the RBC membrane, which provides a signal for macrophages to clear these damages cells from circulation. To compensate for this significant reduction in RBC lifespan in SCD, the body produces significantly more premature RBCs, reticulocytes, which may also have a different lipid makeup as adult RBCs. Understanding how lipid orientation and metabolism is altered in SCD may provide tools to modulate RBC sickling and downstream processes in SCD.

Sphingolipids are a class of lipids containing a backbone of sphingoid bases.

Sphingolipids can be produced *de novo* and further metabolized through the activity of various enzymes to produce intermediates with diverse roles in cellular processes and signal transduction. As they are significant components of the red blood cell membrane, their expression and orientation may be altered due to sickling events. The orientation of dominant lipids in the RBC membrane has been extensively studied in the context of SCD but the metabolism of these bioactive lipids has not. Sphingomyelin is the most abundant sphingolipid in the RBC membrane and is concentrated on the outer leaflet. Ceramide is produced by the hydrolysis of sphingomyelin by sphingomyelinase and is the sphingolipid at the center of the metabolic network. Ceramide can be metabolized by ceramidase to form sphingosine, which can be phosphorylated to form sphingosine 1-phosphate (S1P). S1P is stored in significant amounts by RBCs and is a ligand for 5 known G-protein coupled receptors that contribute to many cellular processes such as cell proliferation, motility and phenotype. These lipids not only exist in the RBC plasma membrane, but also can be secreted and bound to carrier proteins in blood plasma to signal to other cells.

Sphingolipid metabolism has been implicated in membrane-derived microvessel formation. Specifically, sphingomyelinase activity has been shown to result in the production of membrane derived microparticles and exosomes. While the exact mechanism is unknown, it is thought that conversion of the large polar head sphingolipid to the smaller ceramide causes microdomain formation in the RBC membrane and subsequent budding. These microparticles can be secreted from RBCs or released into circulation upon RBC hemolysis where they can signal to other cells. Microparticles have been shown to contribute to many processes in sickle cell disease including vaso-

occlusions, inflammatory cell activation, thrombosis and apoptosis.

As microparticles are membrane-derived, they contain bioactive sphingolipids, which can signal to other cells in circulation. Additionally, monocytes are known to interact with RBCs at a much higher frequency in SCD. Not only do these two cells interact, they exchange protein and lipid signals. Monocytes exist in an "activated" state in SCD and are more adhesive and pro-inflammatory. Sphingolipids, many of which are bioactive, may be transferred from RBCs and activate signaling cascades on circulatory monocytes. S1P, in particular, has been shown to modulate monocyte phenotype, adhesion and recruitment through receptor signaling and intracellular metabolism. In this work, we hypothesized that sickling in SCD may alter sphingolipid metabolism and microparticle generation. As a result, sphingolipid-rich microparticles may enhance activation of inflammatory cells, like monocytes and neutrophils, in circulation. This work examines the metabolism of sphingolipids and generation of microparticles in SCD using sphingolipidomic profiling, enzymatic assays and computational modeling. Secondly, the crosstalk between S1P, microparticles and monocyte/macrophage phenotypes is examined in the context of sickle cell disease and immunomodulation. Lastly, the therapeutic potential for altering sphingolipid metabolism to regulate microparticle generation and inflammation during SCD is examined. This work, taken together, shows that acid sphingomyelinase activity is significantly elevated in RBCs during SCD. This results in the production of sphingolipid-rich RBC-derived microparticles, which are present in circulation. These microparticles interact with myeloid cells and alter pro-inflammatory cytokine secretion and endothelial cell adhesion. Pharmacological inhibition of acid sphingomyelinase reduces microparticle

generation and subsequent inflammation in a mouse model of SCD.

CHAPTER 1

INTRODUCTION

Sickle cell disease (SCD) is a hereditary genetic blood disorder caused by a point mutation in the gene encoding hemoglobin. This mutation causes hemoglobin molecules to polymerize during de-oxygenation of erythrocytes leading to rod-shaped polymers that bend and distort the red blood cell (RBC) membrane, making it more rigid and "sickled". This sickling causes RBC to lose their flexibility and become trapped in small capillaries and arteries. This vaso-occlusion has the potential to cut off blood supply to downstream tissues and is often associated with pain but can also lead to many complications such as chronic inflammation, ischemia, peripheral artery disease, stroke, myocardial infarction and even death (1, 2). The current standards of care for those with SCD are blood transfusions and pain management. Transfusions provide a pool of healthy RBC but patients must go to the hospital every time they need treatment. Furthermore, there are still issues associated with transfusions, including graft rejection and hypertension (3). Pain management is reactive and is associated with many side effects and addiction (4).

Sphingolipids are a class of lipids containing a backbone of sphingoid bases. These lipids play diverse roles in cellular processes and signal transduction (5). Sphingomyelin is the most abundant sphingolipid in the plasma membrane and is hydrolyzed to ceramide by sphingomyelinases. Ceramide can then be converted to sphingosine by ceramidases and ultimately sphingosine 1-phosphate (S1P) with sphingosine kinases. Sphingosine 1-phosphate, a bioactive intermediate in sphingolipid metabolism is stored at high concentrations in red blood cells. S1P acts as an extracellular signaling molecule by activating 5 known G-protein coupled receptors ($S1P_{1-5}$) and as an

intracellular signaling metabolite to direct a wide array of cellular processes (6). Sphingolipids are integral components of cell plasma membranes. Sphingomyelin metabolism and ceramide production have been implicated in processes regulating membrane integrity, apoptosis, deformability, cell shape and budding (7, 8), all of which are factors that affect red blood cells in SCD. Additionally, RBC store, metabolize and transport a significant amount of sphingolipids. RBC-derived microparticles may interact with inflammatory cells in circulation, and are potential carriers for sphingolipids. Sphingolipid metabolism has been shown to alter the receptor expression, cytokine secretion, growth and differentiation of inflammatory cells (9-11). We hypothesized that sphingolipid metabolism is altered in SCD and that regulation of sphingolipid metabolism may be an effective therapeutic strategy to modulate inflammation-related pathologies in the disease.

We believe that the dysregulation of sphingolipid metabolism in sickle cell disease serves as a feed-forward mechanism of inflammation associated with SCD. Our **central hypothesis** is that chronic inflammation and associated plasma secretion of key enzymes of sphingolipid metabolism evokes the hyper-production of ceramide and sphingosine, the precursors of S1P. Geometric and biological changes associated with sickle cell disease and exacerbated by dysregulated sphingolipid metabolism in sickle erythrocytes, leads to the generation of microparticles that can activate monocyte/macrophage populations, further enhancing systemic inflammation. Thus, regulating sphingolipid metabolism may be a novel tool to therapeutically treat the pathogenesis of sickle cell disease. In this proposal, we address the following three specific aims:

1. Evaluate the role of systemic inflammation in the dysregulation of sphingolipid metabolism and subsequent microparticle generation in SCD erythrocytes. Increases in the secretion of sphingolipid metabolizing enzymes and geometrical changes in the RBC membrane, which occur in SCD, may alter the presence of membrane-borne sphingolipids and the activities of membrane-bound enzymes. The *objective* of this aim is to evaluate the role of SCD-associated inflammation in sphingolipid metabolism, the resulting changes in the erythrocyte sphingolipidome and the subsequent generation of RBC-derived microparticles. To this end we will quantify sphingomyelinase expression and activity from inflamed endothelial and myeloid cells with plate-based enzyme activity kits, western blotting and ELISA. Additionally, we will measure sphingomyelinase activity in the plasma and RBC from SCD donors. We will also measure the concentration of sphingosine kinases and ceramidases, enzymes that metabolize sphingolipids downstream of sphingomyelin, and bioactive sphingolipids in the blood, plasma and red blood cells from SCD donors with lipid extraction and HPLC-MS quantification. We will quantify the generation of RBC-derived microparticles with flow cytometry in SCD and characterize their sphingolipid content through lipidomic profiling. Lastly, we will develop a computational model of sphingolipid metabolism in AA and SS RBCs to elucidate altered reactions that might be therapeutic targets. This aim will reveal whether alterations in sphingolipid metabolism are associated with microparticle generation as well as the sphingolipid content of microparticles. It will also allow us to utilize our predictive mathematical model to reveal reaction fluxes and enzyme activities that might be altered in SS RBCs. This model will be validated experimentally and probed for therapeutic intervention to alter sphingolipid enzyme

activity and sphingolipid production.

2. Evaluate the interaction between microparticles and myeloid cells. The *objective* of this aim is to evaluate the interaction of RBC-derived microparticles with inflammatory cells and their biological consequences. To this end, we will use fluorescent microscopy and lipid-transfer experiments to examine how microparticles are internalized, distributed and processed within myeloid cells. We also plan to examine the potential of myeloid cells to metabolize microparticle-derived sphingolipids during SCD. We will do this through single cell transcriptional analysis of sphingolipid-metabolizing enzymes in SCD and non-SCD peripheral blood mononuclear cells. Additionally, we will assess monocyte-endothelial cell adhesion and cytokine production after incubation of myeloid cells with S1P, RBC and RBC-derived microparticles. This aim will elucidate the capacity of myeloid cells to metabolize sphingolipids delivered via microparticles in SCD.

3. Evaluate the therapeutic potential of pharmacological perturbations to sphingolipid metabolism to reduce pathological effects of inflammation in SCD. The *objective* of this aim is to determine if pharmacological regulation of sphingolipid metabolism can be used to modulate inflammation-associated pathogenesis in SCD. We *hypothesize* that pharmacological reduction of sphingomyelinase activity will reduce the production of microparticles, and subsequent chronic inflammation, in mouse models of hypoxia- mediated vaso-occlusion in SCD. In this aim, we will utilize a murine model of SCD with or without hypoxia to drive microparticle generation. Mice will be housed in a hypoxic chamber for 2 hours to induce RBC sickling and chronic inflammation with or without a sphingomyelinase inhibitor, amitriptyline. We expect that animals given the

sphingomyelinase inhibitor will have reduced microparticle generation and systemic inflammation. This aim will allow us to examine the potential of pharmacological inhibitors of sphingomyelinase improve systemic inflammation and pathogenesis associated with sickle cell disease in a mouse model of acute inflammation and hypoxia.

This overall project seeks to understand the role of sphingolipid metabolism and immunomodulation during SCD pathogenesis. The project develops pharmacological platforms to modulate cellular processes that contribute to the pathologic red blood cell sickling and inflammatory cell activation in Sickle Cell Disease.

CHAPTER 2

BACKGROUND

Sickle Cell Disease is characterized by morbidity, affects quality of life and can be deadly

Sickle cell disease (SCD) is a hereditary genetic blood disorder caused by a point mutation in the gene encoding hemoglobin. This mutation causes hemoglobin molecules to polymerize during de-oxygenation of erythrocytes leading to rod-shaped polymers that bend and distort the RBC membrane, making it less flexible and "sickled". This sickling results in the propagation of vaso-occlusion, when RBCs become trapped in small capillaries and arteries, potentially cutting off blood supply to downstream tissues. Vaso-occlusion is often associated with pain but can also lead to many complications such as chronic inflammation, ischemia, peripheral artery disease, stroke, avascular necrosis and even death. While bone marrow transplants and gene therapy have been explored in the cure of SCD none have been widely used for donor-matching and regulatory reasons. The current standard of care for those with SCD is blood transfusions and pain management. Transfusions provide a pool of healthy RBC but patients must go to the hospital every time they need treatment and there are still issues with graft rejection and hypertension (3). Pain management is reactive and is associated with many side effects and addiction (4). While medical advancements have improved life expectancy of SCD over the years, it remains significantly less than those without the disease. Furthermore, the pain associated with SCD is often disruptive to educational, social and recreational life and worsens quality of life (12).

Vaso-occlusive crisis

One of the most common complications of SCD is the vaso-occlusive crisis. This crisis comes about when blood vessels are obstructed by sickle cells, causing ischemia in tissues and organs down stream of those vessels. While pain is the most common effect, irreversible organ damage can also result from the painful crisis. Sickled erythrocytes that lose their flexibility and ability to navigate small vessels are thought to initiate vaso-occlusion by interacting with the vascular endothelium (13). Circulatory inflammatory cells have also been implicated in the propagation of vaso-occlusion. Monocytes from those living with SCD have been shown to be activated and cause the activation of the endothelium, enhancing cellular adhesion (14). Neutrophils have also been shown to enhance pathologic cell adhesion through cytokine and ROS production (15). While inflammatory cells are key contributors to endothelium activation and vaso-occlusion there are no therapies that attempt to regulate inflammatory cell activation and adhesion in SCD.

Treatment for Sickle Cell Disease

While advances in gene therapy have elucidated mechanisms to correct the mutation for hemoglobin in mutated cells (16, 17), bone marrow transplants remain the only clinical cure for SCD. Finding a donor, however, is very difficult and the procedure has many associated risks, including death.

Blood transfusions are employed to prevent crisis by increasing the pool of normal red blood cells in a patient. Transfusions prevent many vascular complications of SCD by overcoming anemia associated with the disease and preventing vaso-occlusion from sickled cells. Blood transfusions however, contain iron and buildup of iron after

transfusions can result in heart and liver damage (18). Medicines such as antibiotics, hydroxyurea and pain medications have also been used to treat complications of the disease. While morbidity is improved through these therapies none of them are long-term solutions to the complications of the disease and may require life-long prescriptions and visits to the hospital. Additionally, none of these interventions target the cellular basis of sickle cell disease: the patient's red blood cells themselves. There is a critical need for therapies that regulate the processes of red blood cell sickling and immunomodulation in sickle cell disease.

Sphingolipid metabolism

Sphingolipids are a class of lipids containing a backbone of sphingoid bases. These lipids play diverse roles in cellular processes and signal transduction (5). Many cells can synthesize sphingolipids *de novo* from the initial rate-limiting enzyme, serine Palmitoyl transferase (19). Sphingomyelin is the most abundant sphingolipid in cell membranes. Ceramide, lies at the center of the sphingolipid metabolic pathway. It can be produced through the metabolism of Serine and Palmitoyl CoA or by hydrolyzing sphingomyelin. Ceramide is the direct precursor of sphingosine, which can be phosphorylated to produce sphingosine 1-phosphate (S1P) (**Figure 2.1**). Red blood cells do not maintain the ability to produce the enzymes that metabolize sphingolipids but they instead can adopt these cells from their surroundings. Sphingomyelinase can be secreted from endothelial cells and myeloid cells during many biological processes (20). Specifically, erythrocyte apoptosis and chronic inflammation can trigger the secretion of acid sphingomyelinase (21-23). As chronic inflammation is characteristic of SCD, it is likely that elevations in sphingomyelinase secretion also occur in the disease state.

Additionally, sphingosine kinase (SK) 2 can be cleaved and secreted from apoptotic cells (24). SK exists in two isoforms and phosphorylates sphingosine into S1P two steps down stream of sphingomyelinase activity. S1P is the most studied bioactive sphingolipid and is stored at high concentrations in red blood cells. It acts as an extracellular signaling molecule by activating 5 known G-protein coupled receptors and as an intracellular signaling metabolite to direct a wide array of cellular processes (6).

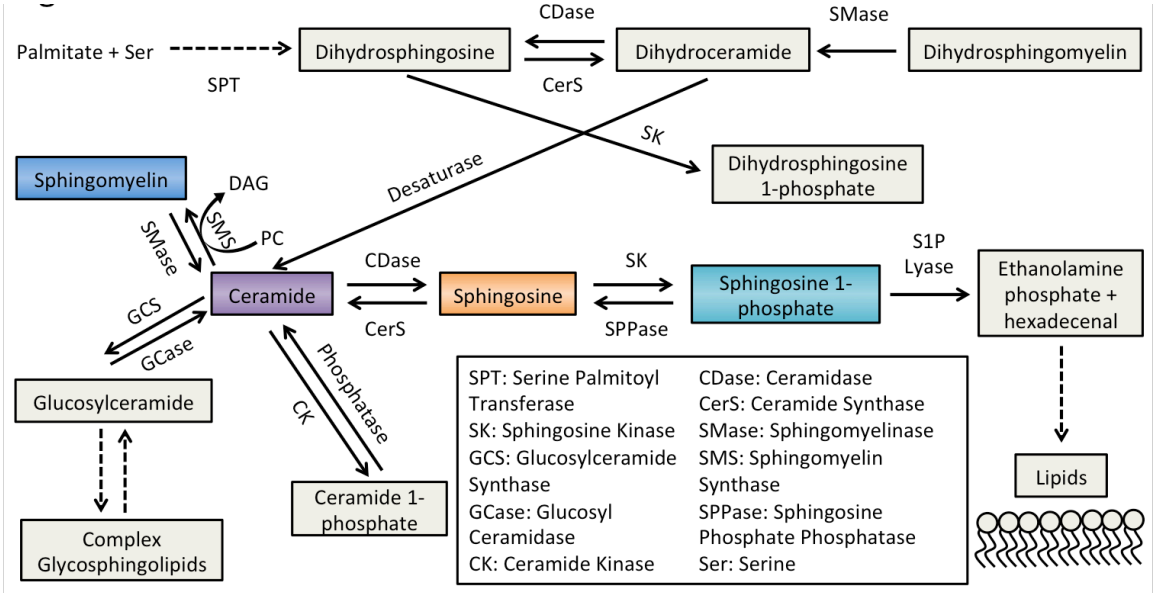

Figure 2.1. Diagram of sphingolipid metabolism. *De novo* sphingolipid production starts with the reaction of serine and palmitoyl CoA, mediated by serine palmitoyl transferase. Sphingolipids are metabolized in many reversible and irreversible reactions. Ceramide is at the center of the sphingolipid metabolism network and can result from the hydrolysis of sphingomyelin and result in the production of sphingosine and S1P downstream (25).

Sphingosine 1-phosphate is a small bioactive signaling lipid

Sphingosine 1-phosphate (S1P) is one of the most studied sphingolipids and is an intermediate in sphingolipid metabolism (**Figure 2.1**). S1P acts as an extracellular signaling lipid by activating 5 known G-protein coupled receptors ($S1P_{1-5}$) to initiate

diverse cellular functions, including chemotaxis and recruitment of cells (26-28) migration and trafficking of hematopoietic stem and progenitor cells within extra medullary tissues (29), and regulation of blood recirculation of osteoclastic precursors (30). S1P is also a lipid intermediate and can be secreted and then internalized and metabolized by other cell types (31).

Sphingosine 1-phosphate as been shown to recruit monocytes/macrophages to atherosclerotic plaques via $S1P_3$ (32). Fueller et al. discovered that S1P acted as a pro-inflammatory mediator by activating human monocytes, which contribute to inflammation and atherogenesis (33). Weis et al. followed up on this by evaluating the role of S1P on monocyte activation and adhesion (34). S1P was shown to induce E-selectin expression and the adhesion of monocytes to endothelial cells (35). All of these processes can contribute to the pathogenesis of sickle cell disease by exacerbating inflammation associated with vaso-occlusion (14).

Sphingolipid metabolism in membrane vesicle formation

The erythrocyte cell membrane plays critical roles in the size, shape, structure and deformability of the cell. Healthy RBCs have flexible membranes that allow the cells to bend and navigate through small vessels. As RBC age, loss in the deformability of the cells enhances splenic sequestration and clears old/damaged cells from circulation (36). Sphingolipids are integral components of cell plasma membranes and contribute to membrane integrity, deformability and cell shape. Sphingolipid metabolism changes the balance of membrane sphingolipids and can result in changes in cell shape, integrity and deformability. Dinkla et al. found that chronic inflammation enhances the secretion of acid sphingomyelinase, an enzyme that catalyzes the hydrolysis of sphingomyelinase to

ceramide (7). Membrane ceramide synthesis in erythrocytes was associated with the appearance of phosphatidyl serine (37) on the outer leaflet of RBC, enhancing apoptosis and clearance and contributing to anemia. Additionally, Dinkla et al. found that sphingomyelin removal enhanced membrane fragility, vesiculation and invagination (7). Consistent with this observation, Trajkovic et al. revealed that ceramide synthesis in plasma membranes, through sphingomyelinase, induces the coalescence of membrane microdomains promoting membrane budding and exosome formation (8). Increased erythrocyte bending, as occurs in SCD, has also been shown to activate neutral sphingomyelinase (38). Membrane-derived particles produced through sphingolipid metabolism contain bioactive metabolites and can be secreted or released upon apoptosis.

Microparticles in sickle cell disease

Microparticles, once termed "cell dust", are small vesicles with diameters between 100 and 1000nm that bud from the plasma membrane of mechanically stressed, dying or activated cells. These particles express antigens and membrane components specific to their parent cells and can act as protein/lipid transport vesicles in circulation. As these particles are membrane derivatives, sphingolipids can also bud off and be stored in these particles. Additionally, microparticles have been shown to be elevated in the circulation of those living with sickle cell disease. Particles derived from erythrocytes (39), platelets (40) and monocytes (41) have all been evaluated.

Though microparticle formation is a physiological phenomenon, many pathologies are associated with increases in microparticles in circulation such as inflammation, atherosclerosis and auto-immunity (42). In 2003, Shet et al. showed that tissue factor microparticles contribute to coagulation during SCD (41). Recently,

Tantawy et al. expanded on this by attributing platelet- and RBC-derived microparticles to coagulation as well as other cardiovascular complications in SCD (40). Soon after, Camus at al. discovered that erythrocyte-derived microparticles induce vaso-occlusion in the kidney during SCD (43). As sphingolipids are integral parts of RBC membranes it is likely that they are present in microparticles and contribute to cell-cell cross talk.

Microparticles and monocyte modulation

Microparticles have been shown to interact with monocytes in circulation. Bardelli et al. discovered that monocyte-derived microparticles induce, in an autocrine fashion, cytokine release, NF-κB activation and oxygen radical production (44). Barry et al. first discovered that platelet-derived microparticles enhanced the adhesion of monocytes to endothelium in a dose and time dependent fashion (45). Rautou et al. isolated microparticles from atherosclerotic plaques from humans and confirmed their thrombogenic potential (46). These authors, however, did not examine the cellular source of these pro-thrombotic microparticles. The microparticles, however, were more potent at stimulating monocyte adhesion than microparticles derived from asymptomatic plaques. More recently, Vasina et al. discovered that microparticles were internalized by monocytes and subsequently promoted cytoskeleton rearrangement, hydrogen peroxide production, and pro-inflammatory cytokine secretion (47). Pro-inflammatory cytokines are known to be elevated in the blood and plasma of those living with sickle cell disease and contribute to vascular inflammation. Since monocytes interact with erythrocytes and their microparticle products in circulation, this has the potential to enhance their inflammatory state and exacerbate inflammation-mediated pathogenesis in SCD. To this

date, however, no one has explored the role of RBC-derived microparticles in monocyte activation in SCD.

CHAPTER 3

ACID SPHINGOMYELINASE IS ACTIVATED IN SICKLE CELL ERYTHROCYTES AND CONTRIBUTES TO INFLAMMATORY MICROPARTICLE GENERATION IN SICKLE CELL DISEASE

Introduction

Sickle cell disease (SCD) is a hereditary blood disorder characterized by mutated hemoglobin molecules, which polymerize during deoxygenation to form fibers that deform the erythrocyte membrane. These red blood cells (RBCs) contribute to significant vascular pathology, including stroke, myocardial infarction, peripheral artery disease and even death (48). As the initiating event in the pathology of SCD is the sickling of the RBC membrane, it is important to understand how modifications in membrane composition might play a role in the disease.

Sphingolipids are a class of lipids containing a backbone of sphingoid bases. They play diverse roles in cellular processes and signal transduction and are significant components of cell membranes (5). Sphingomyelin, which comprises 10% of the mammalian plasma membrane, is degraded by the hydrolyzing enzyme sphingomyelinase (SMase). In recent studies, membrane curvature, and associated increases in mechanical bending stresses in RBCs, activated SMase, reducing sphingomyelin and increasing ceramide (38). Production of ceramide has a direct effect on a wide range of cell processes and alters production of other immediately descendent metabolites such as sphingosine and sphingosine 1-phosphate (S1P), which are key regulators of inflammation (26-28, 30, 49). Furthermore, SMase has been implicated in lipid

microdomain formation, membrane fragility, vesiculation and microparticle formation (7, 50). While the orientation of plasma membrane lipids in SCD and other hemolytic anemias has been studied, the consequences of altered distribution and metabolism of sphingolipids have been largely unexplored.

Sickle RBCs are a particularly interesting model system for the relationship between membrane stresses, inflammation and sphingolipid metabolism. Acid SMase is secreted from endothelial cells and myeloid (20) and erythrocyte apoptosis and chronic inflammation, both of which occur in SCD, enhance the secretion of acid SMase (7, 21-23). The role of acid SMase, and sphingolipid dysregulation more generally, has not been studied in the context of SCD.

In this work, we elucidate mechanisms contributing to the dysregulation of sphingolipid metabolism and subsequent MP generation by RBCs in SCD. Membrane stresses enhance the activity of acid SMase in the blood, plasma, and RBCs of people living with SCD. This results in a significant increase in the presence of sphingosine and S1P in RBCs as well as the generation of RBC-derived MPs (**Figure 2.1 and Figure 3.1**).

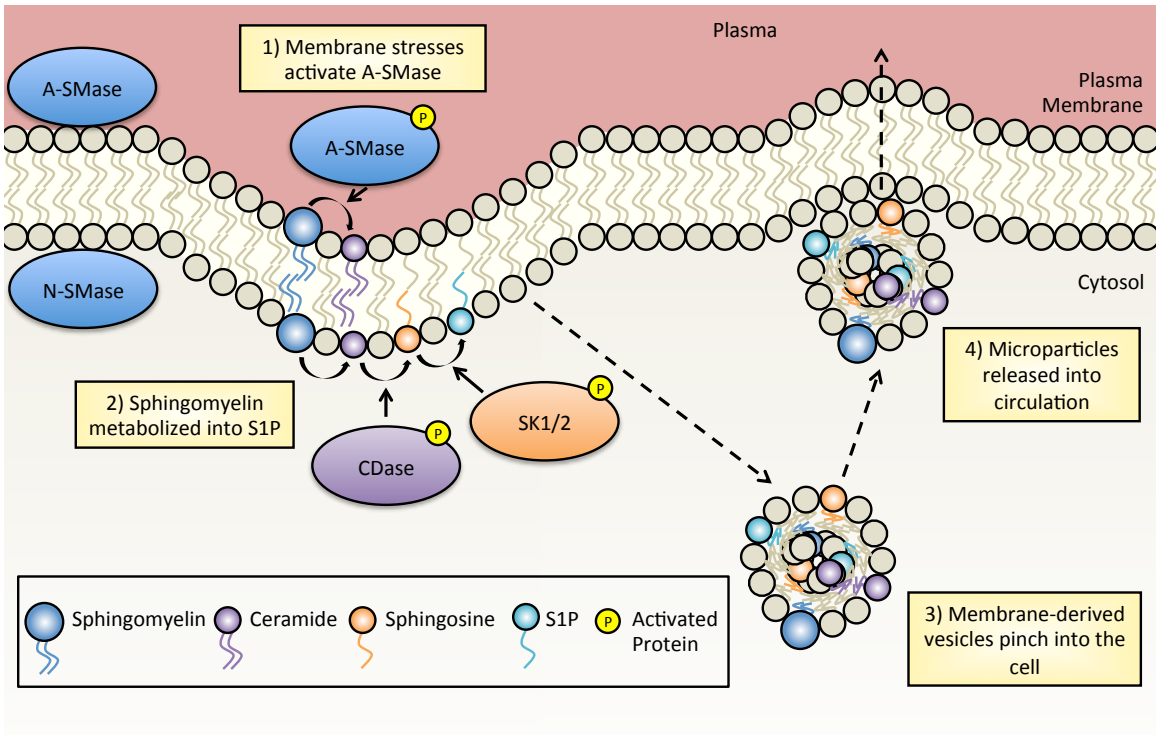

Figure 3.1. Schematic of Sphingolipid metabolism and microparticle generation in SS RBC. When RBC undergo reversible sickling cycles, their membranes curve, introducing membrane stresses caused by the closer interaction of lipids. This increased membrane force activates acid sphingomyelinase (A-SMase) on the outer leaflet of the plasma membrane (1). Acid SMase hydrolyzes sphingomyelin to form ceramide which has a smaller head group and can cause an inward curvature of the membrane which reduces membrane stresses. Sphingomyelin can be further metabolized into sphingosine and S1P with alkaline ceramidase (CDase) and Sphingosine Kinase (SK1/2), respectively (2). Membrane budding results in the formation of membrane-derived vesicles (3), containing sphingolipids and proteins, which are internalized into the cell and subsequently released into circulation through secretion or hemolysis as microparticles (4).

These factors enhance monocyte adhesion to endothelial cells and inflammatory cytokine production. Pharmacological inhibition of acid SMase with an FDA-approved drug, amitriptyline, reduces MP generation and cytokine production. These results elucidate a novel mechanism for MP-mediated inflammatory cell activation in SCD (51). Additionally, these findings may be relevant to other hemolytic anemias such as

paroxysmal nocturnal hemoglobinuria and autoimmune hemolytic anemia and disorders rooted in aberrant RBC morphology.

Materials and Methods

RBC and MP isolation and fractionation

Whole blood samples obtained from donors homozygous for sickle (SS) or normal (AA) hemoglobin were centrifuged against a Ficoll-Paque density gradient (density: 1.077g/mL; GE Healthcare) for 30 minutes at 400 RCF at 4˚C to separate plasma, peripheral blood mononuclear cells (PBMCs) and packed RBCs (**Figure 3.2**).

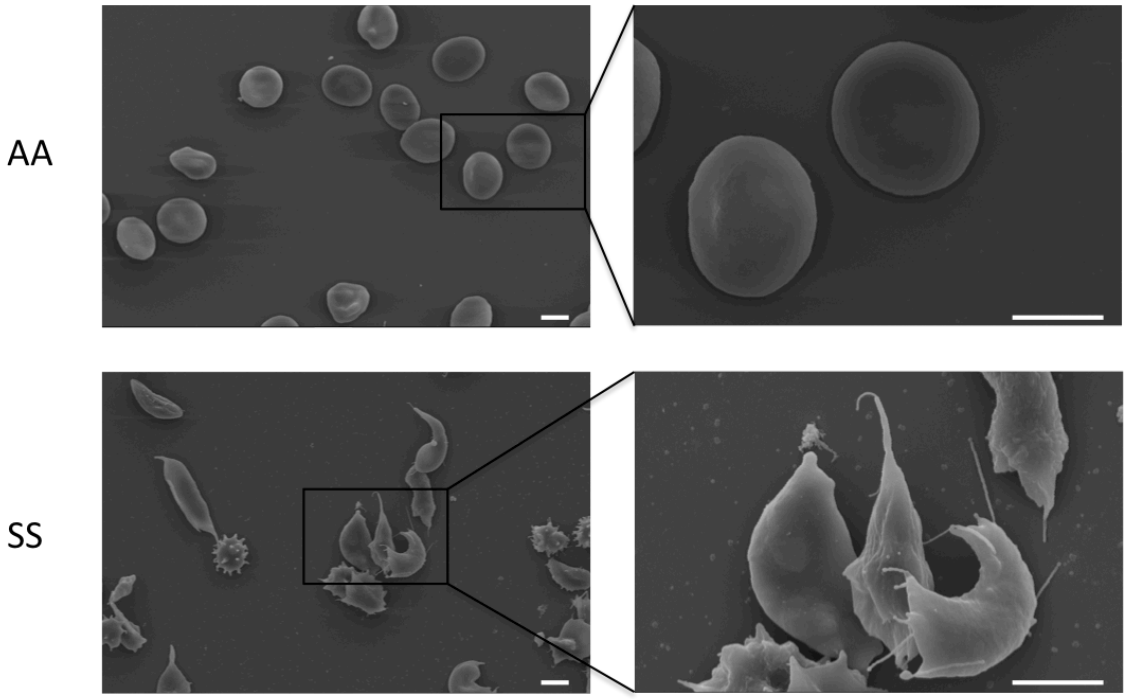

Figure 3.2. Scanning electron microscopy images of AA and SS RBCs. Donor blood was harvested and fractionated in a Ficoll density gradient to separate plasma and RBCs. RBCs were fixed, dehydrated and prepared for SEM imaging. While AA RBCs (top) display a normal, discoid shape, SS (bottom) RBCs are sickled and misshapen. SS RBCs also appear to have spindle-like protrusions from hemoglobin polymerizations. These alterations significantly enhance membrane forces. *Scale bars = 5μm.*

RBCs were separated into high and low density fractions using stacked Percoll solutions centrifuged at 41,000rpm for 30 minutes using a Beckman SW 41 Ti rotor (52). RBC-derived MPs were obtained by ultracentrifugation of packed RBCs at 10,000 (P2), 37,000 (P3) or 200,000 (P4) RCF for 1 hour at 4^{o}C.

Flow cytometry for microparticle quantification

Whole blood, cultured RBCs or isolated MPs were incubated with antibodies against Glycophorin A (catalog #Ab91163, Abcam) and Annexin V (catalog #640906, Biolegend). Events were counted with Accucheck counting beads (catalog #PCB100, Life Technologies) and analyzed on a BD FACS Aria flow cytometer.

Protein and enzyme quantification

Enzyme expression and activation were quantified from biological samples using the following kits: SMase activity: catalog #10006964, Cayman Chemical Company, Acid SMase expression: catalog #SEB360Hu, USCN Life Science, ACER1 expression: catalog #CSB-EL001151HU, CUSABio, Sphingosine kinase 1 and 2 western blot: catalog #1000-6822, Cayman Chemical Company and catalog #AB37977, Abcam, ICAM-4 antibody: catalog #ABIN901654 (antibodies online), Total and phosphor-ERK1/2 western blot: catalog #9102, #9101, Cell Signaling. Western blot measurements were standardized by loading an equal volume of protein. An equal volume of blood was used for activity assays.

Lipid Extraction and Quantification

Lipids were extracted following a protocol from Shaner et al. (53) and analyzed using a Shimadzu LC-10 AD VP binary pump system coupled to a Perkin Elmer Series

200 autoinjector coupled to a 4000 quadrupole linear-ion trap (QTrap) LC-MS/MS system.

Monocyte differentiation and MP internalization

THP-1 monocytes were seeded at $2x10^5$ cells/well on poly-d-lysine-coated coverslips and treated with 100 nM phorbol myristate acetate (PMA) for 72 hours to promote adhesion. Primary AA PBMCs were seeded at $1x10^6$ cells/mL in 12 well plates in media supplemented with macrophage colony stimulating factor (MCSF) (Peprotech). P3 MPs were isolated from packed RBCs as described above and incubated 1:1 with 1μM CFSE (Abcam) for 20 minutes at room temperature followed by ultracentrifugation at 37,000 RCF for 20 minutes at 4^oC. The MP pellet was resuspended in PBS and seeded at $1x10^6$ particles/well on THP-1 or primary isolated monocytes. After 30 minutes, 2 hours or 24 hours the conditioned media was collected, and the cells were washed three times with PBS before imaging or cell lysis with RIPA buffer. Collected proteins were assessed for cytokines using a Milliplex MAP Human Cytokine/Chemokine Premixed 42 Plex Assay (catalog #MPXHCYTO60KPMX42, Millipore) on the Luminex platform.

Monocyte adhesion studies

GFP-HUVECs (Angioproteomie) were seeded in either an 8 chamber slide or a 96-well plate and grown to confluence. DRAQ5 (eBioscience) or DiI (Life Technologies) labeled THP-1 monocytes or primary isolated PBMCs were pre-treated with vehicle media, 1μM S1P or 10% AA/SS plasma for one hour, co-incubated with AA/SS RBCs (1:10 Monocyte:RBC) for 18 hours or co-incubated with AA/SS P3 MPs at high (50%), medium (20%) or low (10%).concentrations for 18 hours and washed then allowed to adhere to confluent HUVECs for 4 hours. Non-adherent cells were washed away with

PBS three times and nuclei of adherent cells were stained with DAPI (4,6-diamindino-2-phenylindole) and imaged with fluorescent microscopy (DRAQ5- or DiI-labeled monocytes appear in red).

Ex vivo RBC studies

RBCs were isolated as described above and resuspended 1:100 in PBS + 20mmol/L glucose with 0, 1, 10 or 100μM amitriptyline and incubated at 37^{o}C for 1, 2 or 24 hours. Cells were resuspended in diH_20 for acid SMase activity measurement or PBS for flow cytometric measurement of MPs.

Animals

Wild-type C57BL/6 mice were obtained from The Jackson Laboratories; Heterozygous AS and homozygous SS mice were initially obtained from the sickle transgenic breeding colony at Georgia Institute of Technology. Townes' model sickle transgenic mice were heterozygous (AS) or homozygous (SS) for the sickle mutation. Saline and 10mpk amitriptyline (dissolved in sterile saline) injections were performed via intraperitoneal injection and peripheral blood was drawn via retro-orbital bleed. For hypoxia studies, mice were housed in polypropylene hypoxia chamber (Coy Laboratory products) and kept at 8% oxygen (using pure O_2 and N_2 as background gas) for 24 hours. All surgical procedures and animal care protocols were approved by the Georgia Institute of Technology Animal Care and Use Committee.

Results

Sphingolipid metabolism is dysregulated in SCD

Neutral SMase is known to be activated upon membrane bending (38). While neutral SMase activity was largely undetectable in plasma and AA RBCs, there was a

small but significant (10pmol/min/mL) increase in neutral SMase activity in SS RBCs (**Figure 3.3A-B**).

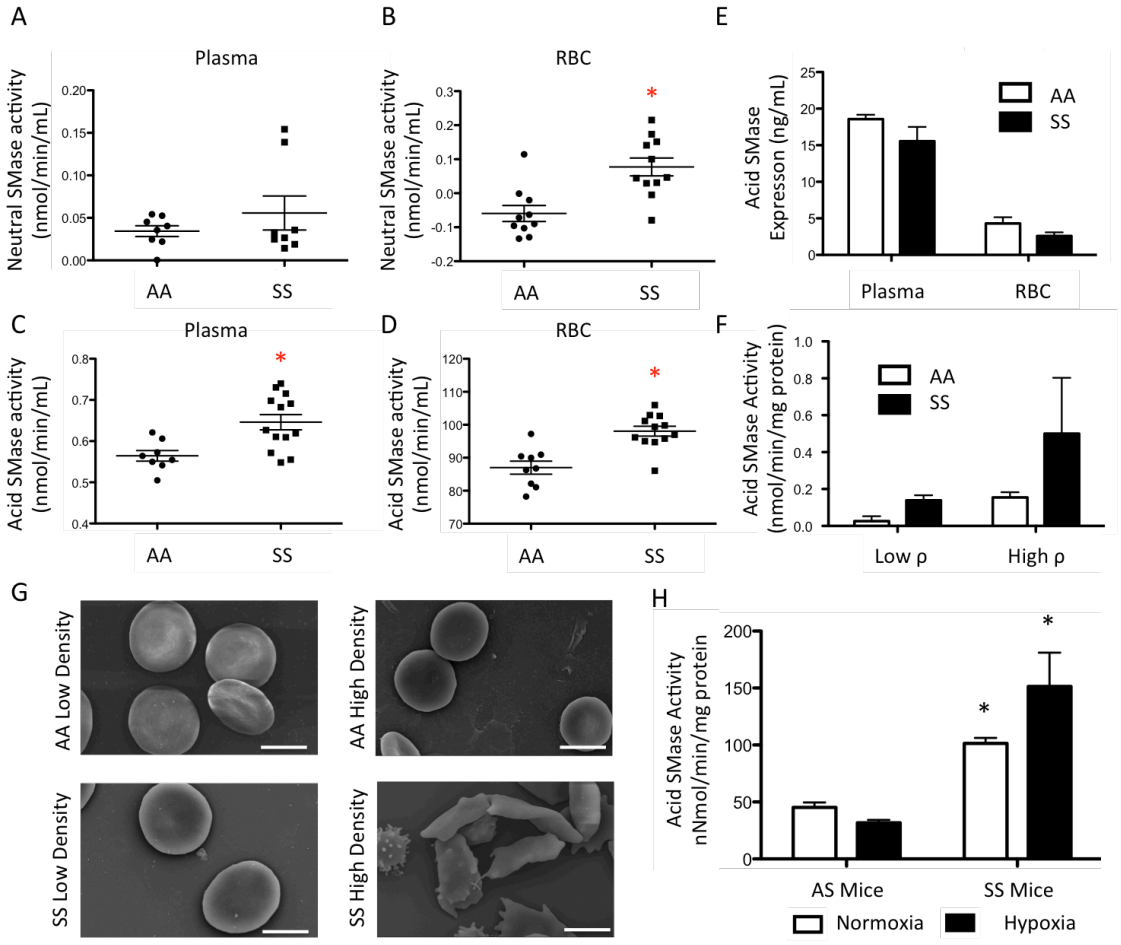

Figure 3.3. Acid and Neutral Sphingomyelinase activity in AA and SS RBC and plasma. Donor blood was harvested and fractionated in a Ficoll density gradient to separate plasma and RBC. A plate based assay for sphingomyelinase activity was performed at a neutral pH on equal volumes of plasma (A) and RBC (B). Neutral sphingomyelinase activity was very low or undetectable in both plasma (A) and RBC (B). SMase activity, while still low, was significantly increased in SS RBC (B) relative to AA RBC. This is likely due to residual (sub-optimal) acid SMase activity at neutral pH or activation of neutral SMase. A plate based assay for acid sphingomyelinase activity was performed on equal volumes of plasma (C) and RBC (D). Acid sphingomyelinase activity was elevated in both plasma and RBC from SCD donors relative to non-diseased donors. A plate based ELISA for sphingomyelinase expression was performed on plasma and RBC (E). Sphingomyelinase expression was not altered in the plasma (left) or RBC (right) of those living with SCD. Packed RBC from AA and SS donors were stacked onto

Percoll density discontinuous layers and spun with ultracentrifugation to separate two distinct density (high and low) fractions of cells. F) High density RBC had higher sphingomyelinase activity than low density RBC. Low density RBC from SS donors had much higher sphingomyelinase activity than low density AA cells and high density RBC from SS donors had much higher sphingomyelinase activity than high density AA cells. Morphological differences were apparent between the four fractions (G). H) AS and SS mice were conditioned with hypoxia (8% oxygen) for 24 hours. Normoxic SS mice displayed a significant increase in acid SMase activity relative to normoxic AS mice. Hypoxic conditioning further enhanced acid SMase activity in SS mice. Scale bar = 5μm. * $p < 0.05$ measured in a ANOVA relative to AA or AS normoxia.

Acid SMase activity in AA plasma was 0.56 nmol/min/mL but was significantly elevated (0.64 nmol/min/mL) in SS plasma (**Figure 3.3C**). Acid SMase activity in SS RBCs (98.06nmol/min/mL) was also significantly elevated in comparison to AA RBCs (87nmol/min/mL) (**Figure 3.3D**). There was a positive correlation (r^2=0.84) between acid SMase activity in RBCs and plasma (data not shown). Acid SMase expression was not altered in plasma and RBCs, suggesting that its increased activity in SCD is due to activation (**Figure 3.3E**). We sought to determine if sickled RBCs had higher levels of acid SMase activity, so we used Percoll density centrifugation to separate high- (irreversible sickled) and low-density fractions of RBCs (**Figure 3.3G**) (54). Low density SS RBCs, many of which were sickled, displayed increased acid SMase activity relative to AA RBCs. Irreversible sickled SS RBCs had the highest acid SMase activity (**Figure 3.3F-G**). To confirm the role of RBC sickling in acid SMase activation, we induced sickling in SS mice with hypoxic conditioning for 24 hours. Consistent with humans, SS mice displayed a significant increase in acid SMase activity in whole blood at normoxic baseline. Deoxygenation by hypoxic conditioning further enhanced acid SMase activity in SS mice (**Figure 3.3H**).

Multiple lipids can be metabolized downstream of sphingomyelin (**Figure 2.1**). Alkaline ceramidase (ACER1), which converts ceramide to sphingosine (55), was measured in RBCs and plasma. ACER1 levels were not altered between AA (73.02pg/mL) and SS (79.68pg/mL) RBCs (**Figure 3.4A**).

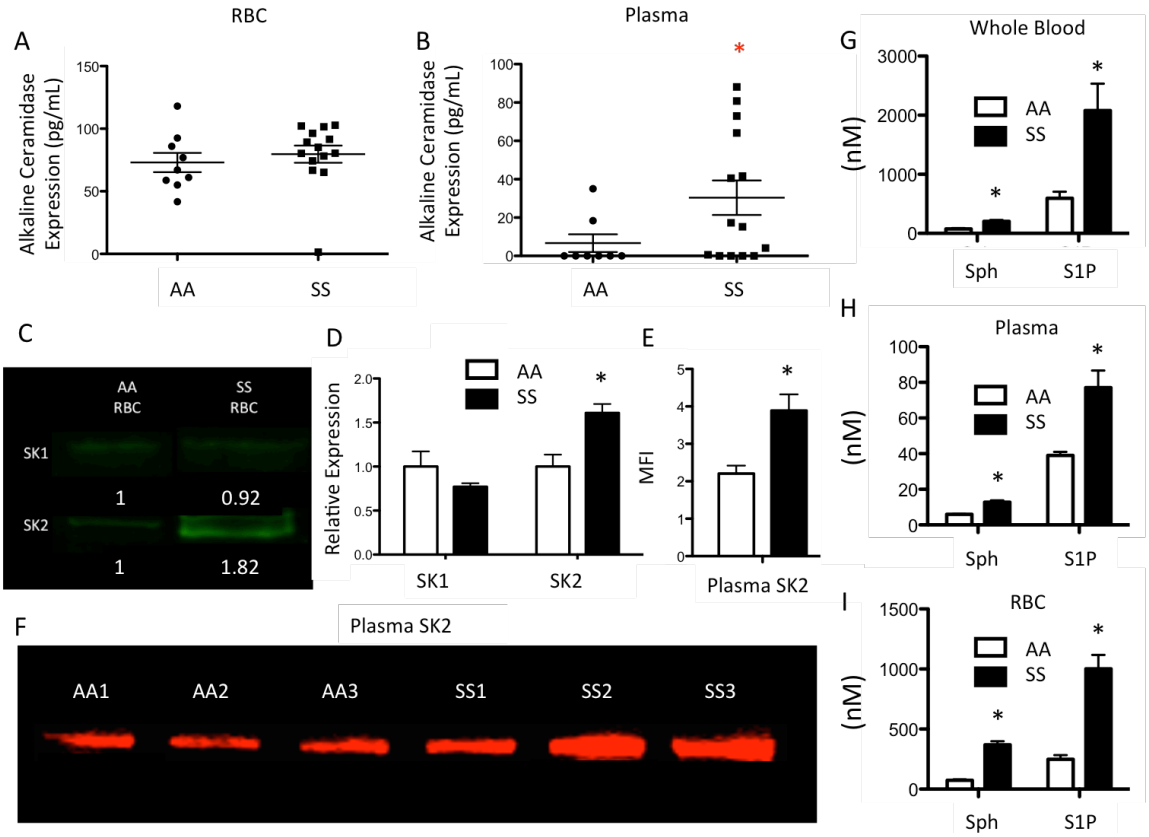

Figure 3.4. Alkaline ceramidase, sphingosine kinase 2, S1P and sphingosine elevated in SCD. Donor blood was harvested and fractionated in a Ficoll density gradient to separate plasma and RBC. A plate based assay for alkaline ceramidase (ACER1) expression was performed on RBCs (A) and plasma (B). ACER1 expression was not altered in SCD RBC. ACER1 was not detected in the plasma of those without SCD but was elevated in the plasma of those with SCD. RBC were fractionated from donor blood and lysed in RIPA buffer. C) Western blotting shows expression of both SK1 and SK2, but only SK2 was visibly elevated in SS RBC. D) Relative fold changes in SK1 and K2 expression reveal a significant increase in SK2 expression in SS RBC. E-F) Donor plasma was assessed for SK2 expression and plasma from those living with SS had significantly more SK2, relative to AA, suggesting that SK2 is secreted during SCD. Lipids were extracted from donor samples and sphingosine and S1P levels in whole

blood (G), plasma (H) and RBC (I) was quantified with HPLC-MS. * $p < 0.05$ measured in a t-test.

ACER1 was present at a concentration of 30.39pg/mL in SS plasma, but was not detected in AA plasma (**Figure 3.4B**). Sphingosine is phosphorylated to form the bioactive signaling lipid, S1P, by sphingosine kinase 1 and 2 (SK1/2). As S1P is stored at high concentrations in RBCs (56), we hypothesized that they would express SK1 and SK2. SK1 was expressed at low levels in both AA and SS RBCs. SK2 was also expressed by both cell types but was significantly elevated in SS RBCs (**Figure 3.4C-D**). SK2 levels in plasma were assessed via western blot and were significantly increased in SS relative to AA plasma (**Figure 3.4E-F**), suggesting that SK2 may be secreted into circulation in SCD. As these enzymes are upstream of sphingosine and S1P, we hypothesized that they would be elevated in SCD. HPLC-MS was used to quantify lipids were extracted from whole blood, plasma or RBCs. Both sphingosine (202.84nM vs. 77.42nM) and S1P (2080nM vs. 593.5nM) were significantly elevated in SS whole blood relative to AA blood (**Figure 3.4G**). Sphingosine and S1P levels were much lower in the plasma but there were still significant increases in sphingosine (12.82nM vs. 5.97nM) and S1P (77.03nM vs. 35.01nM) levels in SS plasma relative to AA plasma (**Figure 3.4H**). SS RBCs also had significantly more sphingosine (369.71nM vs. 73.41nM) and S1P (1000.22nM vs. 249.3nM) compared to AA RBCs (**Figure 3.4I**).

RBC-derived MPs express sphingolipids

We employed the Townes mouse model of SCD to determine whether SS RBCs produced more MPs. SS mice have both mouse alpha and beta hemoglobin knocked out and human alpha sickle beta globin knocked in. Blood was collected from these mice and

stained for CD41+ platelet MPs and Glycophorin A+ RBC MPs (57). While platelet MPs comprised the vast majority of blood-borne MPs, there was a significant increase in RBC-derived MPs in SS mice relative to AS mice (**Figure 3.5**), corroborating the finding that RBC-derived MPs are significantly elevated in SCD (39).

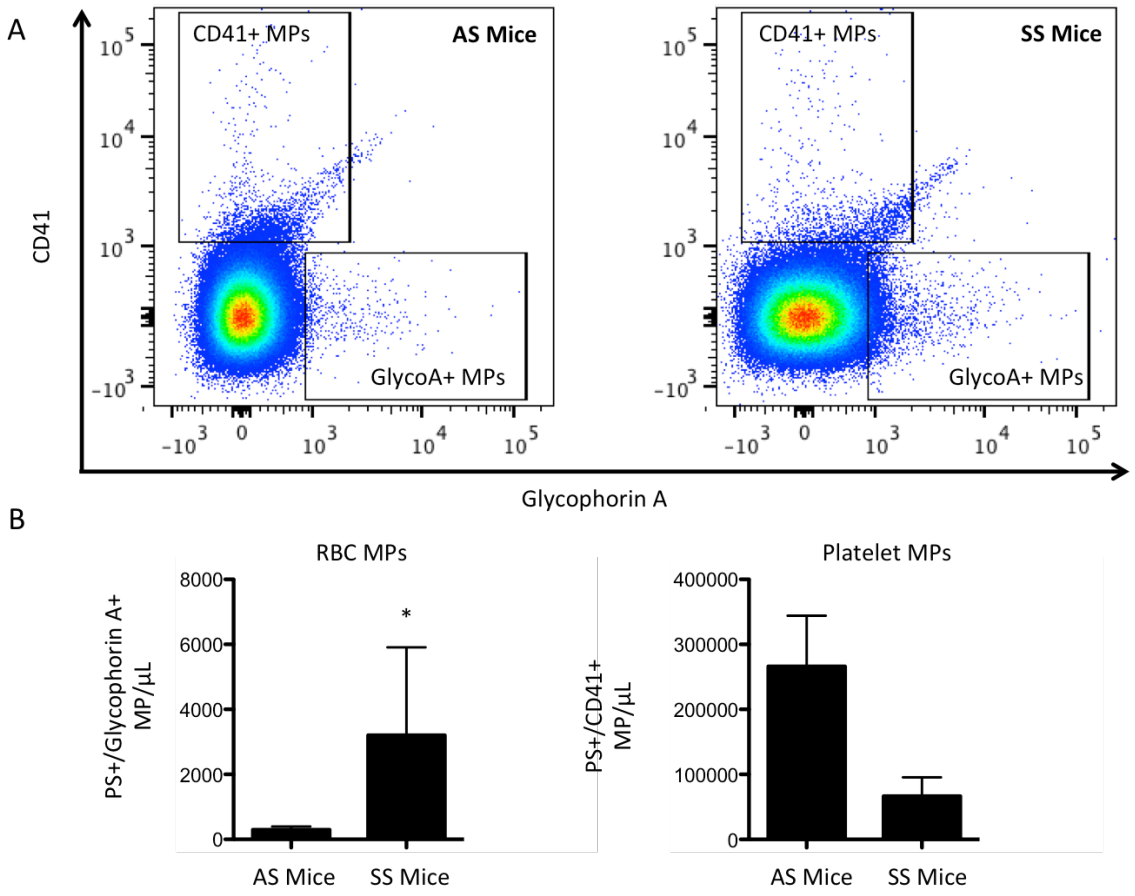

Figure 3.5. Platelet and RBC derived Microparticles in AS and SS mice. A) Blood was drawn via retro-orbital bleed from AS (left) or SS (right) Townes mice and stained with antibodies against PS, CD41 and Glycophorin A. B) Analysis reveals a significant increase in Glycophorin A+ (RBC-derived) microparticles in SS mice relative to AS mice (left). There were significantly more CD41+ (platelet-derived particles) in both mice but no significant differences in their concentration (right). * $p<0.05$ compared to AS.

Preliminary image analysis of human RBC-derived MPs revealed a heterogeneous size distribution so we employed ultracentrifugation at 10,000, 37,000 and 200,000 RCF to isolate P2, P3 and P4 MPs, respectively (**Figure 3.6A**).

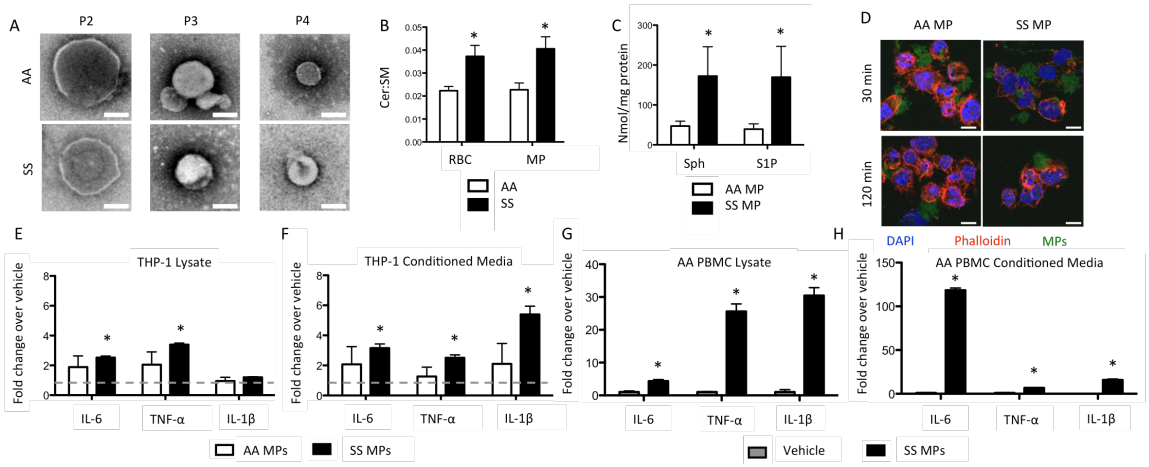

Figure 3.6. RBC derived microparticles contain sphingolipids, are internalized by macrophages and enhance cytokine production. A) TEM images were taken of microparticles harvested at 10,000 (P2), 37,000xg (P3) or 200,000xg (P4) for one hour. *Scale bar = 200nm.* B) P3 microparticles derived from SS RBCs have an increase in the ceramide: sphingomyelin ration. C) P3 particles derived from SS RBCs contain significantly more sphingosine and S1P. D) P3 microparticles were labeled with CFSE and incubated with M0 THP-1 macrophages for 30 (top) or 120 (bottom) minutes. *Scale bar = 10μm*. E-F) SCD RBC-derived P3 microparticles were incubated with M0 THP-1 macrophages for 24 hours. Microparticle incubation enhanced the production (E) and secretion (F) of inflammatory cytokines IL-6, TNF-a and IL-1β relative to vehicle-treated cells (dotted line). G-H) AA and SS RBC-derived P3 microparticles were incubated with primary AA macrophages for 24 hours. Microparticle incubation enhanced the production (G) and secretion (H) of inflammatory cytokines IL-6, TNF-a and IL-1β relative to vehicle-treated cells. * $p < 0.05$ measured in one-way ANOVA relative to vehicle.

Their size distribution was between 150 and 400nm (**Figure 3.7A**).

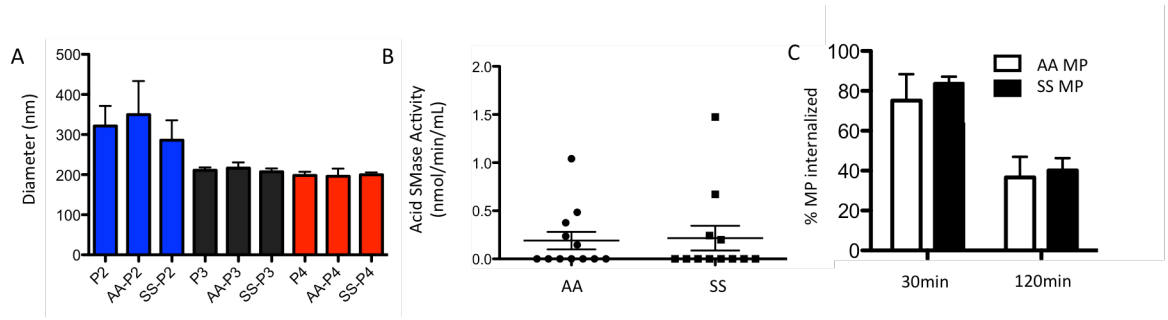

Figure 3.7. Microparticle Characterization and pro-inflammatory cytokine production in primary AA PBMCs. A) P2 microparticles were around 300nm on average while P3 and P4 microparticles were around 200nm. B) A plate based assay for acid sphingomyelinase activity was performed. Acid sphingomyelinase activity was largely undetectable in both AA and SS microparticles suggesting that the enzyme is not present in these particles. C) P3 microparticles were labeled with CFSE and incubated with M0 THP-1 macrophages for 30 or 120 minutes. Flow cytometry was used to quantify the number of particles internalized. A higher proportion of cells was internalized in 30 minutes than 120 minutes suggesting that microparticles can be internalized and subsequently secreted but there were no differences between AA and SS microparticles.

Acid SMase activity was largely undetectable in MPs (**Figure 3.7B**) suggesting that the enzyme is not internalized within particles upon generation. Sphingomyelin and ceramide were measured in RBCs and MPs. As expected, both RBCs and MPs had an increase in the ceramide: sphingomyelin ratio, indicating a shift towards ceramide production consistent with SMase activity (**Figure 3.6B**). Both AA- and SS- derived MPs expressed sphingosine and S1P and similar to SS RBCs, SS RBC-derived MPs contained significantly more sphingosine and S1P (**Figure 3.6C**).

<u>MPs are internalized and modulate cytokine production by monocytes</u>

To determine whether monocytes internalized RBC-derived MPs, PMA-treated THP-1s were incubated with $1x10^6$ CFSE-stained MPs for 30 or 120 minutes. Confocal microscopy revealed that MPs were internalized as early as 30 minutes (**Figure 3.6D**). Within 30 minutes, 75% of AA MPs and 84% of SS MPs were internalized (**Figure**

3.7C). Surprisingly, after 120 minutes, a smaller proportion of MPs (37% for AA and 40% for SS) was internalized by PMA-treated THP-1s, suggesting that MPs can be internalized and secreted as intact MPs (**Figure 3.7C**). MP internalization increased the production and secretion of many inflammatory cytokines after 24 hours. Interestingly, SSMPs, and not AAMPs, significantly enhanced the production and secretion of IL-6, TNF-α and IL-1β, markers of systemic inflammation during SCD (58), relative to vehicle-treated cells (**Figure 3.6E-F**). To interrogate the effects of SSMPs on primary AA PBMCs, we incubated PBMCs with SSMPs. SSMPs significantly enhanced the production and secretion of these cytokines in primary AA monocytes as much as 120-fold (**Figure 3.6G-H**).

S1P, SS plasma and SS RBC co-incubation enhances monocyte adhesion to endothelial cells

S1P, an immunomodulatory lipid, signals through the activation of 5 known G-protein coupled receptors ($S1P_{1-5}$) with diverse biological functions (6). As SS plasma and MPs express significantly more S1P than AA plasma and MPs, we wished to explore their effects on PBMC adhesion. 1μM S1P or AA/SS plasma was used to pre-treat primary AA PBMCs for 1 hour before co-incubation with confluent HUVECs for four hours. S1P (43%) and SS plasma (28%) but not AA plasma (-1.7%) resulted in an elevation in endothelial adhesion relative to vehicle (**Figure 3.8A-B and Figure 3.9**).

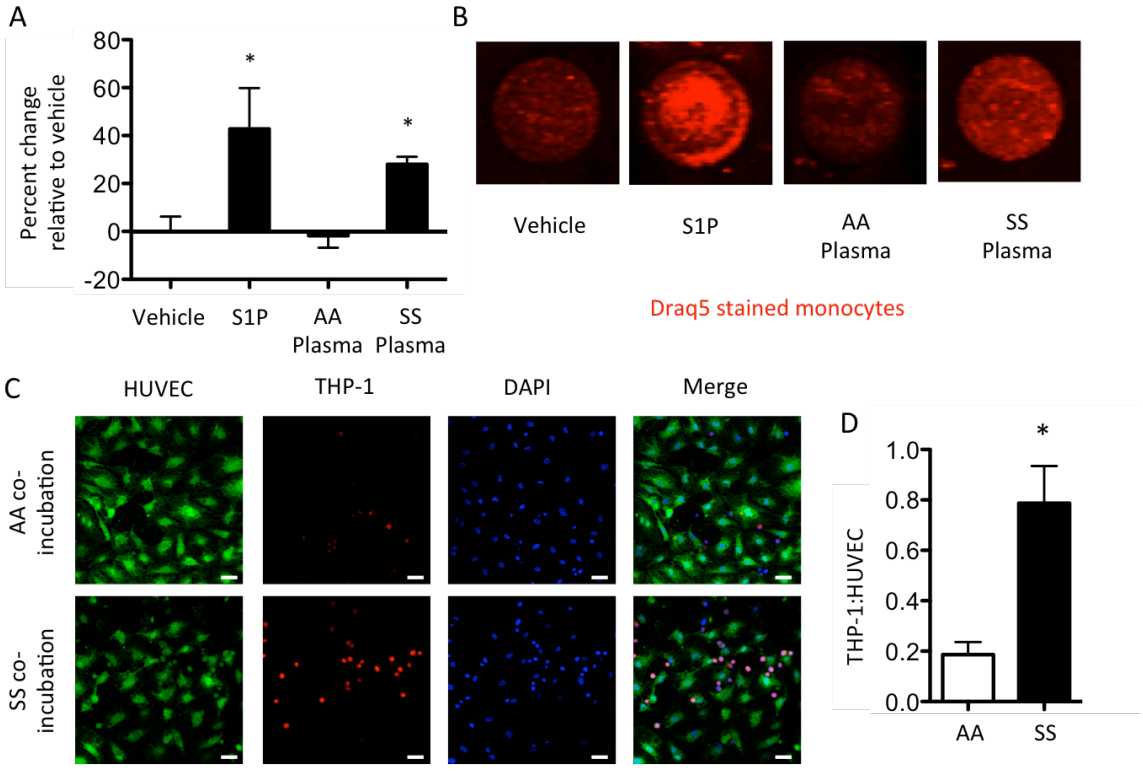

Figure 3.8. S1P treatment and SS RBC co-incubation of monocytes enhances endothelial adhesion. A-B) DRAQ5 stained AA PBMCs were incubated with media, media with 1μM S1P, media with 10% AA plasma or media with 10% SS plasma for 1 hour and allowed to adhere to confluent HUVECs for 4 hours. S1P and SS plasma enhanced monocyte adhesion while AA plasma reduced monocyte adhesion relative to vehicle treated cells. C-D) AA or SS RBCs were co-incubated with THP-1 monocytes (10:1) for 18 hours before HUVEC adhesion. Co-incubation of THP-1 monocytes with SS RBC significantly enhanced monocyte: HUVEC ratio after 4 hour adhesion (D). Representative images (C) show enhanced THP-1 monocytes (red cells) adhered to a HUVEC (59) monolayer. *Scale bar = 10μm.* * $p < 0.05$ measured in one-way ANOVA or t-test relative to vehicle or AA.

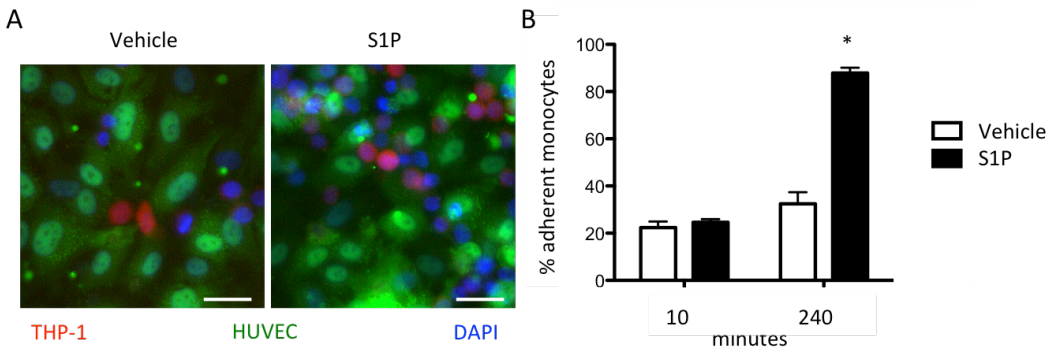

Figure 3.9. SS plasma, but not AA plasma, enhances primary PBMC adhesion to endothelial cells. A-B) GFP HUVECs (59) were grown to confluence and co-incubated with THP-1 monocytes (DiI-red) for 10 minutes or 4 hours after 1 hour vehicle treatment or 1μM S1P treatment of monocytes. S1P treatment of monocytes significantly enhanced the proportion of adherent monocyte after 4 hours. * $p<0.05$ relative to vehicle.

As RBCs are known to interact with monocytes in circulation (60, 61) we sought to interrogate the potential of SS RBCs to directly alter monocyte-endothelial adhesion. AA or SS RBCs were incubated with THP-1s at a 10:1 ratio for 18 hours. Thereafter, THP-1s were co-incubated with HUVECs and allowed to adhere for four hours (**Figure 3.8C**). Co-culture with SS RBCs significantly enhanced THP-1 adhesion to endothelial cells, measured by the THP-1:HUVEC ratio (0.78) relative to co-culture with AA RBCs (0.19) (**Figure 3.8C-D**).

SS RBC-derived MPs enhance PBMC adhesion and express ICAM-4 and elevated p-ERK1/2

To confirm whether MPs alone could enhance monocyte-endothelial cell adhesion, we incubated primary AA PBMCs with AA- or SS RBC-derived MPs for 24 hours and allowed them to adhere to endothelial cells for 4 hours. Interestingly, AA RBC-derived MP incubation did not enhance adhesion while SS RBC-derived MP

incubation resulted in a significant increase in PBMC adhesion at all concentrations (**Figure 3.10A**).

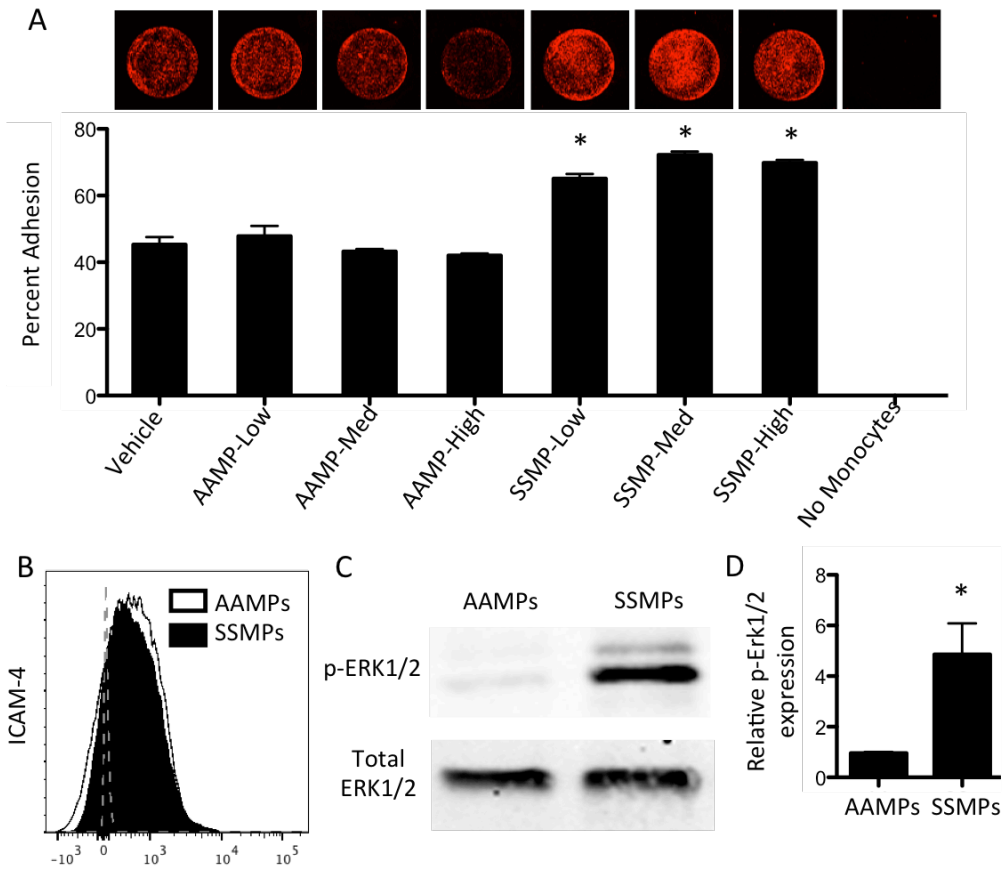

Figure 3.10. SS RBC-derived MPs enhanced endothelial adhesion and express LW and significantly more pErk1/2 than AA RBC-derived MPs. A) RBC-derived microparticles were incubated with primary AA PBMCs (62) at three different concentrations (low, medium and high) for 18 hours before HUVEC adhesion. AAMPs reduced PBMC adhesion, while SSMPs enhanced PBMC adhesion. B) AAMPs and SSMPs express ICAM-4 (LW). C-D) Phosphorylated Erk1/2 significantly elevated in SSMPs relative to AAMPs. $p < 0.05$ measured in ANOVA relative to vehicle or AAMPs.

Zennadi et al. established an ERK1/2 mediated mechanism for ICAM-4 expression on SS RBCs, which mediates RBC adhesion to both monocytes and endothelial cells (37, 61). Both AA and SS RBC-derived MPs expressed ICAM-4 (**Figure 3.10B**). SS RBC-derived

MPs, however, express significantly activated ERK1/2 as indicated by significantly higher phosphor-ERK1/2 to total ERK1/2 than AA RBC-derived MPs (**Figure 3.10C-D**). These results suggest that, similar to SS RBCs, SS RBC-derived MPs may enhance monocyte adhesion in an ERK1/2 – ICAM-4 mediated fashion.

Acid SMase inhibition reduces MP generation and pro-inflammatory cytokine production

As spleen dysfunction and reduced MP clearance are characteristic of SCD we sought to establish a unique role for SMase in MP generation. SS RBCs were cultured in media with amitriptyline, a tricyclic anti-depressant and acid SMase inhibitor for 1 or 24 hours and MPs were quantified by flow cytometry. While 1-hour amitriptyline treatment did not alter the production of MPs at any dose, by 24 hours amitriptyline significantly reduced the generation of RBC-derived MPs *in vitro* in a dose-dependent fashion (**Figure 3.11A-C**).

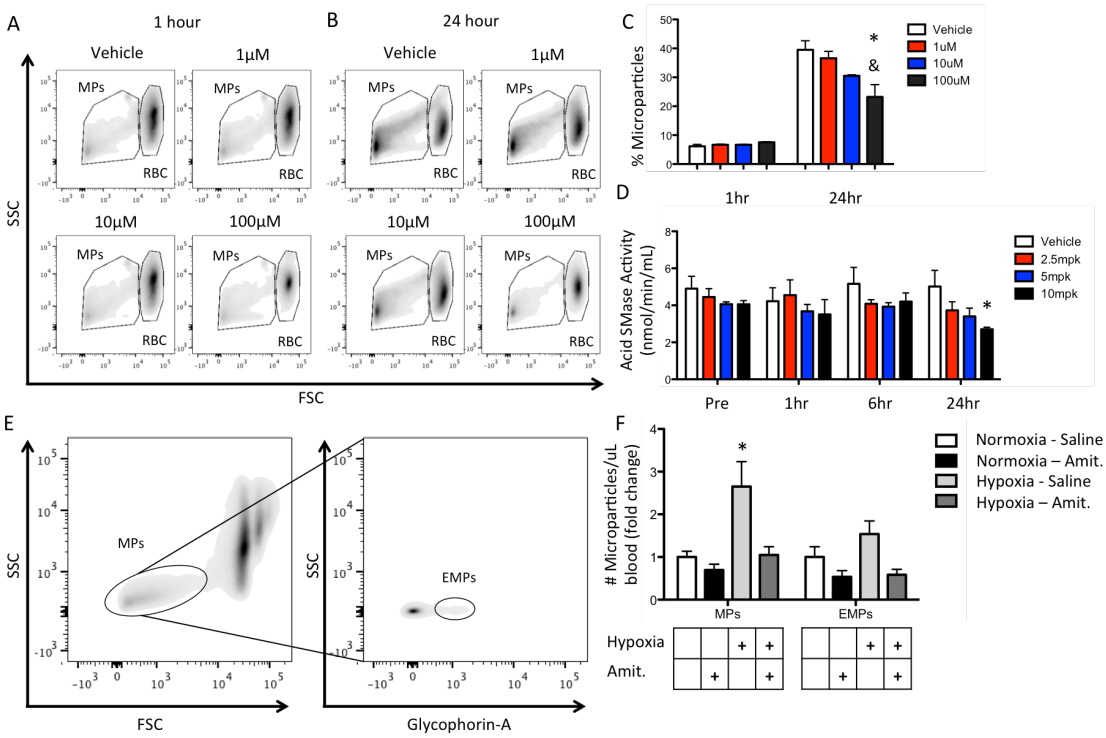

Figure 3.11. Amitriptyline reduces microparticle generation in RBCs. A-B) Flow cytometry showing microparticles and RBC at 1 hour (A) and 24 hours (B). C) 100μM Amitriptyline significantly reduces the percentage of microparticles produced from SS RBCs 24 hours after treatment. D) 10mpk Amitriptyline significantly reduces acid sphingomyelinase activity in C57/Bl6 mice 24 hours after injection. E) Gating strategy for identifying microparticles and erythrocyte derived microparticles (EMPs) *in vivo*. F) Amitriptyline reduces the hypoxia-induced increase in microparticle generation relative to vehicle treated groups as early as 24 hours after injection. * $p<0.05$ compared to vehicle or normoxia-saline, & $p<0.05$ compared to 1uM.

We next injected amitriptyline at four concentrations into wild type C57Bl/6 mice and found that acid SMase activity was significantly reduced after 24 hours of the highest dose. (**Figure 3.11D**). Hypoxia has been shown to enhance microparticle generation *in vivo* (63). After 24 hours of hypoxic conditioning MPs in blood and erythrocyte-derived MPs in blood were significantly elevated relative to pre-hypoxic conditioning (**Figure 3.11F**). Amitriptyline reduced hypoxia-induced MP and erythrocyte-derived MP (EMP) generation (**Figure 3.11E-F**). Additionally, two of the three cytokines we showed to be

modulated by MPs in monocytes *in vitro* (IL-6 and IL-1β) were reduced in amitriptyline-treated mice relative to saline treated mice (**Figure 3.12**).

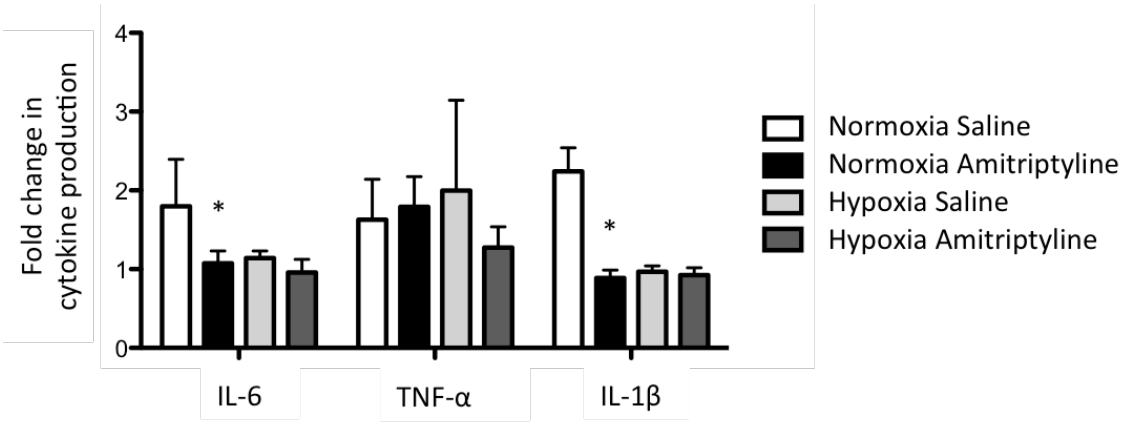

Figure 3.12. *In vivo* hypoxia cytokine production in mice. Wild type mice were conditioned normoxia/hypoxia with intraperitoneal injections of saline or amitriptyline for 24 hours. The fold change in IL-6, TNF-a and IL-1B were quantified. Amitriptyline significantly reduced the expression of IL-6 and IL-1B during normoxic conditioning, relative to saline-injected mice.

These results elucidate a role for acid SMase in RBC-derived MP generation and systemic inflammation *in vivo* and establish pharmacological modulation of acid SMase as a strategy to modulate these phenomena in SCD.

Discussion

SCD is a complex disease with severe pathophysiological effects. In recent years, it has been discovered that MPs, which are elevated in SCD, contribute to SCD pathogenesis (39-42). In this work, we examined the dysregulation of sphingolipid metabolism, MP production and inflammatory cell activation in SCD. Lopez et al. found that stresses in RBC membranes transiently enhanced the activation of neutral SMase (38). Similarly, Urbina et al. found that SMase activity in unilamellar vesicles in *Clostridium perfringens* α-toxin increased with membrane curvature (64). Our work

shows that SS RBCs, which may undergo membrane stresses due to sickling events, oxidative damage, ion fluxes and enhanced adhesion have a significant increase in acid SMase activity relative to AA RBCs (Figure 3**.3D**). Irreversibly sickled RBCs had the highest acid SMase activity, corroborating these findings (**Figure 3.3F-G**). Furthermore, when RBC sickling was induced in SS mice by hypoxic deoxygenation, there was an increase in acid SMase activity confirming that sickling is upstream of acid SMase (**Figure 3.3H**). More studies need to be performed to elucidate the mechanism underlying the sensing of local forces and subsequent activation of SMase in cell membranes.

SMase activity has been implicated in vascular inflammation (65, 66). Becker et al. discovered that ceramide production in the lung contributed to inflammatory cytokine production during cystic fibrosis and amitriptyline reduced ceramide production, inflammatory cytokine production and inflammatory cell recruitment in a mouse model of CF (2, 67). Other groups have shown that SMase-mediated ceramide synthesis in plasma membranes promotes microvessel formation (7, 8). We found that the ceramide: sphingomyelin ratio in SS RBCs and MPs was reduced, which corroborates the finding that acid SMase is activated in SS RBCs (**Figure 3.6B**).

MPs have been shown to enhance atherosclerosis (42), coagulation (41), vaso-occlusion in the kidney (43), inflammation (44, 47) and monocyte adhesion (45). RBC-derived MPs from AA and SS donors were both internalized by THP-1s (**Figure 3.6D**). The internalization, processing and secretion of RBC-derived particles deserves significant attention and future studies are needed to completely understand these mechanisms. Interestingly, SS MPs enhanced the production and secretion of three

cytokines consistently associated with inflammation in SCD, TNF-α, IL-1β and IL-6 (58), to a much larger extent than AA MPs (**Figure 3.6E-H**). Additionally, we show that SS MPs, and not AA MPs, enhance monocyte adhesion to endothelial cells (**Figure 3.10A**) and, similarly, co-incubation of monocytes with SS RBCs enhances monocyte-endothelial adhesion relative to AA RBCs (**Figure 3.8C**). Zennadi et al. established an ERK1/2 mediated mechanism for ICAM-4 expression on SS RBCs which mediates monocyte and endothelial cell adhesion and activation (37, 61), so we wished to determine whether RBC derived MPs expressed both ICAM-4 and p-ERK1/2. Interestingly, while both AA and SS RBC-derived MPs expressed roughly the same level of ICAM-4, SS RBC derived MPs express significantly more activated ERK1/2 (**Figure 3.10C-D**). Taken together, these results suggest that, similar to SS RBCs, SS MPs may enhance monocyte adhesion in an ERK1/2 – ICAM-4 mediated fashion. Additional studies are needed to elucidate this mechanism and lipidomic and proteomic profiling of RBC-derived MPs might provide critical insights into the molecules contributing to these phenotype-specific alterations in inflammatory cell adhesion and cytokine secretion. Others have described inflammatory cell activation in SCD (51). As both SS plasma, RBC and MPs contain significantly more S1P (**Figure 3.4H-I, Figure 3.6C**), we wished to explore the direct effects of S1P on monocyte adhesion. S1P can be pro-inflammatory by activating S1P receptors on monocytes (33), inducing E-selectin expression and the adhesion of monocytes to endothelial cells (35), and cathepsins-mediated endothelial cell activation (68). We recently showed that S1P receptor 3 activation enhances the recruitment of anti-inflammatory monocytes to inflamed tissues (49). In this work we found that both SS plasma and S1P directly enhance monocyte-endothelial cell adhesion

(**Figure 3.8A-B**). While S1P has been shown to alter monocyte morphology and motility through the activation of rho-kinase (69) and receptor tyrosine kinases (70), more comprehensive studies need to be performed to elucidate the receptor-specific signaling mechanism behind S1P-mediated monocyte adhesion.

It is important to note that SCD is characterized by significant hyposplenism. As the spleen is responsible for the removal of cellular debris, the increase in blood microparticles observed in SCD is also a result of impaired spleen function (71). We wished to establish a non-redundant role for acid SMase in RBC-derived MP generation, so we interrogated MP generation from SS RBCs *in vitro*, in the absence of spleen clearance. Inhibition of acid SMase with amitriptyline significantly reduced MP generation from SS RBCs *in vitro* (**Figure 3.11A-C**). As amitriptyline and other tricyclic antidepressants have been shown to reduce acid SMase activity and exosome formation *in vivo* (2, 67, 72) we explored the ability of acid SMase inhibition to reduce MP production in mice. Hypoxia has been shown to enhance MP generation (63) and we confirmed that in non-sickled mice with normal functioning spleens, MP production was significantly elevated after 24 hours hypoxia. Amitriptyline significantly reduced MP generation in normoxic and hypoxic conditioned wild-type mice, confirming a role for acid sphingomyelinase in MP generation independent of dysfunctional spleen clearance (**Figure 3.11F**). Additionally, these changes occurred in concert with pro-inflammatory cytokine reduction *in vivo* (**Figure 3.12**). Taken together, these results show that acid SMase, which is activated in sickled RBCs (**Figure 3.3C-H**), enhances RBC-derived MP production and systemic inflammation in a mechanism independent of impaired spleen clearance in SCD. The role of systemic hypoxia, and local hypoxia in sickle cell due to

transient vasoocclusions, in acid SMase activation cannot be ruled out by these studies and needs to be explored.

There are multiple lipids metabolically downstream of sphingomyelin that have diverse biological effects. Erythrocytes convert ceramide into sphingosine with ACER1 (55). To date, this enzyme has not been detected in plasma; however, we detected ACER1 in SS plasma (**Figure 3.4B**), suggesting that it can be released into circulation through secretion or hemolysis. Ceramide synthesis in erythrocyte membranes is associated with eryptosis and clearance (73). Additionally, the chronic stress induced by sickled RBCs in circulation during SCD results in an increase in the apoptosis of white blood cells (74). Weigert et al. found that cellular apoptosis leads to the activation and secretion of SK2 (24). Consistent with these findings, we found that SK2 is increased in both the plasma and RBCs of SCD donors (**Figure 3.4C-F**). While more studies need to be performed to fully understand the source and mechanism of ACER1 and SK2 secretion into plasma, it is apparent that complex mechanical and biological cues in SCD result in dysregulated sphingolipid enzyme expression and activation, causing a significant increase in sphingosine and S1P (**Figure 3.4G-I**).

Our findings reveal for the first time that sphingolipid metabolism is dysregulated in SCD. As this dysregulation is a result of altered enzyme activation and expression in stressed cells, these results are likely applicable to other hemolytic anemias and their interrogation is warranted. Additionally, they elucidate a novel mechanism for microparticle generation in SS RBCs. Membrane stresses imposed on RBCs in SCD activate acid SMase, which, in concert with other sphingolipid enzymes, results in elevated S1P and MP production (**Figure 3.1**). SS RBC-derived MPs, containing S1P,

activate monocytes by enhancing endothelial cell adhesion and pro-inflammatory cytokine production. These findings elucidate potential new strategies to regulate inflammatory processes in SCD through modulating sphingolipid metabolism but are not unique to SCD. These results are not unique to SCD and can be applied to many other diseases rooted in alterations in sphingolipid metabolism. Modulating sphingolipid metabolism may be a novel way to pharmacologically control systemic inflammation present in many human diseases.

CHAPTER 4

EXTENSIVE SPHINGOLIPIDOMIC CHARACTERIZATION AND MODELING OF SS AND AA RED BLOOD CELLS AND MICROPARTICLES

Introduction

Many diseases have very complex pathologies, despite having very simple origins. This is the case with sickle cell disease (SCD), which causes a host of vascular complications as a result of a single point mutation in the gene encoding hemoglobin. The pathophysiology of SCD involves many organ systems, signaling systems and cell types. The complexity of diseases like SCD makes it difficult to find biological targets for therapy or cure. In recent years, the "-omics" movement has dominated much of the exploration around human diseases and disorders (75, 76). Researchers are taking a much more top-down approach to elucidate genetic and molecular targets for therapy. With the advent of tools and techniques that can characterize complete genetic, proteomic and lipidomic profiles from biological samples, researchers are generating large sets of data that can be mined to elucidate unique states and dysregulations that exist in SCD and other diseases.

Sickle cell disease is caused by the polymerization of hemoglobin molecules in red blood cells (RBCs). These hemoglobin polymers form rod-like structures that distort the RBC plasma membrane and leads to severe vasculopathy such as stroke, atherosclerosis and peripheral arterial disease. While the genetic basis of SCD has been known for decades (77), molecular dysregulation in SCD has been widely understudied. As alterations in the RBC membrane are pathognomonic in SCD, there is reason to

believe that the balance of lipids, which comprise the RBC plasma membrane, may be altered in the disease state. Sphingolipids are membrane-derived lipids which have been shown to act as bioactive signaling mediators (5, 78). We sought to determine whether sphingolipid metabolism was dysregulated in SCD and whether distinct lipid species were up- or down- regulated in the disease state.

The contribution of sphingolipids to diseases is not a new discovery. Niemann-Pick disease (NPD), for example, is a group of lysosomal storage diseases caused by the mutation of the gene which encodes for acid sphingomyelinase (SMase) (79). Acid SMase hydrolyzes sphingomyelin into ceramide, and thus loss of acid SMase function in NPD results in the accumulation of sphingomyelin in lysosomes, which can be harmful to the spleen, lungs, liver, brain and bone marrow (80). Similarly, Farber disease is a much rarer lysosomal storage disease caused by deficiency in the enzyme ceramidase, which leads to pathological storage of sphingolipids in various parts of the body (81). While sphingolipid metabolizing enzymes are not directly mutated in SCD, others have shown dysregulation in S1P (82), sphingosine and ceramides (83). Sphingolipids are significant components of RBC plasma membranes, so it is important to understand how alteration of these lipids might play a role in the disease.

Sphingomyelin is the most abundant sphingolipid in the red blood cell RBC membrane (84) and is hydrolyzed by a class of enzymes known as sphingomyelinases. Our previous work has shown that acid SMase is activated in SS RBCs and may be a result of membrane sickling (83). Not only does this activity alter the balance of sphingolipids in RBCs, it contributes to the generation of membrane-derived vesicles called microparticles. Others have implicated SMase in RBC membrane modifications

and invaginations (7), and membrane bending has been shown to activate neutral sphingomyelinase in red blood cell membranes (38). In 1982 Allan et al. showed that SS RBCs lose 2-3% of their lipid content due to the sickling cycle. Lipids are lost as spectrin-free spicules in the form of rods and microspheres (39). These rods can eventually degrade to form sub-micron sized microparticles. RBC-derived MPs, which can also bud directly from the membrane, contain sphingolipids and thus can serve as signaling mediums to cells in circulation. We sought to determine whether the expression of sphingolipids that exist in the metabolic network was altered in RBCs and MPs in SCD. We hypothesized that there would be distinct sphingolipidomic differences in RBCs and their MP byproducts between AA and SS donors. To this end, we performed an extensive sphingolipidomic analysis of AA and SS RBCs and MPs to determine if there were distinct differences in their lipid profiles. From this lipidomic analysis we were able to distinguish the disparities in sphingolipid distribution between AA and SS samples at steady state. However, this information did not tell us which enzymes or reactions might be altered, revealing potential areas of therapy.

Mathematical modeling has been employed in conjunction with proteomics and lipidomics to predict changes in reaction flux between metabolites. For instance, Cowart et al. discusses the importance of combining lipidomic data with modeling to reveal novel signal transduction pathways involved in sphingolipid metabolism elucidating potential therapy targets (85). Models of sphingolipid metabolism have also been developed by incorporating transcriptomic and lipidomic data in order to predict enzyme targets for anti-cancer drugs and changes in sphingolipid metabolism during infection (86, 87). To investigate dysregulation in the sphingolipid metabolic pathway in SCD we utilized

lipidomic data as inputs in a computational model in order to predict changes in sphingolipid metabolic reaction flux and enzyme activity between AA and SS RBCs. Of the 29 reactions modeled, 7 were decreased and 1 was increased more than 2-fold in SS RBCs relative to AA RBCs. Importantly the model reveals several rate-limiting steps in sphingolipid metabolism (i.e. phosphatase and ceramidase activity) that may control the maximum flux of metabolites. These findings show, for the first time, that several reactions in sphingolipid metabolism are altered in SCD and contribute to the altered sphingolipid state in SCD. Additionally, the discovery of rate-limiting steps may provide more potent therapeutic targets for sphingolipid modulation.

Methods

RBC and MP isolation and fractionation

Whole blood samples from donors homozygous for sickle (SS) or normal (AA) hemoglobin were centrifuged against a Ficoll-Paque density gradient (density: 1.077g/mL; GE Healthcare) for 30 minutes at 400 RCF at 4˚C to separate plasma, peripheral blood mononuclear cells (PBMCs) and packed RBCs. RBCs were separated into high and low density fractions using stacked Percoll solutions centrifuged at 41,000rpm for 30 minutes using a Beckman SW 41 Ti rotor (52). RBC-derived MPs were obtained by ultracentrifugation of packed RBCs at 10,000 (P2), 37,000 (P3) or 200,000 (P4) RCF for 1 hour at 4^{o}C.

Flow cytometry for microparticle quantification

Whole blood, cultured RBCs or isolated MPs were incubated with antibodies against Glycophorin A (catalog #Ab91163, Abcam) and Annexin V (catalog #640906,

Biolegend). Events were counted with Accucheck counting beads (catalog #PCB100, Life Technologies) and analyzed on a BD FACS Aria flow cytometer.

Protein and enzyme quantification

Enzyme expression and activation were quantified using the following kits: SMase activity: catalog #10006964, Cayman Chemical Company; Acid SMase expression: catalog #SEB360Hu, USCN Life Science; ACER1 expression: catalog #CSB-EL001151HU, CUSABio; Sphingosine kinase 1 and 2 western blot: catalog #1000-6822, Cayman Chemical Company and catalog #AB37977, Abcam; ICAM-4 antibody: catalog #ABIN901654, Antibodies online; Total and phosphor-ERK1/2 western blot: catalog #9102, #9101, Cell Signaling. Western blot measurements were standardized by loading an equal volume of protein. An equal volume of blood was used for activity assays.

Lipid Extraction and Quantification

Lipids were extracted following a protocol from Shaner et al. (53) and analyzed using a Shimadzu LC-10 AD VP binary pump system coupled to a Perkin Elmer Series 200 autoinjector coupled to a 4000 quadrupole linear-ion trap (QTrap) LC-MS/MS system. Sphingolipids of various variable chain lengths (13-26) in 9 classes (**Table 4.1**) were quantified. Separate protocols were used for quantifying long chain bases (with no variable chains) and complex sphingolipids (with 13-26 long side chains). C12 and C17 sphingolipids, which are not naturally produced, were used as internal controls.

Table 4.1. Classes of sphingolipids quantified by HPLC-MS. Table 4.1 continued.

Name	Abbreviation	Class
Ceramide	Cer	Complex
Ceramide 1-phosphate	C1P	Complex
Dihydroceramide	DHCer	Complex
Dihydrosphingosine	DHSphingosine (Sa)	Long chain base

(sphinganine)		
Dihydrosphingosine 1-phosphate (sphinganine 1-phosphate)	DHS1P (SaP)	Long chain base
Glucosylceramide	GluCer	Complex
Sphingomyelin	SM	Complex
Sphingosine		Long chain base
Sphingosine 1-phosphate	S1P	Long chain base

Mathematical Modeling

Lipidomic Data

For the modeling component of our study we used the average total value of each lipid class (ceramides, sphingomyelins, etc.) in AA and SS RBC samples.

Flux Balance Analysis

The first component of our modeling strategy is to compute biologically feasible sets of steady-state fluxes for AA and SS RBC sphingolipid networks. This is accomplished through flux balance analysis which has been described extensively elsewhere (88). In short, for each metabolite in the network, a flux balance is written as follows

$$\frac{dX_i}{dt} = \sum_j s_{ij} v_j$$

where X_i is the concentration of metabolite i, s_{ij} is the stoichiometric coefficient of metabolite i in reaction j, and v_j is the flux through reaction j. This can be compactly represented in matrix form as follows

$$\frac{dX}{dt} = Sv$$

where X is the vector of the concentration of all metabolites in the network, S is the stoichiometric matrix of the network, and v is the vector of all reaction fluxes in the network. At steady-state, this reduces to

$$0 = Sv$$

In order for a set of reaction fluxes to be biologically feasible, they must not only satisfy this equation (the steady-state constraint), they must also fall within reasonable values based on experimental data. Thus, irreversible reactions should not have negative flux values which corresponds to flux in the reverse direction. Nor should they exceed a maximum rate based on experimental measurements. Thus, any feasible set of fluxes must obey the constraints

$$0 \leq v \leq vmax$$

where vmax is the vector maximum value that each flux is allowed to take. The vmax values may be different between AA and SS RBCs.

The stoichiometric matrix, S, is based on the known or supposed architecture of the network. It is know that RBCs contain the enzymes sphingosine kinase (89), sphingomyelinase (38), and alkaline ceramidase (55). There are conflicting reports in the literature as to whether RBCs contain sphingomyelin synthase and lipid phosphate phosphatases. It is also possible that RBCs contain glucosylceramidase activity. We also include ceramide kinase because of the observed high concentration of ceramide-1-phosphate though the presence of this enzyme has never been investigated in RBCs. Additionally, it is likely that all sphingolipids exhibit some degree of exchange with the plasma (90). Thus, the master stoichiometric matrix used in this model is as follows

$$S = \begin{bmatrix}
1 & 0 & -1 & 1 & 0 & 0 & 0 & 0 & 0 & 0 & 0 & 1 & 0 & 0 & 0 & 0 & 0 & 0 & 0 & 0 & -1 & 0 & 0 & 0 & 0 & 0 & 0 & 0 & 0 \\
-1 & 0 & 0 & 0 & 0 & 0 & 0 & 0 & 0 & 0 & 0 & 0 & 1 & 0 & 0 & 0 & 0 & 0 & 0 & 0 & 0 & -1 & 0 & 0 & 0 & 0 & 0 & 0 & 0 \\
0 & -1 & 0 & 0 & -1 & 1 & 0 & 0 & -1 & 1 & 1 & 0 & 0 & 1 & 0 & 0 & 0 & 0 & 0 & 0 & 0 & 0 & -1 & 0 & 0 & 0 & 0 & 0 & 0 \\
0 & 1 & 0 & 0 & 0 & 0 & -1 & 1 & 0 & 0 & 0 & 0 & 0 & 0 & 1 & 0 & 0 & 0 & 0 & 0 & 0 & 0 & 0 & -1 & 0 & 0 & 0 & 0 & 0 \\
0 & 0 & 1 & -1 & 0 & 0 & 0 & 0 & 0 & 0 & 0 & 0 & 0 & 0 & 0 & 1 & 0 & 0 & 0 & 0 & 0 & 0 & 0 & 0 & -1 & 0 & 0 & 0 & 0 \\
0 & 0 & 0 & 0 & 1 & -1 & 0 & 0 & 0 & 0 & 0 & 0 & 0 & 0 & 0 & 0 & 1 & 0 & 0 & 0 & 0 & 0 & 0 & 0 & 0 & -1 & 0 & 0 & 0 \\
0 & 0 & 0 & 0 & 0 & 0 & 1 & -1 & 0 & 0 & 0 & 0 & 0 & 0 & 0 & 0 & 0 & 1 & 0 & 0 & 0 & 0 & 0 & 0 & 0 & 0 & -1 & 0 & 0 \\
0 & 0 & 0 & 0 & 0 & 0 & 0 & 0 & 1 & -1 & 0 & 0 & 0 & 0 & 0 & 0 & 0 & 0 & 1 & 0 & 0 & 0 & 0 & 0 & 0 & 0 & 0 & -1 & 0 \\
0 & 0 & 0 & 0 & 0 & 0 & 0 & 0 & 0 & 0 & -1 & 0 & 0 & 0 & 0 & 0 & 0 & 0 & 0 & 1 & 0 & 0 & 0 & 0 & 0 & 0 & 0 & 0 & -1
\end{bmatrix}$$

The advantage of including all speculative reactions into the master stoichiometric matrix is that the effects of their presence or absence can easily be investigated by changing the vmax value for that reaction (setting vmax to a value of zero for absence) while using the same stoichiometric matrix throughout.

In order to locate solutions which satisfy both the steady-state and flux limit constraints we use a linear least-squares optimization algorithm implemented through the MATLAB program lsqlin. Because there are generally an infinite number of solutions to this problem we randomly generate a large number of initial values for each flux to initialize the algorithm in order to get a full sampling of the solution space.

Once we have sets of biologically feasible fluxes for AA and SS RBCs we move on to the second component of our modeling strategy. For this, we propose that each reaction can be represented as a power law as follows

$$v_j = \gamma_j \prod_i X_i^{f_{j,i}}$$

where v_j is the rate of reaction j, γ_j is the rate constant for reaction j, X_i is the concentration of metabolite I, and $f_{j,i}$ is the kinetic order for the effect of metabolite I on reaction j. For this model, the only metabolite affecting a reaction will be its substrate. The rate constant effectively lumps together all aspects of the system which affect the rate of the reaction that are not dependent on the concentrations of metabolites. This

includes concentration of enzymes, enzyme phosphorylation, ion concentrations, etc. Using this rate law we can separate out the influence of metabolite concentrations on reaction rates. This can be seen as follows

$$\gamma_j = \frac{v_j}{\prod_i X_i^{f_{j,i}}}$$

Thus, we can use the biologically feasible sets of fluxes from the first component of our model together with the lipidomic data to determine whether the change in a flux between AA and SS is driven by changes in substrate concentration or by a change in some other variable affecting the reaction rate.

Statistical analysis

All correlation analyses, volcano analyses and principal component analysis for sphingolipidomic data were performed on statistical analysis software. All other analyses were performed with t-tests or ANOVA at a significance level of 5% unless otherwise stated.

Results

Extensive sphingolipidomic analysis of AA/SS RBCs and MPs

Lipids were extracted from RBCs and MPs harvested from AA and SS human donors and prepared for HPLC-MS quantification of sphingolipids. Nine sphingolipid classes were quantified. Five of these sphingolipids have variable fatty acyl side chains and are referred to as complex sphingolipids: sphingomyelins, ceramides, glucosylceramides, ceramide 1-phosphates and dihydroceramides. Four of the sphingolipids do not have fatty acyl side chains and are known as long chain bases (LCBs): dihydrosphingosine, dihydrosphingosine 1-phosphate, sphingosine and sphingosine 1-phosphate. The fatty acyl-chain of the complex sphingolipids can range in

length from 13 (C13) to 26 carbons (C26) and have variable degrees of unsaturation. Within each species, we quantified the amount of each of the detectable varied chained lipids, which resulted in 86 measurements for each sample. While the distribution of lipids varied from class to class, the majority of the complex lipids were C16 or C24 in both AA and SS RBC and MP samples (**Figures 5.1 and 5.2**).

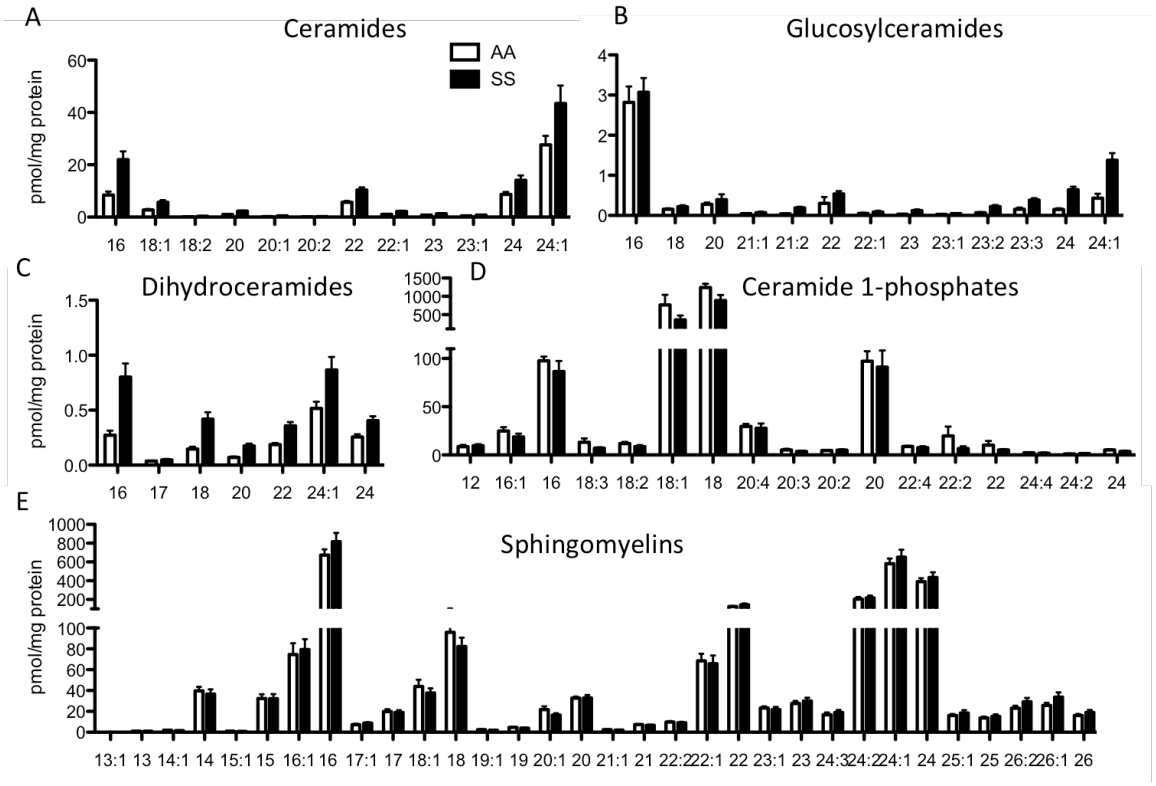

Figure 4.1 Extensive quantitative analysis of complex sphingolipids in AA and SS RBCs. Complex sphingolipids between 13 and 26 fatty acyl chain lengths were detected and quantified under the ceramide (A), glucosylceramide (B), dihydroceramide (C), ceramide 1-phosphate (D) and sphingomyelin (E) families. C16 and 24 ceramides, glucosylceramides, dihydroceramides and sphingomyelins were the most prevalent lipids while C18 C1P was the most prevalent in AA and SS RBCs.

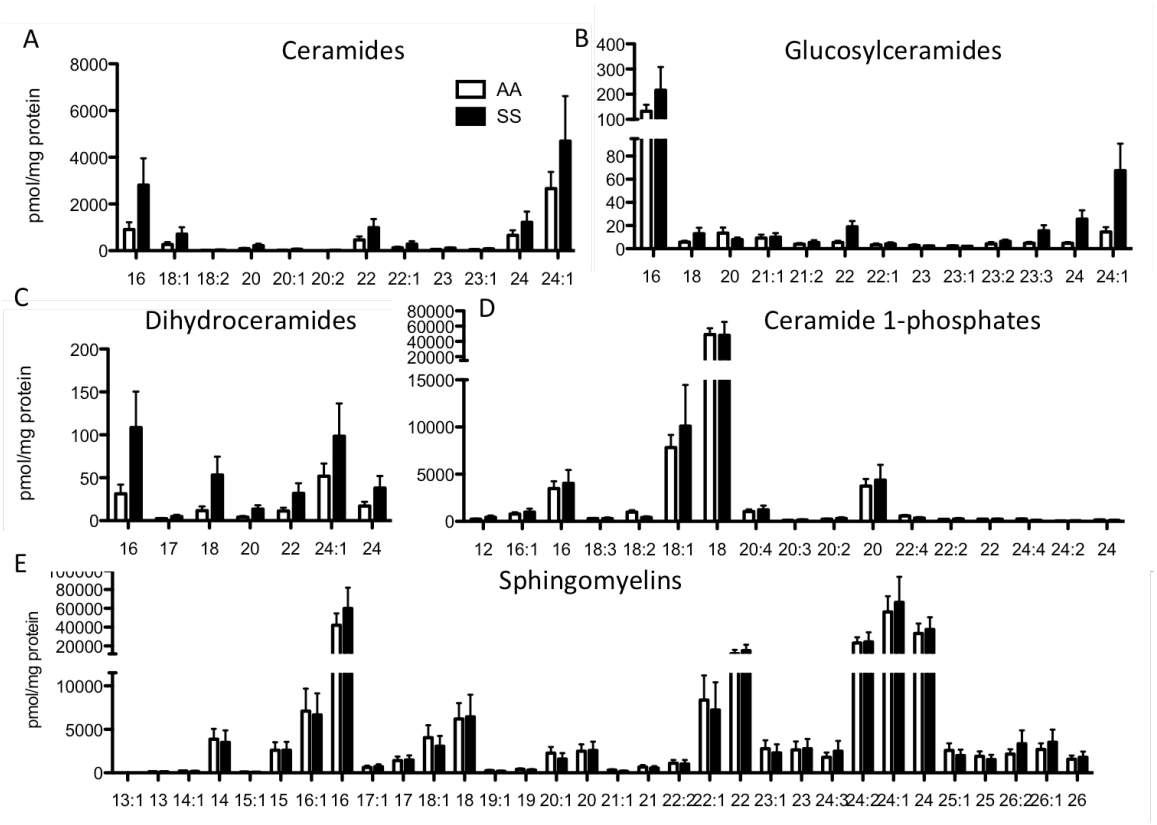

Figure 4.2 Extensive quantitative analysis of complex sphingolipids in AA and SS MPs. Complex sphingolipids between 13 and 26 fatty acyl chain lengths were detected and quantified under the ceramide (A), glucosylceramide (B), dihydroceramide (C), ceramide 1-phosphate (D) and sphingomyelin (E) families. C16 and 24 ceramides, glucosylceramides, dihydroceramides and sphingomyelins were the most prevalent lipids while C18 C1P was the most prevalent in AA and SS MPs.

Ceramides and LCBs elevated in SCD

Statistical analysis of large sphingolipid metabolome-wide data can be performed to elucidate alterations in lipid metabolism (91). We sought to use our 86 sphingolipid measurements across all samples to determine if specific lipids were significantly up- or down-regulated in SCD. These differences in lipids, if existent, may serve as potential therapeutic targets for pathological processes in SCD. To this end we employed volcano plot analysis, which visualizes the relationship connecting changes between genotypes and significance of differences in expression for all 86 lipids we quantified in each

sample. We found eight sphingolipids that were significantly different between AA and SS RBCs (**Figure 4.3**). Seven of them were increased (ceramide 16:0, ceramide 18:1, ceramide 22:0, sphingosine, sphinganine, sphingosine 1-phosphate and sphinganine 1-phosphate) while one was decreased (sphingomyelin 19:0) (**Figure 4.3B-C**).

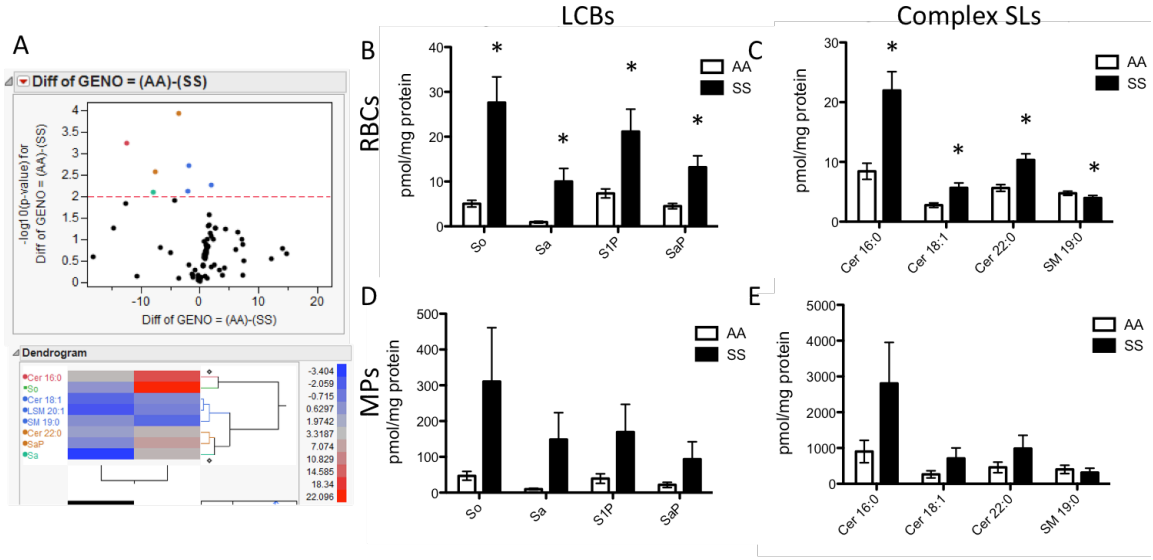

Figure 4.3 Long chain bases, ceramides and sphingomyelin significantly altered in SS RBCs and MPs. A) Volcano analysis reveals 8 sphingolipids that are significantly altered ($p < 0.05$) between AA and SS RBCs. B) LCBs (sphingosine, sphinganine, S1P and SaP) are significantly increased in SS RBCs relative to AA RBCs. C) Ceramides 16:0, 18:1 and 22:0 are significantly increased and sphingomyelin 19:0 is significantly decreased in SS RBCs, relative to AA RBCs. D) LCBs also increased in SS MPs relative to AA MPs. E) Ceramides 18:0, 18:1 and 22:0 are increased in SS MPs and SM 19:0 is decreased in SS MPs relative to AA MPs.

Interestingly, 4 of the 7 lipids that were increased in SS RBCs were the 4 LCBs (**Figure 4.3B**) and the other 3 were ceramides (**Figure 4.3C**). We have previously shown that acid sphingomyelinase, the enzyme the produces ceramides from sphingomyelin, is activated in sickle erythrocytes (83) and elevated ceramide is consistent with this result. Consistent with this observation, sphingomyelin 19:0 was the only sphingolipid significantly

reduced in SS RBCs (**Figure 4.3C**). We sought to determine if RBC-derived microparticles harbored similar changes in sphingolipid content so we looked at expression levels of these 8 lipids in MPs as well. As expected, LCBs (**Figure 4.3D**) and ceramides 16:0, 18:1 and 22:0 (**Figure 4.3E**) were significantly elevated in SS MPs relative to AA MPs and sphingomyelin 19:0 was reduced (**Figure 4.3E**).

Chain length distribution within species

Sphingolipids are known to play roles in biological processes, but much is unknown about the specific roles that distinct lipids play in biology. Recent evidence, however, has shown that sphingolipids of specific chain lengths can produce distinct biological responses (92, 93). We wished to determine if there were changes in the proportion of sphingolipids within the lipid classes between AA and SS RBCs or MPs. SS RBCs expressed roughly the same amount of sphingomyelin, increased amounts of ceramide, dihydroceramide and glucosylceramide and decreased amounts of ceramide 1-phosphate as AA RBCs (**Figure 4.4A-E**).

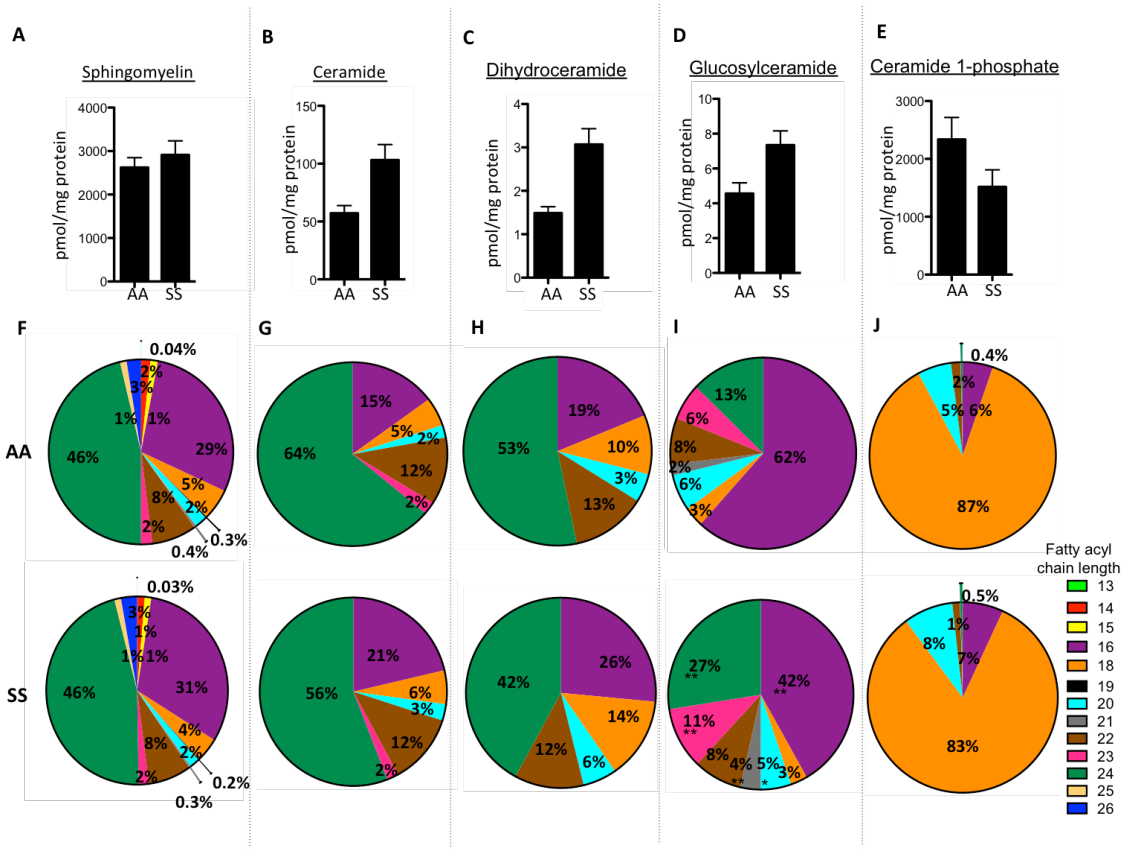

Figure 4.4 Complex sphingolipid expression and fatty acyl chain in AA and SS RBCs. A-E) Sphingomyelin (A), ceramide (B), dihydroceramide (C), glucosylceramide (D) and ceramide 1-phosphate (E) expression was quantified in AA and SS RBCs. F-J) The percentage of each fatty acyl chain (13-26) within each complex sphingolipid class for AA (top) and SS (bottom) RBCs is shown. (n=10). *p< 0.01, ** p<0.0001 measured in ANOVA relative to AA RBCs.

C16 and C24 lipids are the most abundant in AA and SS RBCs in the sphingomyelin, ceramide, dihydroceramide and glucosylceramide classes while C18, C16 and C20 lipids are the most abundant for C1P (**Figure 4.4F-J**). Interestingly, several differences emerged when we looked at the distribution of the ceramides, dihydroceramides and glucosylceramides in SS and AA RBCs. The two most abundant chain lengths in all three classes are the C16- and C24- carbons (**Figure 4.4G-I**). SS RBCs express a higher proportion of C16 ceramides and a lower proportion of C24 ceramides relative to AA

RBCs (**Figure 4.4G**). The same trend is observed with dihydroceramides in SS RBCs relative to AA RBCs (**Figure 4.4H**). These data suggest that acid SMase, which is activated in SS RBCs, may preferentially hydrolyze C16 ceramides and dihydroceramides relative to C24 sphingolipids. Interestingly, the opposite trend was observed with glucosylceramides. C24 glucosylceramides are increased and C16 glucosylceramides are decreased in SS RBCs relative to AA RBCs (**Figure 4.4D**).

SS MPs showed very similar trends. SS MPs expressed roughly the same amount of sphingomyelin and C1P and increased amounts of ceramide, dihydroceramide and glucosylceramide and decreased amounts of ceramide 1-phosphate as AA RBCs (**Figure 4.5A-E**).

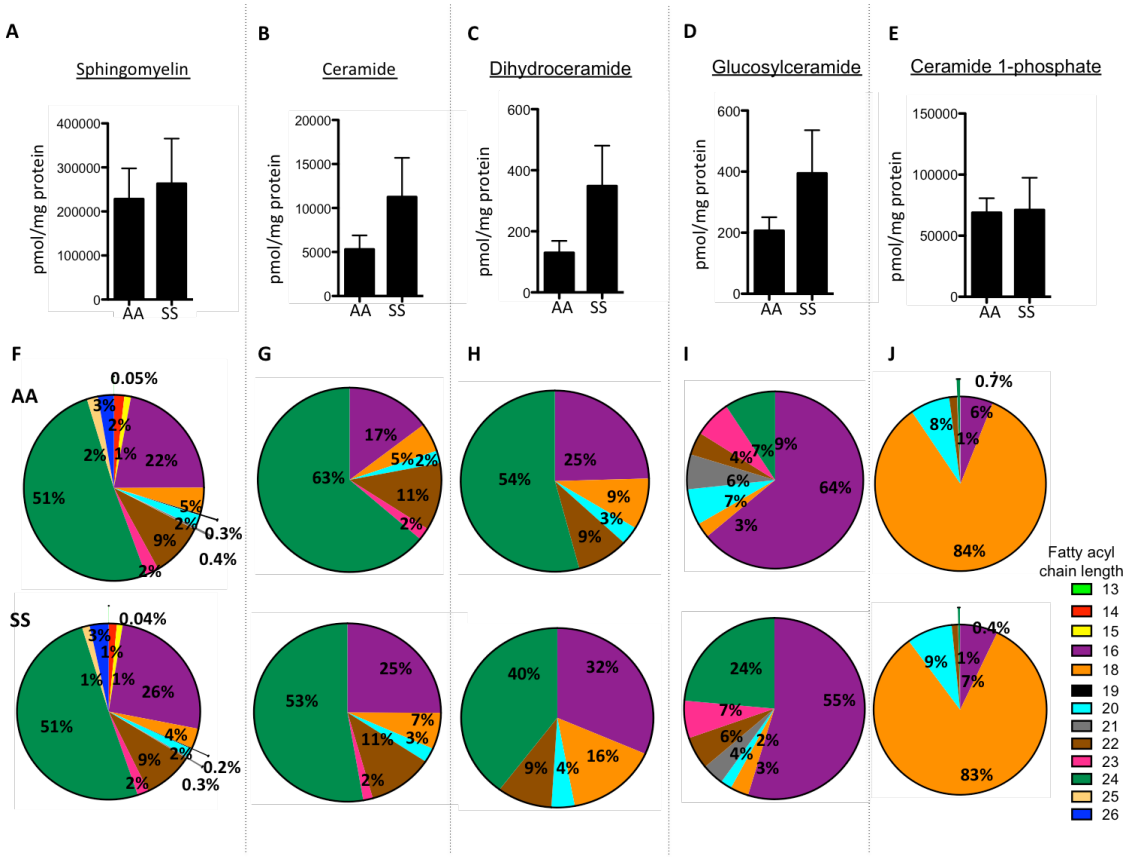

Figure 4.5 Complex sphingolipid expression and fatty acyl chain in AA and SS MPs. A-E) Sphingomyelin (A), ceramide (B), dihydroceramide (C), glucosylceramide (D) and

ceramide 1-phosphate (E) expression was quantified in AA and SS MPs. F-J) The percentage of each fatty acyl chain (13-26) within each complex sphingolipid class for AA (top) and SS (bottom) MPs is shown. (n=10). *p< 0.01, ** p<0.0001 measured in ANOVA relative to AA MPs.

As with RBCs, C16 and C24 lipids are the most abundant in AA and SS MPs in the sphingomyelin, ceramide, dihydroceramide and glucosylceramide classes while C18, C16 and C20 lipids are the most abundant for C1P (**Figure 4.5F-J**). The two most abundant chain lengths in ceramides, dihydroceramides and glucosylceramides are the C16- and C24- carbons (**Figure 4.5G-I**). SS MPs express a higher proportion of C16 ceramides and a lower proportion of C24 ceramides relative to AA MPs (**Figure 4.5G)**. The same trend is observed with dihydroceramides in SS MPs relative to AA MPs (**Figure 4.5H**). As with SS RBCs, opposite trend was observed with glucosylceramides in MPs. C24 glucosylceramides are increased and C16 glucosylceramides are decreased in SS MPs relative to AA MPs (**Figure 4.5D**).

Changes in total lipid class in SS RBCs and MPs

In addition to exploring differences in unique lipids between AA and SS RBCs and MPs, we wished to determine if specific classes of lipids were altered in SCD. All of the lipids within each class of lipids (sphingomyelin, ceramide, dihydroceramide, ceramide 1-phosphate, glucosylceramide, sphingosine, sphinganine, sphingosine 1-phosphate and sphinganine 1-phosphate) were summed for each of the four types of samples measured and averaged across the sample set. When all of these lipids, normalized to protein content, are summed together, we get an idea of the total amount of lipid in the RBCs or MPs. The total concentration of sphingolipids (pmol/mg protein)

was reduced in SS RBCs (4615.7pmol/mg protein) relative to AA RBCs (5031.11 pmol/mg protein) (**Figure 4.6A**).

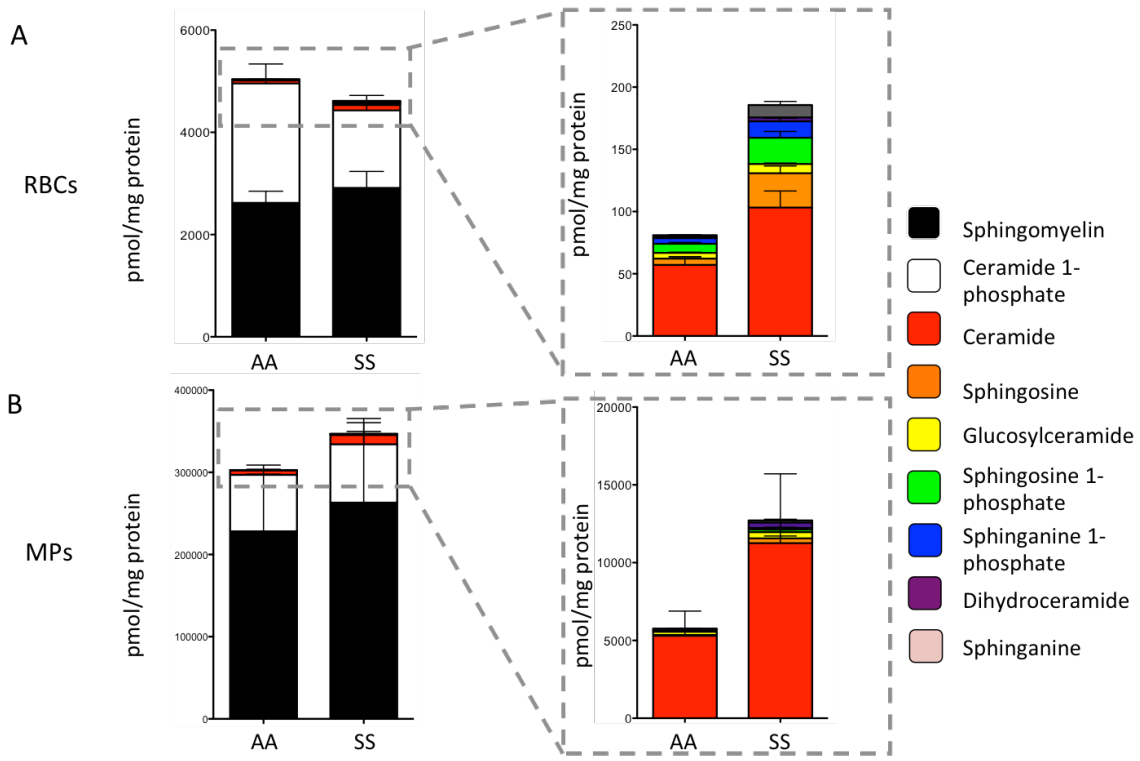

Figure 4.6 Sphingolipid concentration is reduced in SS RBCs, increased in SS MPs and AA/SS donors express different proportions of sphingolipids. A-B) The total concentration (pmol sphingolipids per mg protein) of sphingolipids is reduced in SS RBCs (A) and increased in SS MPs (B). Sphingomyelin is the most abundant lipid in both RBCs and MPs, followed by C1P, which is decreased in SS RBCs (A), and ceramide, which is increased in SS RBCs and MPs (A-B). There is about a 60-fold increase in lipid concentration of MPs relative to RBCs. The distribution of less abundant sphingolipids (ceramide, sphingosine, glucosylceramide, S1P, SaP, dihydroceramide and sphinganine) is also altered between AA and SS RBCs and MPs (A-B).

Consistent with this observation, the sphingolipid concentration in SS MPs (346853.1 pmol/mg protein) was elevated relative to AA MPs (302270 pmol/ mg protein) (**Figure 4.6B**). This supports the finding, from Allan et al., that sickled RBCs lose their membrane lipid content to microparticles (39). More interestingly, however, we also

observed differences in the proportion of sphingolipid classes in RBCs and MPs. Specifically, SS RBCs expressed less C1P, more ceramide and more LCBs than AA RBCs and SS MPs expressed more ceramide and more LCBs than AA MPs (**Figure 4.6**).

Modeling approach

To develop a mathematical model of sphingolipid metabolism we relied on flux balance analysis. A metabolic network can be created by outlining the reaction fluxes (arrows) through metabolites (letters) (**Figure 4.7A**).

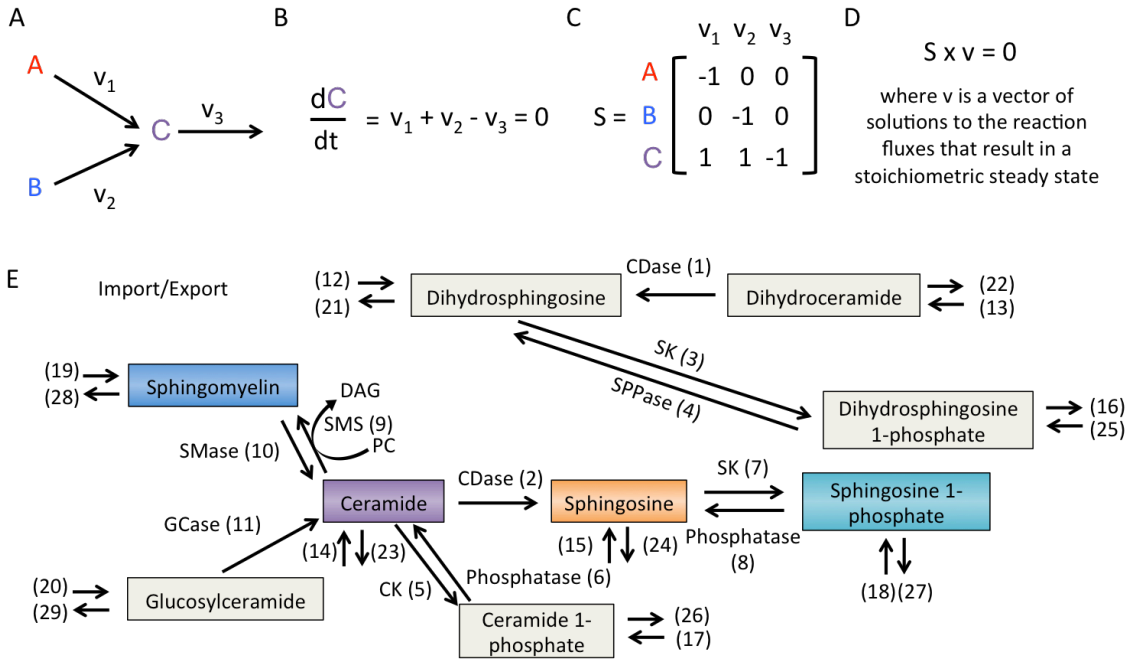

Figure 4.7 Modeling approach to elucidating enzyme/transport flux in RBCs. A) Schematic showing how molecular species can be represented by the reactions that create and consume them. B) At steady state, consistent with conservation of mass, the summation of these fluxes must be zero. C) A stoichiometric matrix (S) can be created based on the network architecture to define the bounds of the reactions. D) Solving this matrix for the reaction fluxes, v_i, gives flux for each reaction in the network. E) Simplified sphingolipid metabolism network including import and export processes (arrows).

At steady state, the time derivative of all of the metabolites must be zero (**Figure 4.7B**). A stoichiometric matrix (S) can be generated to define the architecture of the metabolic network including all reactions, reactants and fluxes (**Figure 4.7C**). This matrix can be solved for the reaction fluxes to determine the relative amounts of flow through each reaction (**Figure 4.7D**). These reaction fluxes are constrained on the low end by zero because flux cannot be negative and on the high end by biologically reasonable values for RBC sphingolipid transport which were experimentally measured. Ultimately, these fluxes can be used to calculate the reaction rate constants, or activity, of the enzymes/transport processes based on metabolite concentrations. By comparing changes in reaction and transport flux and reaction constants between AA and SS RBCs we can predict reactions that may be dysregulated in SCD.

Modeling Results

A metabolic model of sphingolipid metabolism accounting for enzymatic and transport flux between sphingolipid metabolites measured in RBCs contains 29 distinct reactions. (**Figure 4.7E**). Eleven of these reactions represent enzymatic flux between metabolites while the other 18 represent import (9) and export (9) of the metabolites from the RBC. Modification of enzymatic and transport parameters between AA and SS RBCs based on experimentally measured changes allows the model to predict biologically feasible reaction fluxes for all of these processes between AA and SS RBCs.

Table 4.2. Simulated sphingolipid reaction flux in AA and SS RBCs. 29 biologically accurate sphingolipid reaction fluxes (column 1) were computed for AA and SS RBCs. Column 2 describes the metabolites involved in the reaction. Column 3 lists the enzymes controlling the reaction. Columns 4 and 5 list the flux of metabolites through the reaction for AA and SS RBCs, respectively. Column 6 lists the fold change (SS flux over AA flux) for all 29 reactions. *, reactions that were altered more than 2-fold between AA and SS RBCs. Sa: sphinganine, DHC: dihydroceramide, So: sphingosine, Cer: ceramide, SaP: sphinganine 1-phosphate, C1P: ceramide 1-phosphate, S1P: sphingosine 1-phosphate,

SM: sphingomyelin, GCer: Glucosylceramide, (L): Long chain base (LCB), (C): Complex sphingolipid. Table 4.2 continued.

Rxn #	Description	Enzyme	AA RBC (pmol/min/ mg protein)	SS RBC (pmol/min/mg protein)	SS/AA flux
1	Sa from DHC	Ceramidase	0.65	0.22	0.34*
2	So from Cer	Ceramidase	4.17	0.49	0.12*
3	SaP from Sa	Sphingosine Kinase	1.32	3.60	2.73*
4	Sa from SaP	Phosphatase	0.95	0.94	0.99
5	C1P from Cer	Ceramide Kinase	34.52	44.29	1.28
6	Cer from C1P	Phosphatase	0.98	0.99	1.01
7	S1P from So	Sphingosine Kinase	2.89	3.70	1.28
8	So from S1P	Phosphatase	0.21	0.10	0.46*
9	SM from Cer	Sphingomyelin Synthase	184.29	195.27	1.06
10	Cer from SM	Sphingomyelinase	220.73	242.73	1.10
11	Cer from GCer	Glucosylceramidase	5.68	2.07	0.37*
12	Sa import (L)	na	19.81	20.90	1.06
13	DHC import (C)	na	0.10	0.10	0.99
14	Cer import (C)	na	0.10	0.10	1.00
15	So import (L)	na	65.74	66.00	1.00
16	SaP import (L)	na	20.96	21.00	1.00
17	C1P import (C)	na	0.08	0.06	0.76
18	S1P import (L)	na	65.93	66.00	1.00
19	SM import (C)	na	44.79	44.88	1.00
20	GCer import (C)	na	0.55	0.55	1.00
21	Sa export (L)	na	22.69	18.34	0.81
22	DHC export (C)	na	0.18	0.01	0.03*
23	Cer export (C)	na	0.21	0.40	1.85
24	So export (L)	na	115.47	198.62	1.72
25	SaP export (L)	na	20.65	23.64	1.14
26	C1P export (C)	na	33.47	43.83	1.31
27	S1P export (L)	na	668.21	931.66	1.39
28	SM export (C)	na	21.91	4.45	0.20*
29	GCer export (C)	na	0.25	0.04	0.16*

Transport (import/export) flux of LCBs, which have one hydrophobic carbon chain, which would allow for relatively fast transport across the cell membrane, is much faster than enzymatic flux (**Table 4.2, (L)**). Import and export of sphingosine, sphinganine, SaP and S1P were between 19.81 (AA RBC sphinganine import) and 931.66 pmol/min/mg

protein (SS RBC S1P export) while the enzymatic fluxes producing these species were between 0.22 (SS RBC sphinganine production from dihydroceramide) and 4.17 pmol/min/mg protein (AA RBC sphingosine production from ceramide) (**Table 4.2**). Complex sphingolipids, conversely, which have two hydrophobic carbon chains, have much higher enzymatic fluxes than transport fluxes. Enzymatic flux producing complex sphingolipids are as high as 242.73 pmol/min/mg protein (SS RBC ceramide from sphingomyelin) while transport fluxes are limited to 44.88 pmol/min/mg protein (SS RBC sphingomyelin import) (**Table 4.2**). Of the 29 reactions assessed eight were altered by more than two fold between AA and SS RBCs. Sphinganine production from dihydroceramide (ceramidase), sphingosine production from ceramide (ceramidase), sphingosine production from S1P (phosphatase), ceramide production from glucosylceramide (glucosylceramidase), dihydroceramide export, sphingomyelin export and glucosylceramide export were all decreased by more than 2-fold while sphinganine 1-phosphate production from sphinganine (sphingosine kinase) was increased by more than 2-fold (**Table 4.2**). Importantly, alterations in reactions with relatively smaller fluxes (rate limiting reactions) seem to dominate changes observed between AA and SS RBCs. Acid sphingomyelinase, for example, which is activated in SS RBCs controls the formation of ceramide from sphingomyelin (83). The model predicts, however, that flux through this reaction is not altered significantly in SS RBCs. This is likely because its speed is determined by the downstream speed of other reactions (i.e. sphingosine kinase-mediated production of S1P from sphingosine). These results suggest that reactions with smaller fluxes (rate limiting steps) are the best therapeutic targets for modulating sphingolipid metabolism in SCD given their control of the metabolic speed.

Discussion

In this work we show, for the first time, that sphingolipid metabolism is significantly dysregulated in SCD. While many groups have studied the asymmetry of phospholipids in SCD (94, 95) few have thoroughly studied the expression, metabolism and orientation of sphingolipids in the context of SCD. Sphingolipids are an important component of RBC membranes and have been shown to regulate many biological processes. These lipids are also present in RBC-derived microparticles, which are known to be elevated in SCD. The production of these inflammatory MPs is known to contribute to much of the pathology of SCD. By using systems biology and modeling approaches, we can learn valuable information about disease from information collected from donor samples. In this work, HPLC-MS was used to quantify 86 distinct sphingolipid species from AA and SS RBCs and their MP byproducts. We show, for the first time, the distribution of an extensive panel of membrane-derived sphingolipids in RBCs and MPs derived from AA and SS individuals. Specifically, not only had a thorough sphingolipid characterization across classes never been performed on RBCs, the differences present in the sickle cell disease state had also never been interrogated. These results elucidated two distinct sphingolipidomic states between AA and SS RBCs and MPs that may contribute to the disease pathology.

In this work we quantified complex and long chain bases existent in RBCs and found that, by in large, most lipids were present at about the same level in AA and SS RBCs (**Figure 4.1**). In MPs, which can be a product of sphingolipid metabolism (83), we found that the distribution of sphingolipids between AA and SS donors was also roughly the same (**Figure 4.2**).

To determine whether any lipids were significantly altered in SCD from our data set we performed a volcano analyses on all 86 sphingolipids to identify any lipids that were significantly elevated or reduced in SS RBCs. This analysis revealed 8 lipids that were significantly altered in SS RBCs and MPs. Four of them (sphingosine, sphinganine, sphingosine 1-phosphate and sphinganine 1-phosphate) (**Figure 4.3B,D**) are long chain bases, some of which have been shown to have bioactivity. Sphingosine 1-phosphate is the most widely recognized bioactive sphingolipid. It is stored at high concentrations in RBCs and is a ligand for 5 known G-protein coupled receptors ($S1P_1$-$S1P_5$) (5). In our previous work we showed that inflammatory cells respond differentially to $S1P_3$ activation and contribute to microvascular remodeling and inflammation (96). Given that these bioactive lipids are significantly increased in SS RBCs and MPs, their consequences on cellular processes and inflammation in SCD should be thoroughly evaluated. Of the other 4 lipids, the 3 increased lipids were ceramides and the 1 decreased lipid was a sphingomyelin in SS RBCs and MPs, consistent with our previous observation that sphingomyelinase activity is increased in SS RBCs (83). RBC-derived microparticles have been shown to contribute to vasculopathy (97) and inflammation (41) in SCD, and the contribution of these particular lipids to these phenomena should be explored moving forward.

In recent years, evidence supporting unique roles of distinct chain-length sphingolipids is growing. Grosch et al. provided a comprehensive review of how many specific ceramides contribute to apoptosis, inflammation, cancer autophagy and Alzheimer's (98). Osawa et al. discovered that C16 ceramide regulates hepatocyte apoptosis in a TNF- mediated fashion (92) and Seumois et al. discovered that C16- and

C24-ceramide production results in spontaneous neutrophil apoptosis (93). To determine whether SS RBCs or MPs expressed a different distribution of complex chain lengths, we summed the C13-C26 complex lipids across species and compared the distribution of different fatty acyl length lipids between AA and SS RBCs and MPs. While there were few differences in the distribution of most lipids (**Figures 5.4 and 5.5**), the ceramide species seemed to have the most altered states in SCD. We found that the levels of C16- and C24- ceramides were altered in SS RBCs and MPs, relative to AA samples. SS RBCs and MPs expressed more C16- ceramides and dihydroceramides and a less C24- ceramides and dihydroceramides than AA RBCs and MPs (**Figure 4.4B-C and 5.5B-C**). These data suggest that SMase, which is activated in SS RBCs, may preferentially hydrolyze C16 ceramides and dihydroceramides relative to C24 sphingolipids. Interestingly, C24 glucosylceramides were increased, and C16 glucosylceramides were decreased, in SS RBCs and MPs relative to AA RBCs and MPs (**Figure 4.4D and 5.5D**). More extensive studies need to be performed to fully understand the mechanism behind this shift in the balance of distinct chain length ceramides as well as the functional consequences of this shift in the context of SCD.

We next looked at changes in the proportion of total lipid families. The concentration of sphingolipids was reduced in SS RBCs relative to AA RBCs (**Figure 4.7A**). The exit pathway in sphingolipid metabolism is the degradation of sphingosine 1-phosphate to yield ethanolamine phosphate and hexedecanal, or sphinganine 1-phosphate to yield hexadecanal, by S1P lyase. As S1P lyase is not active in RBCs (99) we reasoned that some form of sphingolipid export was occurring in SS RBCs. We, and others, have shown that SS RBCs produce membrane-derived microparticles which can be released

into circulation and contribute to vascular pathology (83, 100, 101). In fact, 2-3% of their lipid content is lost to membrane-derived spicules and microparticles due to RBC sickling (39). To this end, we examined RBC-derived microparticles from AA and SS donors and found that sphingolipid content was increased by roughly 15% in SS particles (**Figure 4.7B**). Our recent work showed that acid sphingomyelinase, which hydrolyzes sphingomyelin, the most abundant sphingolipid in plasma membranes, to ceramide, is activated in sickle RBCs and contributes to MP production (83). Consistent with this observation, we found that SS RBCs and MPs contained significantly more ceramide species than AA RBCs and MPs. Interestingly, ceramide has been shown to induce the budding of exosomes to form multivesicular endosomes in a mouse cell line (8). Further studies need to be performed to examine the role of ceramide in RBC vesicle formation, fusion and trafficking. Ceramide is also at the hub of sphingolipid metabolism and is the precursors for many sphingolipid species. The long chain bases are produced when ceramide and dihydroceramide are cleaved by ceramidase. Our previous work showed that ceramidase is secreted into the plasma in SCD and sphingosine is significantly increased in SS RBCs and MPs which is consistent with these findings (83). C1P was reduced in SS RBCs and bioactive long chain bases (sphingosine, sphinganine, S1P and sphinganine 1-phosphate) were also found to be significantly increased in SS RBCs and MPs (**Figure 4.7**).

While these findings are interesting, they only tell us about the distribution of sphingolipids at steady state and nothing about the reactions, or enzymes, that produce them. Mathematical models have been used to predict changes in reaction flux between metabolites in sphingolipid metabolism (86, 87). We used a similar approach to model

sphingolipid metabolism in AA and SS RBCs. Using experimentally measured enzymatic and transport fluxes, or relative changes between AA and SS RBCs, we constrained the model to produce biologically feasible fluxes for 29 reactions that are present in sphingolipid metabolism. Interestingly, transport (import and export) flux was much larger than enzymatic flux for AA and SS LCBs (**Table 4.2, (L)**). This is likely due to their smaller hydrophobic domain and relatively larger water solubility than complex sphingolipids. Conversely, enzymatic fluxes were larger than transport fluxes for complex sphingolipids (**Table 4.2, (C)**). Our model simulation revealed 7 fluxes, of 29 total, which are altered by more than two fold between AA and SS RBCs. These fluxes suggest that ceramidase, phosphatase and glucosylceramidase activity may be decreased in SS RBCs (**Table 4.2**) but these enzyme activities should be measured experimentally. Additionally, the export of dihydroceramide, sphingomyelin and glucosylceramide were reduced. It will be interesting to see if these lipids occur at smaller concentrations in SS plasma and the biological consequences of their altered expression. The one enzymatic flux that was increased more than 2-fold was sphinganine 1-phosphate production from sphinganine, which is mediated by sphingosine kinase. This is consistent with reports that sphingosine kinase is activated in SS RBCs (89). Interestingly, the model predicts that flux through sphingomyelinase (which is elevated in SS RBCs (83)) is not altered significantly in SS RBCs. This is likely because its speed is determined by the downstream speed of other reactions (i.e. sphingosine kinase-mediated production of S1P from sphingosine – which has a much smaller flux). These results suggest that reactions with smaller fluxes (rate limiting steps) are the best therapeutic targets for modulating sphingolipid metabolism in SCD given their control of the metabolic speed. Directly

inhibiting sphingosine kinase activity, instead of sphingomyelinase, for example might have a much larger effect on the bioactive S1P expression in SCD. This work reveals for the first time that sphingolipid metabolism is significantly dysregulated in SCD, leading to altered balance of specific lipids, specific fatty acyl chain lengths and specific reactions modulated by enzymes. Additionally, this work may elucidate many sphingolipid molecules and metabolizing-enzymes that can be used as effective therapeutic targets in SCD.

CHAPTER 5

FUTURE CONSIDERATIONS

Background

Sickle cell disease is a hereditary genetic blood disorder caused by a point mutation in the gene encoding for hemoglobin. This mutation causes hemoglobin molecules to polymerize during de-oxygenation of erythrocytes leading to rod-shaped polymers that bend and distort the red blood cell membrane, making it more rigid and "sickled". This sickling causes RBC to lose their flexibility and become trapped in small capillaries and arteries. This vaso-occlusion has the potential to cut off blood supply to downstream tissues and is often associated with pain but can also lead to many complications such as chronic inflammation, ischemia, peripheral artery disease, stroke, myocardial infarction and even death. Reorganization of the RBC membrane due to sickling has been explored in the context of phospholipids, which are significant components in the RBC membrane. Phosphatidyl serine, in particular, is translocated from the inner to the outer leaflet of RBCs and serves as a sign for clearance. Sphingolipids, which are also integral components of RBC membranes, can be bioactive signaling molecules but their orientation and metabolism in RBCs during SCD has not been studied extensively. By exploring the orientation and metabolism of sphingolipids in SCD, and their consequences in the disease state, we may be able to develop more effective therapies to treat the disease.

Erk1/2 signaling in SS RBCs and MPs

Sickle cell disease and systemic inflammation go hand in hand. Sickle RBCs can activate a variety of cell types including platelets, smooth muscle cells, endothelial cells

monocytes, macrophages and neutrophils through direct interaction, adhesion or molecule-mediated stimulation (14, 51). Numerous studies have shown the relationship between sickle RBCs and inflammatory cells (51, 68). Erk phosphorylation in sickle RBCs has been shown to activate ICAM-4 and lead to monocyte and endothelial cell adhesion (37, 61). Zennadi et al. showed that sickle RBCs signaled through Erk1/2 to promote RBC adhesion and activation but the idea that their microparticle byproducts could also signal, independent of the RBCs, is a novel one. An interesting insight from this chapter was the discovery that RBC-derived MPs from SS RBCs contained constitutively activated Erk1/2. Interestingly, Erk1/2 has been shown to be activated downstream of $S1P_1$ activation. In ongoing studies, we are measuring the expression of $S1P_1$ on RBCs and MPs from people living with or without sickle cell disease. As S1P is significantly elevated in both SS RBCs and MPs, relative to AA particles, it is possible that the Erk1/2 activation observed in SS RBCs and MPs is mediated by S1P. Our work shows, for the first time, that SS RBC-derived MPs also have constitutively active Erk and may potentially use this signaling cascade to activate monocytes in a fashion similar to RBCs. It will be interesting to see if MPs can also modulate their expression and activation of membrane-bound proteins like ICAM-4 in a fashion similar to SS RBCs. The location of Erk in SS RBCs and MPs will also be important to look at in the future. It will be interesting to see if the membrane localization of Erk in RBCs or MPs permits it to respond to biophysical changes produced in SS membranes.

Microparticle sources in SCD

Sphingolipids have been shown to play roles in lipid raft formation and membrane vesiculation (7). Interestingly, the production of ceramide caused the production of

membrane-derived micro-vessels and the loss of the biconcave discoid shape of red blood cells (7, 8). Furthermore, both hypotonic and hypertonic forces in RBCs activate neutral sphingomyelinase, the enzyme that mediates the conversion of sphingomyelin to ceramide in RBCs (38). The pro-inflammatory interaction of RBC-derived microparticles with monocytes in sickle cell combined with the role of sphingolipids in microparticle production creates a particularly interesting area of exploration rooted in sphingolipid metabolism and inflammation. However, microparticles from multiple cell sources have been shown to play significant roles in systemic inflammation in SCD. RBCs, platelets and other cells have been shown to produce these membrane-bound particles when activated which can activate other cells in circulation (41-45, 47). While this work focused on RBC-derived MPs there is much room for exploration into the roles of MPs from other cell types in SCD. Platelets in particular have been shown to contribute to vascular pathology in vaso-occlusion in SCD (40). Platelets, which also contain bioactive lipids, may also harbor sphingolipid dysregulations similar to those discovered in RBCs and their interrogation deserved attention.

Sphingolipid modulation of monocyte phenotype

In Appendix A of this work show how local polymeric delivery of S1P receptor compounds can be immunomodulatory and, specifically, recruit regenerative cells, which lead to enhanced vascular remodeling. Our results demonstrate that $S1P_3$ activation in remodeling tissues can preferentially recruit anti-inflammatory monocytes, which contribute to wound healing and microvascular remodeling. The major contribution of this work is the discovery that S1P receptor agonists can be used in polymeric scaffolds to preferentially recruit subsets of inflammatory cells. Others have explored the role of

sphingolipids in immunomodulation but it remains to be discovered whether these lipids can directly differentiate and polarize monocytes (102). It will be very valuable to perform systematic experiments using unique sphingolipids at varying doses and time periods *in vitro* to assess changes to monocyte phenotype. In the context of sickle cell, it will be interesting to assess whether the sphingolipids found to be significantly altered in this work also promoted monocyte/macrophage phenotype transition. To this end, we have begun experiments to perform single cell transcriptional analysis for all of the sphingolipid metabolizing enzymes as well as pro- and anti-inflammatory markers, cytokines, integrins, cathepsins and matrix metalloproteases (see Appendix B) on primary-isolated peripheral blood mono-nuclear cells from people living with and without sickle cell disease. Preliminary results have shown differences in the mRNA content of both sphingolipid metabolizing enzymes and markers of inflammation in AA and SS PBMCs. By correlating changes in sphingolipid metabolizing enzyme production with changes in markers of monocyte transition, we may be able to determine which lipids, if any, promote phenotype changes in monocytes and ultimately inflammation in SCD. Additionally, genome-wide exploration of distinct phenotypes of inflammatory cells in people living with and without SCD may provide more valuable information regarding the sphingolipid changes in distinct inflammatory states.

Our work also shows, for the first time, that RBC-derived MPs are internalized by monocytes and macrophages and elicit biological responses. Monocyte adhesion as well as macrophage cytokine production/secretion and enzyme expression are altered upon SS MP internalization. Preliminary work is also showing increased expression of cathepsins, which contribute to vascular inflammation in SCD, in SS MP-treated macrophages. As

monocytes are known to exist in at least two distinct phenotypes, it will be interesting to explore what distinct phenotypes internalize circulating MPs in vivo. Anti-inflammatory, or patrolling, monocytes that contribute to wound healing and neovascularization or inflammatory monocytes that respond to infection and inflammation may respond very differently to MP internalization and this should be explored.

Amitriptyline in acid sphingomyelinase inhibition

In chapter 3 of this work I describe results showing that acid sphingomyelinase is activated in sickle RBCs, leading to microparticle production and downstream activation of monocytes and macrophages. Blood collected from people with SCD revealed consistent elevation in acid SMase in RBCs consistent with increases in ceramide, sphingosine and S1P in whole blood, plasma, RBCs and MPs from people living with SCD. I also show that inhibition of acid sphingomyelinase with a tricyclic antidepressant, amitriptyline, significantly reduces acid SMase activity, MP production and systemic inflammation both *in vitro* and in mouse models of SCD. A limitation of this work, however, is the sole us of amitriptyline as a SMase inhibitor. The mechanism by which amitriptyline inhibits SMase is indirect. Amitriptyline inserts into the inner leaflet of the RBC membrane and subsequently cases acid sphingomyelinase to detach: functionally inhibiting its activity. Amitriptyline, therefore, is not specific to acid SMase and also has other targets (i.e. NO and PGE2). Indeed, the drug may act on acid lipase, phospholipase A and C and other sphingolipid hydrolases by a similar mechanism. Furthermore, amitriptyline, as a tricyclic antidepressant, inhibits the uptake of adrenaline, dopamine, and serotonin and affects the cholinergic and histaminergic systems (67). These studies should be repeated with a putative acid SMase inhibitor or with genetic knockdown to

demonstrate whether a more selective pharmacological inhibition of SMase is effective in reducing the generation of RBC MPs in SCD. Becker et al. began to systematically explore other acid SMase inhibitors for cystic fibrosis but many of these compounds work through the same mechanism (2, 67).

C1P and complex sphingolipid expression in erythrocytes

Another interesting observation from chapter 4 was the abundance of ceramide 1-phosphayte (C1P) in both AA and SS RBCs. While it has been shown that S1P is present in abundance in RBCs, no studies to date, have measured the amount of C1P in RBCs and it was not expected to be present at such a high concentration. Measuring individual enzymes is a much more difficult task than measuring their sphingolipid products, but it will be interesting to measure the enzymes that regulate C1P production (i.e. ceramide kinase and ceramide phosphatase). C1P has also been shown to be a stem cell chemoattractant, along with S1P, so measuring the respective affects of these lipids on other cells may be particularly valuable in cell mobilization and homing. In addition to C1P abundance, the balance of C16- and C24- ceramides in SCD was particularly interesting. SS RBCs and MPs shifted towards a higher proportion of C16 ceramides and a lower proportion of C24 ceramides relative to AA RBCs and MPs. The same trend was observed with dihydroceramides in SS RBCs and MPs relative to AA RBCs and MPs. In future studies, it will be valuable to explore whether acid SMase, which is elevated in SS RBCs, preferentially hydrolyzes C16 ceramides and dihydroceramides relative to C24 sphingolipids. Additionally, the role of these distinct sphingolipids in the context of SCD will be very interesting to explore. Specifically, *in vitro* experiments should be performed

to explore the role of C16 and C24 ceramides on monocyte adhesion, cytokine production and phenotype transition.

Sphingolipid modeling for disease

For the past several decades, the "-omics" movement has dominated much of the exploration around human diseases and disorders (75, 76). Researchers are taking a much more bottom-up approach to elucidate genetic and molecular targets for therapy. In chapter 4, it is shown that high performance liquid chromatography analysis of all sphingolipids in biological samples can elucidate distinct sphingolipidomic differences between AA and SS samples. Specifically, we show that long chain bases (sphingosine, S1P, dihydrosphingosine and dihydrosphingosine 1-phosphate) and ceramide species are significantly elevated in SS RBCs and MPs relative to AA RBCs and MPs. By generating large sets of data measuring steady state or dynamic levels of sphingolipids we can apply systems biology and statistical analysis approaches to glean metabolic changes that may result in dysregulated balances of sphingolipids, which contribute to inflammation in SCD. While describing these changes is valuable and may elucidate potential biomarkers or therapeutic targets, it is much more powerful to be able to model these changes and build predictive tools based on lipid/enzyme concentrations. All of the work presented in chapter 4 was taken from 'steady state' samples. Donors were not taking any medications for SCD treatment and had not been hospitalized recently. In ongoing efforts, however, we are taking dynamic measurements of sphingolipid content in AA and SS RBCs and MPs to get a better picture of how these lipids change over time. This information will allow us to build flux-based models that elucidate specific reactions, in the metabolic pathway, that may dominate the changes observed at the steady state.

In this work, we used extensive sphingolipidomic quantification of AA and SS RBCs and experimental measurements of enzyme activity and transport flux to mathematically model AA and SS RBC sphingolipid metabolism. The simulation predicts relatively fast import/export for LCBs and enzymatic flux for complex sphingolipids as well as 7 significantly altered fluxes. Importantly, the model elucidates rate-limiting reactions that have relatively slower speeds and would serve as effective therapeutic targets. This work targeted acid sphingomyelinase, which is significantly activated in SS RBCs, to modulate sphingolipid metabolism and MP production. According to the model, however, the maximum flux through this reaction is much faster than other reactions in the metabolic network. Enzymes mediating slower reactions (rate limiting enzymes) may be much better therapeutic targets because of their greater impact on sphingolipid flux. Models like this can be particularly valuable in understanding how enzymatic/transport changes in SS RBCs contributes to the observed dysregulation in sphingolipid metabolism.

Conclusion

In conclusion, this dissertation shows for the first time that sphingolipid metabolism is dysregulated in sickle cell disease and that this dysregulation contributes to vascular inflammation in the disease state. This work shows that membrane stresses in sickle RBCs activate acid sphingomyelinase, a membrane bound enzyme that hydrolyzes sphingomyelin, the most abundant plasma membrane sphingolipid, to ceramide. Other metabolic changes in SCD lead to the production of sphingosine and sphingosine 1-phosphate, which are also elevated in SCD. Additionally, these lipid alterations enhance the production of RBC-derived microparticles, which are released into circulation and

activate monocytes and macrophages, enhancing pro-inflammatory cytokine production and endothelial adhesion. S1P receptor-specific compounds can be used to preferentially modulate the recruitment of distinct monocyte phenotypes to vasculature, which may be useful for regenerative strategies in SCD. Acid SMase inhibition, with amitriptyline, reduced RBC microparticle production and subsequent inflammation *in vitro* and in mouse models of sickle cell disease. Finally, systems biology approaches elucidate many distinct sphingolipids that were altered in SS RBCs and MPs and may be useful biomarkers or therapeutic targets. It will be very interesting to see how these pharmacological strategies pan out in humans and in other hemolytic anemias and whether the lipidomic alterations described here can be used as new pharmacological targets for treating complications of sickle cell disease.

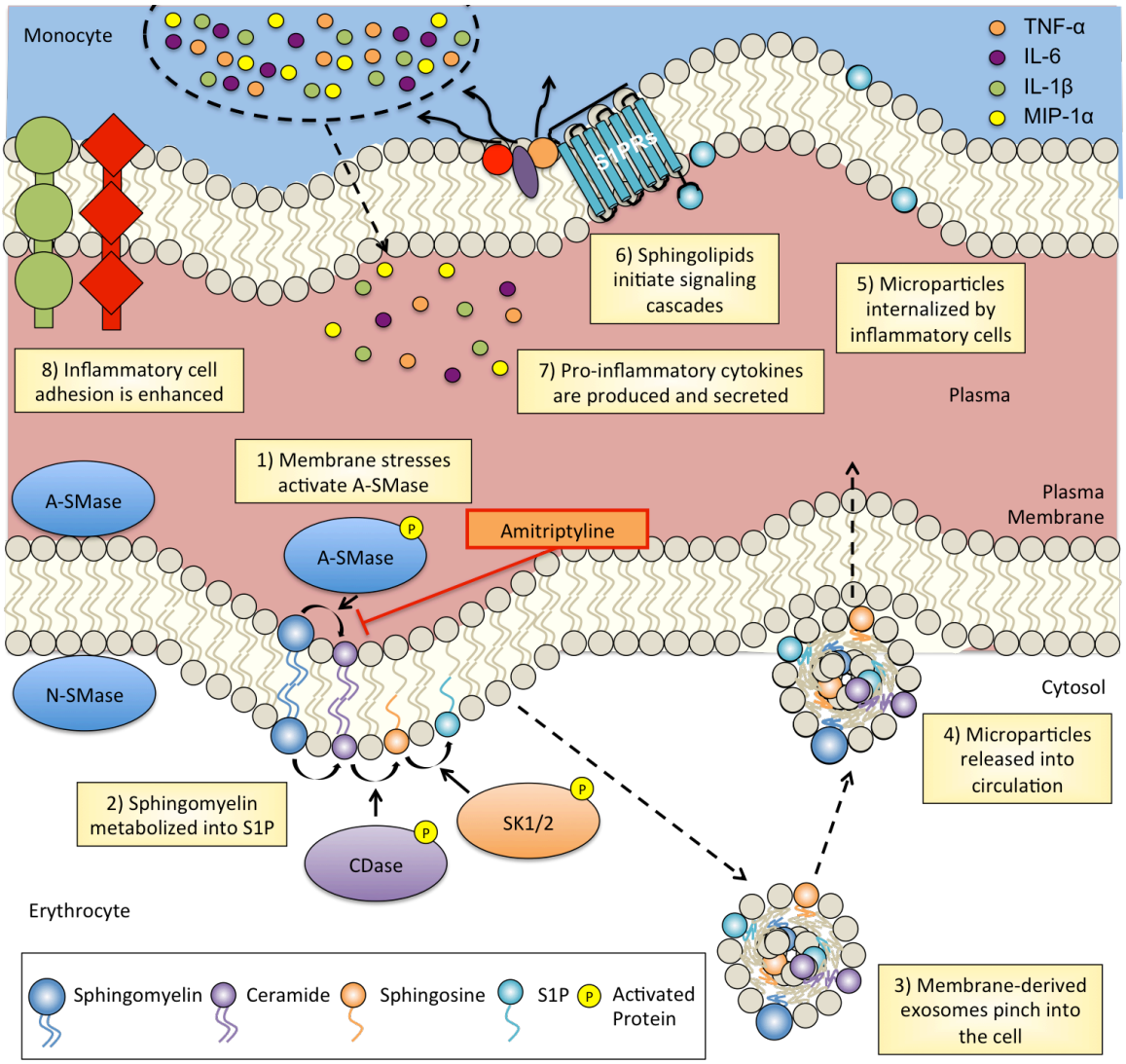

Figure 5.1. Schematic of Sphingolipid metabolism and microparticle mediated inflammation in SCD. 1) Membrane stresses in SS RBCs activate acid sphingomyelinase (A-SMase) on the outer leaflet of the plasma membrane. 2) Sphingomyelin can be further metabolized into sphingosine and S1P with alkaline ceramidase (CDase) and Sphingosine Kinase (SK1/2), respectively. 3) Membrane budding results in the formation of sphingolipid-rich microparticles. 4) Microparticles are released into circulation. 5) Monocytes internalize microparticles. 6) S1P and other sphingolipids initiate signaling cascades. 7) Pro-inflammatory cytokines are produced and secreted. 8) Monocyte adhesion is enhanced. Acid sphingomyelinase inhibition with amitriptyline reduces microparticle formation and subsequent inflammation.

APPENDIX A

SPHINGOSINE 1-PHOSPHATE RECEPTOR 3 REGULATES IMPLANT ARTERIOGENESIS BY RECRUITMENT OF ANTI-INFLAMMATORY MONOCYTES TO MICROVESSELS

Introduction

The microvasculature is an intricate network of blood vessels whose primary purpose is to deliver oxygen and nutrients throughout body. The process of microvascular network growth and remodeling is governed by a continuum of gene expression patterns and molecular signaling events in several cell types working across multiple time and length scales. Microvascular endothelial cells (EC) produce a number of growth factors and cytokines, such as MCP-1 (103), SDF-1α (104, 105) and VEGF (106) that regulate the recruitment, proliferation, differentiation and activation of cells in their proximity. Elucidating these "angiocrine" factors that utilize the body's endogenous repair mechanisms may be critical to improving the treatment of ischemic tissue diseases and enhancing regenerative capacity of biomedical implant materials.

Sphingosine 1-phosphate (S1P) is a naturally occurring bioactive lipid found in nanomolar concentrations in plasma through production by red blood cells, activated platelets and EC. Disrupting the balance of high S1P levels in circulation and low levels in tissues results in extreme conditions such as lymphopenia, neutrophilia, and vascular barrier dysfunction (26). S1P signals pleiotropic cellular functions, including chemotaxis and recruitment of cells (26-28), through the activation of combinations of five known G-protein coupled receptors ($S1P_1$-$S1P_5$) (29, 107, 108). Recent studies also indicate that S1P plays a significant role in the migration and trafficking of hematopoietic stem and

progenitor cells within extra medullary tissues (27) and regulates blood recirculation of osteoclastic precursors (30). Furthermore, S1P receptor signaling plays critical roles in the formation and stabilization of microvascular networks (109). We have shown that local activation of S1P receptors 1 and 3, with the synthetic S1P analog FTY720, enhances microvascular remodeling through expansion of arterioles and capillary networks (110). Modulation of S1P receptors on ECs may be a novel way to control the localization of circulating cells that contribute to tissue regeneration and wound healing.

Monocytes and macrophages were once thought to be homogenous populations of cells, with a uniform role in immunity; however, monocyte/macrophages are now recognized as highly plastic cells that can exist in many subpopulations along a spectrum of activation from pathogen clearance to tissue regeneration (111). These cells are referred to as monocytes while in circulation and macrophages when in the tissue space and have critical roles in injury-induced neovascularization, arteriogenesis and angiogenesis (112-115). In the context of inflammation and wound healing, two subsets of macrophages are dominant (116, 117). Classically activated inflammatory monocytes/macrophages (IM), also known as M1 macrophages, phagocytose debris and clear damaged cells and are recruited from circulation shortly after injury (within hours). On the order of hours to days after injury, a second wave of alternatively activated anti-inflammatory monocytes/macrophages (AM) is recruited that play roles in tissue remodeling and angiogenesis (117, 118). AM are also known as M2 macrophages and exist in at least three states (M2a, M2b and M2c) depending on their roles in allergy, immunoregulation and tissue remodeling, respectively (119). IM express high levels of CCR2, CD16, Ly6C and Gr1 on their surface and secrete inflammatory cytokines such as

TNF-α, IL-6 and IL-1. Conversely, AM express high levels of CX3CR1, CD206 and CD14 and secrete cytokines such as IL-10, TGF-β and IL-1RA (119). Given that monocyte/macrophages respond quickly to local changes in the microvasculature and are often the key targets of signaling from EC, discovering factors that alter the phenotype of, or preferentially recruit, these cells may be critical to controlling healing and regeneration.

In this chapter we explore how local polymeric delivery of S1P receptor compounds can recruit regenerative cells and lead to enhanced vascular remodeling. Our results demonstrate that $S1P_3$ activation on EC is critical for SDF-1α and other pro-regenerative cytokine production and that $S1P_3$ receptor expression in both the bone marrow and the tissue is necessary for FTY720-mediated vascular remodeling. We show that $CX3CR1^{hi}$, CD206+ AM, express higher levels of surface $S1P_3$ and show enhanced SDF-1α mediated chemotaxis after FTY720 treatment. Local AM recruitment to the perivascular niche in tissues after FTY720 treatment results in enhanced arteriogenesis in muscle and soft tissue. Novel strategies, involving S1P receptor signaling, to modulate the secretion of endogenous angiocrine factors that recruit regenerative cells can be employed to enhance blood vessel growth and the integration and functionality of tissue engineered (TE) implants.

Materials and Methods

Animals and Treatments

Wild type C57BL/6 and NG2-DSred mice were obtained from The Jackson Laboratories, heterozygous CX3CR1-eGFP mice were a generous gift from Dr. Klaus Ley (La Jolla) and $S1P_3$-/- mice were a kind gift of Dr. Richard Proia (NIH). NG2-DSred

mice were crossed with the CX3CR1-eGFP mice to generate DsRed-NG2 CX3CR1-eGFP mice. Mice in all studies were male, 8-12 weeks, weighing 18-25 g. The murine dorsal skinfold window chamber model and spinotrapezius ligation model with polymer implantation were performed as described previously (34) and explained in detail in SI methods. All surgical procedures and animal care protocols were approved by the University of Virginia Animal Care and Use Committee.

Fabrication of Poly(Lactic-Coglycolic Acid) Thin Films and Encapsulation of Sphingosine 1-Phosphate Receptor-Targeted Compounds.

Poly(lac- tic-coglycolic acid) (PLAGA) thin films were fabricated by using a solvent-casting technique as described (34). A total of 350 mg of PLAGA was combined with 2 mL of methylene chloride (Fisher Scientific) in a borosilicate liquid scintillation vial (20-mL capacity; Fisher Scientific) and vortexed until completely dissolved. For 1:200 (drug weight:polymer weight) FTY720 (Cayman Chemical), VPC01091, or Compound 26 (Kevin Lynch, University of Virginia) loaded films, 1.75 mg of drug was added to the solution. The polymer/drug solution was quickly poured into a P35 Petri dish (Nunc; area = 8.8cm^2) lined with Bytac Teflon paper. Films were allowed to dry at −20 °C for 7 d, and then were stored at room temperature in a desiccator until needed. All films were lyophilized (Labconco FreeZone 2.5; Labconco) for 24 h before being used for experiments to remove any excess solvent. For implantation in vivo, films with a diameter of 1 mm were extracted by using a 1-mm biopsy punch (Acuderm) and rinsed in 70% (vol/vol) ethanol for ∼30 s and then washed in sterile Ringer's solution (137.9 mM NaCl, 4.7 mM KCl, 1.2 mM $MgSO_4$, 1.9 mM $CaCl_2$, and 23 mM $NaHCO_3$) for an additional 30 s. Films had an average thickness of 517 ± 41 μm, as measured with

calipers (L. S. Starrett Co.).

Fabrication of Nanofiber Scaffolds and Encapsulation of FTY720.

A 1:1 mixture of polycaprolactone (PCL; Sigma) and PLAGA (Lake- shore Biomaterials) was dissolved in a 3:1 (vol/vol) chloroform: methanol solution. The final concentration of polymer solution was 18% (wt/vol). The solution was agitated at room temperature until the polymer dissolved, followed by loading into a 3-mL rubber-free syringe. Electrospinning was performed at a flow rate of 1.0 mL/h, an applied voltage of 19 kV, and a working distance of 10 cm. Nanofibers were collected on a stationary aluminum plate and then stored in a desiccator until use. To make drug- loaded nanofibers, FTY720 (Cayman Chemical) was dissolved in 3:1 chloroform:methanol solution, and 1:1 PCL/PLAGA was added at a concentration of 20% (wt/vol). The final drug:polymer ratio was 1:200.

Generation of Bone Marrow Chimeric Mice.

To generate bone mar- row (BM) chimeric mice, donor mouse tibia were harvested and flushed of marrow. Recipient mice were lethally irradiated with a total dosage of 10.5 gray (33) (5.5- and 5-Gy doses, 3 h apart) before transplantation of 2×10^6 donor cells in 150 μL of PBS via tail vein injection. The cells were allowed to engraft for 6 wk before experimentation.

Dorsal Skinfold Window Chamber Surgical Procedure.

Mice were implanted with dorsal skinfold window chambers (APJ Trading Co.). Mice were treated with a preanesthetic of atropine (0.08 mg/ kg IP) and further anesthetized by using i.p. injections of ketamine (80 mg/kg) and xylazine (8 mg/kg). For nanofiber implantation, anesthesia was induced with isoflurane gas in a chamber (2–3%),

and the surgical plane was maintained with a nose cone (1–2%) equipped with a scavenging apparatus for the procedure. Dorsal skin was shaved, depilated, and sterilized by using triplet washes of 70% ethanol and iodide. A double-layered skin fold was elevated off the back of the mouse and pinned down for surgical removal. The titanium frame of the window chamber was surgically fixed to the underside of the skinfold. The epidermis and dermis were removed from the top side of the skinfold in a circular area (diameter = ∼12 mm) to reveal the underlying vasculature. Exposed tissue was kept hydrated with sterile Ringer's solution (137.9 mM NaCl, 4.7 mM KCl, 1.2 mM $MgSO_4$, 1.9 mM $CaCl_2$, and 23 mM $NaHCO_3$). The titanium frame was then mounted on the top side of the tissue and attached to its underlying counterpart. The dorsal skin was sutured to the two titanium frames, and the exposed tissue was sealed with a protective glass window. Mice were allowed to recover in heated cages and subsequently were administered buprenorphine via s.c. injection (0.1–0.2 mg/kg) as a postoperative analgesic. All mice received a laboratory diet and water ad libitum throughout the time course of the experiment.

Implantation of Thin Films and Intravital Image Acquisition.

PLAGA thin films were implanted into the window chamber 7 d after surgical implantation, hereafter referred to as day 0. Mice were anesthetized via 2% isoflurane mixed with 1 mL/min O_2. Subsequently, the glass window was removed to expose the thin layer of vessel networks. The window chamber was flooded with 1 mM adenosine in Ringer's solution (3 × 5 min) to maximally dilate all vessels and maintain tissue hydration. Following the last ad- ministration of adenosine, the solution was aspirated, and two films (either both loaded or both unloaded) were placed equidistant from one

another and from each edge of the window. The mouse was then mounted to a microscope stage and imaged noninvasively by using a 4× objective on an Axioskope 40 microscope (Carl Zeiss). Images were captured by using an Olympus MicroFire color digital camera and PictureFrame image acquisition software (Optronics). Individual images were later photomerged into a single image of the entire microvascular network by using Adobe Photoshop CS. Mice were initially imaged on day 0 following film implantation and again on days 3 and 7.

Quantitative Microvascular Metrics.

Intravital microscopy montages of entire vascular windows at days 0, 3, and 7 were analyzed by using a combination of Adobe Photoshop CS and ImageJ (http://rsb.info.nih.gov/ij/) software packages. First, circles with a diameter of 5 mm (or 2-mm concentric radius from outer edge of one film) were cropped around each film, with no overlap of the two circles.

Changes in Microvascular Length Density.

For microvascular length density measurements, vessels located within these cropped images were traced by using Photoshop and skeletonized by using ImageJ. These binary images were analyzed by counting the total number of pixels, representing the total length of all traced vessels. Pixels were converted to millimeters by using the conversion factor (350 pixels = 1 mm) calculated from an image of a micrometer at the same imaging conditions (4×). Pixel length was divided by total area of the region of interest (a circle with diameter of 5 mm; A = 19.63 mm^2). The limit of resolution of vessels that can be visualized in this manner is 10 μm.

Changes in Microvascular Diameter.

To assess changes in luminal diameter, arteriole–venule pairs were identified in the 2-mm cropped images. In these intravital images, vessels are visualized by blood column width. Therefore, arterioles and venules were identified on the basis of size only; venule diameters were larger than arteriolar diameters on day 0. Identical vessel segments were labeled on day-0, -3, and -7 images at the bisection of each vessel segment in between branch points. Internal diameters based on blood column widths were measured by using ImageJ. Day-0 diameter measurements were used to bin vessels by size at the onset of the experiment to track how initial size affects lumenal expansion potential. This metric is limited to vessels that are visible at all three time points, and the limit of resolution is ∼10 μm.

BM Harvest and Cell Sorting.

Mice tibia and femurs were harvested with scissors and forceps. The ends of the bone were cut with bone cutters, and marrow was flushed with sterile saline by using a syringe and 25-gauge needle. BM was collected, filtered, and resuspended in sterile PBS + 10% FBS for flow cytometry staining. $SSC^{lo}CD45^{+}CD11b^{+}Gr1^{+}Ly6C^{+}$ inflammatory subtype of monocytes (IM) and $SSC^{lo}CD45^{+}CD11b^{+}Gr1^{-}Ly6C^{-}$ anti-inflammatory subtype of monocytes (AM) were sorted for in vitro and adoptive transfer experiments.

Adoptive Transfer.

$SSC^{lo}CD45^{+}CD11b^{+}Gr1^{-}Ly6C^{-}$ AMs were sorted from mouse BM and stained with 1,1′-dioctadecyl-3,3,3′,3′-tetramethylindo- carbocyanine perchlorate (DiI) for 20 min. Host mice received 800,000 IMs or 175,000 AMs i.v. via retro orbital sinus 24 h before backpack surgery. Blood was collected immediately before surgery and at 1 and 3

d after surgery. Dorsal tissue was also harvested 3 d after surgery for flow cytometric analysis.

Dorsal Tissue Immunohistochemistry.

Five-micrometer-thick sections were cut from paraffin-embedded s.c. dorsal tissue. Sections were de-waxed with 100% xylenes, 100% ethanol, 95% ethanol, 70% ethanol, and 50% ethanol in series for 3 min each. Antigens were retrieved by high-temperature pressure cooking of slides for 15 min in 10 mM sodium citrate buffer (pH 6). Endogenous peroxidase activity was blocked by incubation of specimens with 3% hydrogen peroxide in 40% methanol for 10 min followed by nonspecific blocking with 2.5% horse serum. Slides were incubated with 1:50 rabbit anti-mouse MHCII (Novus), CD206 (Bioss), and F4/80 (AbCam) overnight at 4 °C in a humidified chamber. Slides were washed and fluorescent secondary antibodies or anti-rabbit peroxidase secondary antibodies, and diaminobenzidine–peroxidase substrate kit (Vector Lab) were used to stain slides. Hematoxylin counterstaining was performed for 5 min to stain tissue and cells on specimens.

Dorsal Tissue Digestion for Single-Cell Suspensions and Protein.

To measure the recruitment of cells to inflamed tissue, dorsal skinfold window chambers were implanted on CX3CR1–eGFP mice. Ninety- five percent of CX3CR1, also known as fractalkine, can be attributed to monocytes. Two FTY720-loaded or unloaded PLAGA films were implanted on the day of surgery. Three days after, two 8-mm biopsy punches were taken around each implant in each animal. This dorsal tissue was treated with 1 mg/mL collagenase (Sigma) at 37 °C and further disaggregated with a cell strainer to create a single-cell suspension. For protein analysis, single-cell

suspensions were placed in 1× radioimmunoprecipitation assay buffer with protease and phosphatase inhibitors for 5 min on ice. The lysed cells were then centrifuged to pellet out debris, and the lysate was stored at −80 °C until analysis.

Spinotrapezius Ligation.

Spinotrapezius ligation was performed similarly to previous studies (13). In summary, DsRed–NG2 CX3CR1–eGFP mice were anesthetized via i.p. injection of ketamine/xylazine/atropine (60/4/0.2 mg/kg). The position where the fat pad ends (~1–2 cm from the head posteriorly) was found, and an incision (~0.5 cm, parallel to the spine) was made 1 cm laterally from the spine at this location. Under a dissecting microscope, blunt manipulation of the tissue was performed to locate the spinotrapezius. The main feeding arteriole was located and followed upstream until it exited the spinotrapezius and entered the fat pad. Blunt dissection was used to isolate the arteriole from its associated venule, and care was taken to minimize mechanical manipulation of the muscle and tissue. Two ligatures were placed on the arteriole by using 10-0 sutures followed by ligation of the arteriole between the ligatures. Tissue was returned to its original position. A small 1-mm disk of PLAGA (either empty or loaded with FTY720) was placed between the fascia and spinotrapezius before closing the wound with 8-0 non-resorbable sutures. One week later, the mouse was euthanized, and the whole spinotrapezius was harvested.

Spinotrapezius Tissue Immunohistochemistry.

Both spinotrapezius muscles were harvested from each mouse and permeabilized with 0.2% saponin in PBS overnight (18 h) at 4 °C. Muscles were blocked for 1 h (5% mouse serum, 0.2% saponin, 0.5% BSA in PBS) before being treated with primary

antibody overnight at 4 °C. Spinotrapezius tissues were immunolabeled for smooth muscle α-actin [mural cell stain, IA4-Cy3 (Sigma-Aldrich), 1:300] and isolectin [endothelial cell (EC) stain, IB4–Alexa 647 (Invitrogen), 1:200]. Muscles were washed five times at 20 min per wash (0.2% saponin and 0.5% BSA in PBS) before being whole mounted on a coverslip.

Spinotrapezius Imaging and Data Analysis.

Whole-mounted spinotrapezius tissue was imaged by using confocal microscopy (Nikon; model TE200-E2; 4×, 10×, 20×, and 60× objectives). Analyses of the confocal images were conducted by using ImageJ imaging software to quantify vascular lengths and diameters. Tortuosity of arterioles was determined by tracing the path a vessel took and dividing it by the absolute distance of the start and end point. All tortuosity data were acquired in regions of the vessel where no branching occurred. The 10× images were taken of the primary watershed, i.e., the immediate downstream region of the ligated arteriole. Green fluorescent positive cells were counted. Additionally, cells touching or aligned with vessels were considered to be associated with the vessel. All vascular analysis was performed by a single blinded person who had no knowledge of the treatment groups.

Intravital Microscopy of Rolling in Dorsal Skinfold Window Chamber.

Intravital microscopy of dorsal skinfold window chambers was performed on a Nikon Eclipse 80i microscope equipped with an EXFO XCite 120 xenon light source for epifluorescence microscopy; Nikon 32 B2E/C, G2E/C, and UV2E/C filter cubes; and 10× and 20× objectives. Video was taken by using a high-speed Photometrics HQ2 CCD camera cooled to −30 °C controlled by Nikon NIS Elements Advanced Research

software with a 2D object tracking package (Version 3.22.00; Laboratory Imaging) running on an HP DC7900 PC. Mice were anesthetized by using isoflurane for the duration of the imaging. The glass coverslip was removed from the window chamber before video acquisition. One-minute videos were taken of perfused vessels near implants immediately after surgery and 1 d after surgery. Green fluorescent positive cells captured in the video were separated into three categories, flowing, rolling, and adhered, based on the speed of the cells. Flowing cells had no abnormal changes in velocity. Rolling cells exhibited a stop–start/variable velocity characteristic, whereas adhered cells remained stationary for at least 10 s. In addition, the highest intensity for cells in focus was recorded. One person did all of the video acquisition and analysis.

Flow Cytometry.

Immunostaining and flow cytometry analyses were performed according to standard procedures and analyzed on a FACSCanto flow cytometer (BD Biosciences). Monoclonal antibodies to CD45, CD11b, Ly6C, and Gr1 (Abcam, Biolegend, and eBiosciences) were used to detect and sort inflammatory and anti-inflammatory monocytes and macrophages.

Cell Culture.

Human primary isolated pericyte capillary cells were cultured in Pericyte Growth Medium (Angio-Proteomie) in the presence of 1 μM sphingosine 1-phosphate (S1P) receptor compounds for 160 h with medium change every 48 h. Human umbilical vein ECs (HUVECs) were cultured in EBM-2 medium (Lonza) with 5% FBS and 1% penicillin/streptomycin (Pen/ Strep) in the presence of 1 μM S1P receptor compounds for 24 h. Human THP-1 monocytes were differentiated to macrophages with 100 nM phorbol

myristate acetate treatment for 2 d and polarized to M1 and M2 macrophages with 20 ng/mL IL-4 or 5 ng/mL TNF-α + 20 ng/mL IFN-α, respectively. Murine primary isolated AMs and IMs were serum starved for 2 h before 1-h treatment with 12.5 nM S1P receptor compounds and chemotaxis assays in transwell chambers. For transwell migration assays, cells were plated at the top of 8-μm pore-size transwell inserts and allowed to migrate toward 12.5 nM SDF-1 for 4 h. Murine RAW 264.7 cells (ATCC) were cultured in high-glucose DMEM supplemented with 10% FBS, 2 mM L-glutamine, 1% Pen/Strep, and 1 mM sodium pyruvate. Macrophages were polarized to M1 cells by treatment with 1 μg/mL LPS and 20 ng/mL IFN-γ, or M2 cells by treatment with 10 ng/mL IL-4 for 16 h. Mouse WEHI–274.1 monocytes between passages 25 and 30 were cultured in low-glucose DMEM supplemented with 5% FBS and 1% Pen/Strep. For monocyte polarization, LPS (Sigma) was dissolved in the medium at a concentration of 100 ng/mL Monocytes were incubated in this medium at 37 °C in 5% CO_2 just before seeding. PLAGA thin films were placed in 96-well plates, and 2.5×10^5 cells per mL were seeded onto them and cultured for as long as 14 d. The films were recovered at several time points: 2 h after incubation on day 0 and on days 1–7, 10, and 14, for a total of 30 films.

Protein Analysis.

For Western blotting analysis, total cellular protein was isolated, quantified, and electrophoresed by standard methods. Proteins were transferred to low-fluorescence PVDF membrane, blocked with blocking buffer for fluorescent Western blotting (Rockland Immunochemicals). Membranes were incubated with primary antibodies overnight for S1P1 (Novus Biologicals; NB120-11424), S1P3 (Novus Biologicals; NBP1- 95141), and β-actin (Sigma Aldrich). After washing with Tris- buffered saline

with Tween-20 (TBST), blots were incubated with the appropriate infrared-conjugated secondary for 45 min, washed in TBST, and imaged on the LI-COR Odessey infrared imaging system.

Real-Time PCR.

Total RNA was isolated by Ribozol extraction, and cDNA was generated from 500 ng of total RNA by reverse transcription with random primers (Applied Biosystems). Quantitative PCR with SYBR green was performed on a StepOne Plus thermo cycler (Applied Biosystems). The S1P3 receptor mRNA expression (F: 5′-GTTACTTCAACAGTCCACGAGA-3′; R: 5′- AGATGCGCCTTGCAGAA-3′) was normalized to GAPDH as an internal control (F: 5′-ACCACAGTCCATGCCATCAC-3′; R: 5′-TCCACCACCCTGTTGCTGTA-3′) (IDT). Quantitation was performed by the $\Delta\Delta C_T$ method.

Cytokine Measurement.

Protein isolated from backpack tissue and cell culture-conditioned medium was assayed for cytokine release by using Luminex bead arrays (Millipore). Panels consisting of interferon-γ (IFN-γ), interleukin 1-α (IL-1α), interleukin 1-β (IL-1β), interleukin 6 (IL-6), interleukin 12 (IL-12 - p40), interleukin 17 (IL-17), tumor necrosis factor α (TNF-α), interleukin 12 (IL-12 - p70), granulocyte colony stimulating factor (G-CSF), granulocyte macrophage colony stimulating factor (GM-CSF), macrophage colony stimulating factor (M-CSF), interleukin 5 (IL- 5), interleukin 7 (IL-7), interleukin 8 (IL-8), interleukin 9 (IL-9), interleukin 2 (IL-2), interleukin 3 (IL-3), interleukin 4 (IL-4), interleukin 10 (IL-10), interleukin 13 (IL-13), interleukin 15 (IL- 15), eotaxin, interferon-inducible protein 10 (IP-10), macrophage inflammatory protein 2 (MIP-2), keratinocyte chemoattractant

(KC), leukemia inhibitory factor (LIF), monocyte chemo- attractant protein 1 (MCP-1), macrophage inflammatory protein 1α (MIP-1α), macrophage inflammatory protein 1β (MIP-1β), monokine induced by gamma interferon (MIG), epidermal growth factor (EGF), fibroblast growth factor 2 (FGF-2), transforming growth factor α (TGF-α), Fms-related tyrosine kinase 3 ligand (Flt-3L), fractalkine, interferon α2 (IFNα2), interferon γ (IFNγ), growth-related oncogene (98), monocyte chemoattractant protein 3 (MCP-3), macrophage derived chemokine (MDC), platelet derived growth factor AA (PDGF-AA), platelet derived growth factor BB (PDGF-BB), soluble cluster of differentiation 40 ligand (sCD40L), interleukin 17a (IL-17a), interleukin 1 receptor antagonist A (IL-1RA), vascular endothelial growth factor (VEGF), tumor necrosis factor β (TNF-β) and regulated on activation, normal T-cell expressed and secreted (RANTES) were used to quantify the cytokine secretion profile of monocytes, HUVECs, and in tissue protein ELISA for SDF-1α and MCP-1 (R&D Systems) were used to quantify protein levels from tissue and HUVEC lysate.

Statistical Analyses.

All statistical analyses were performed by using Minitab 15 statistical software (Minitab). Results are presented as mean ± SEM, unless otherwise noted. Comparisons were made by using a one-way ANOVA, followed by Tukey's test for pairwise comparisons. Diameter analysis was performed by using a general linear model (GLM) ANOVA with an unbalanced nested design, followed by Tukey's test for pairwise comparisons. The model for the GLM ANOVA was as follows: drug group film number (drug group), where drug group represents S1P, for example, and film number represents each n number (i.e., mouse 5 left film). Significance was asserted at $P < 0.05$. Where

specified, power calculations were performed with $\alpha = 0.05$ and power = 0.80 to determine statistically significant sample size.

Results

FTY720 enhances inflammation-associated microvascular network growth

Dorsal skinfold window chambers ("backpacks") were implanted on wild type C57Bl/6 mice and a superficial layer of dermis was excised to expose the underlying vasculature (120). FTY720-loaded or unloaded 1mm diameter, 0.5mm height 50:50 poly (lactic-co-glycolic acid) (PLAGA) thin films were implanted directly after surgery (acute treatment) and sham animals underwent surgery with no film implantation (**Figure A.1A**).

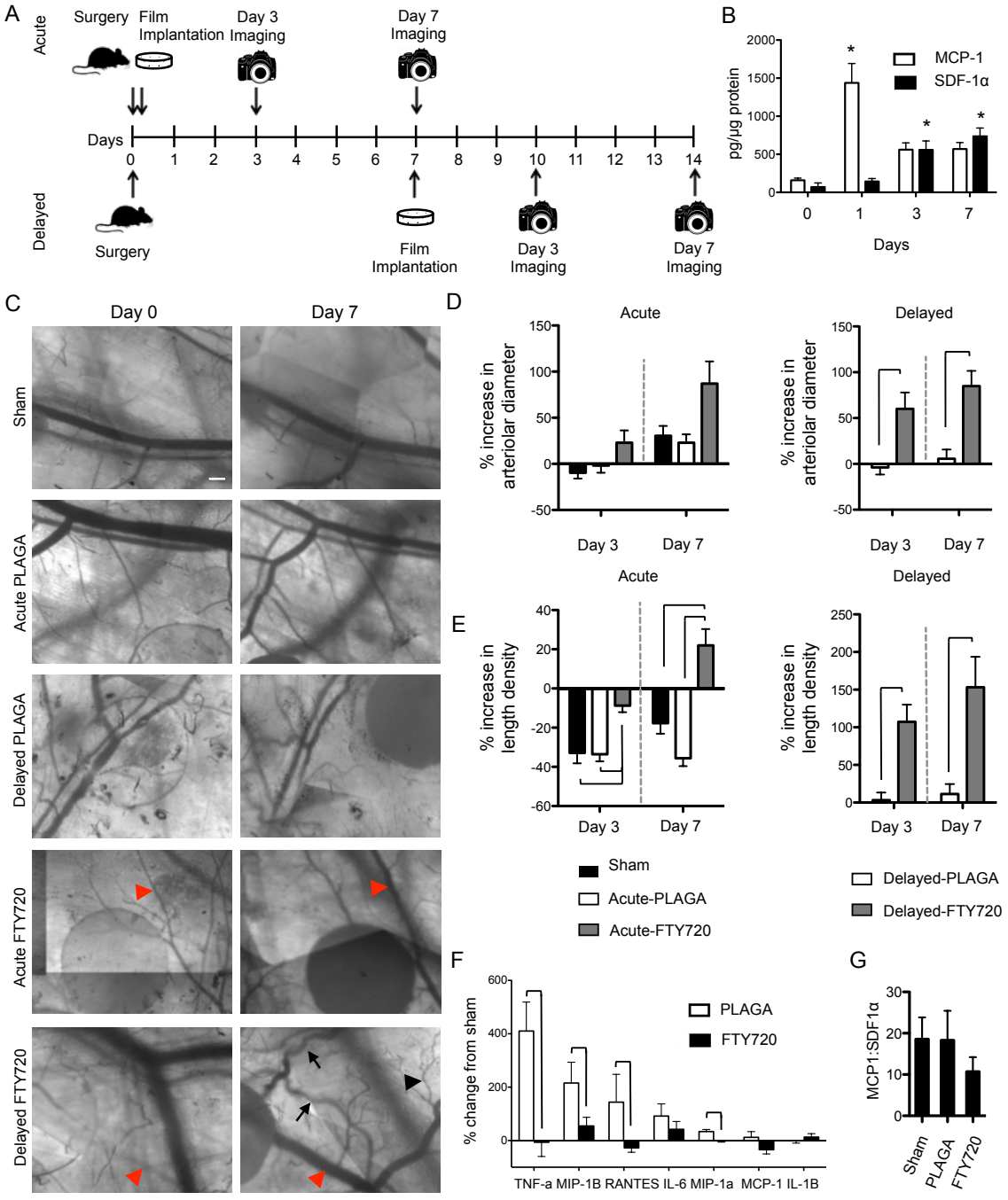

Figure A.1. FTY720 enhances inflammation associated microvascular growth. (A) Schematic of acute and delayed PLAGA film implantation. (B) MCP-1 and SDF-1α in backpack tissue over 7 days. (C) Microvascular networks surrounding PLAGA implants at 0 and 7 days post implantation when implanted on day of surgery (acute) or 7 days after surgery (delayed). Delayed FTY720 promotes growth of new vessels (arrowheads), vessel tortuosity (arrows) and arterial diameter enlargement (red arrowheads). Arteriolar diameter expansion (D) and length density (E) significantly enhanced after acute (left) FTY720 implantation. Delayed FTY720 treatment also significantly enhanced arteriolar

diameter expansion (D) and length density (E) (right). (F) Cytokine quantification (fold change from sham) in tissue surrounding FTY720-loaded implants shows significant reduction of inflammatory cytokines with FTY720 3 days after implantation (G) FTY720 reduces ratio of MCP-1:SDF-1α in tissue around implant on day 1 post surgery. *$P<0.05$ compared to sham or day 0. Scale bar = 100μm.*

These sham animals served as a control for the injury stimulus of the surgery. To investigate the local tissue secretion of inflammatory chemokines in the acute post-surgery period, we evaluated the concentration of the chemokines MCP-1 (a potent IM chemoattractant) and SDF-1α (a potent stem cell chemoattractant) over a 7-day period after backpack implantation. Four-millimeter diameter biopsies were taken from sham-treated backpack tissue and quantification of MCP-1 and SDF-1α was performed by ELISA. The post-surgery period was characterized by early MCP-1 expression peaking at day 1 and later induction of SDF-1α, peaking at day 7. MCP-1 was elevated almost 10 fold from 159.23pg/μg on the day of surgery to 1437.17pg/μg 1 day after surgery. By 3 days post-surgery the level had significantly decreased to 560.32pg/μg and was maintained through day 7 (569.29pg/μg) (**Figure A.1B**). On the other hand, SDF-1α remained relatively low on day 0 and 1 post-surgery (69.72 and 143.09 pg/μg, respectively) but was significantly elevated (558.64pg/μg) by 3 days post-implantation and remained elevated through day 7 (736.28pg/μg) (**Figure A.1B**).

Vascular parameters were assessed by imaging on day 0, 3 and 7 post-acute implantation of the window chamber and films. A reduction in lumenal arteriole diameter was observed from 0- 3 days after implantation in sham (-9.59%) and acute-PLAGA (-1.79%) treated mice while mice with acute-FTY720 implantation had an increase in arteriolar diameter expansion (22.93%) relative to day 0 (**Figure A.1C and Figure A.1D, left**). Mice in the sham (-32.88%) and acute-PLAGA (-33.52%) groups showed

reductions in vascular length density, a measure of network expansion and angiogenesis, as well, while mice in the acute-FTY720 group had much smaller reductions (-8.74%) (**Figure A.1C and Figure A.1E, left**). By 7 days post-implantation lumenal diameter expansion was observed in sham (30.46%) and PLAGA (22.86%) treated mice and FTY720 significantly increased arteriolar diameter expansion (87.02%) (**Figure A.1D, left**). The sham (-17.72%) and acute-PLAGA (-35.61%) groups showed a reduction in length density while there was an increase in length density with acute-FTY720 (21.98%) (**Figure A.1E, left**).

Since FTY720 increases microvascular remodeling when delivered acutely after injury while inflammatory cues dominate relative to regenerative cues, we wished to determine whether FTY720 also enhances remodeling after the peak of the inflammatory response. To this end, we altered our backpack model by adding two "delayed" groups where polymer films were implanted 7 days post-surgical implantation of the window chamber (delayed-PLAGA or delayed-FTY720) (**Figure A.1A**). Images were then taken 7, 10 and 14 days post-implantation of the chamber (0, 3 and 7 days post-implantation of the delayed film). Indeed, mice in the delayed-FTY720 group also show significant increases in both arteriolar diameter expansion (60.10%) and length density (107.34%) relative to delayed-PLAGA mice 3 days after implantation (**Figure A.1C, Figure A.1D, right and Figure A.1E, right**). At 7 days post-implantation there were still more noteworthy increases in arteriolar diameter expansion (84.97%) and length density (153.20%) relative to delayed-PLAGA (**Figure A.1D, right and Figure A.1E, right**). Enhanced vessel tortuosity (arrows), new vessel growth (arrowheads) and diameter enlargement (red arrowheads) are classic signs of arteriogenesis and were observed with

delayed-FTY720 treatment (**Figure A.1C**). These results suggest that with delayed delivery, after macrophage infiltration, FTY720 promotes robust local microvascular network growth in the peri-implant space by the expansion of arterioles. We have termed this effect of both acute and delayed promotion of arteriolar remodeling through biomaterial release of FTY720 "implant arteriogenesis." The goals of the current study were to investigate the role of S1P receptors in the early phase of inflammatory response and therefore the following studies are all acute film implantation unless otherwise noted.

FTY720 reduces inflammatory cytokine secretion in backpack tissue

To test whether the local release of FTY720 modulated the secretion of inflammatory cytokines, we digested backpack tissue 3 days after acute implantation and quantified a panel of inflammatory cytokines with luminex multiplexed magnetic bead technology. Local activation of S1P receptors by FTY720 significantly decreased the expression of many cytokines associated with implant rejection and poor wound healing. Specifically, FTY720 significantly reduced the secretion of TNF-α (410.5 to -6.3), MIP-1β (215.7 to 54.7), RANTES (143.8 to -27.3) and MIP-1α (33.7 to -0.73) relative to unloaded PLAGA films in the backpack model (**Figure A.1F, Figure A.2**).

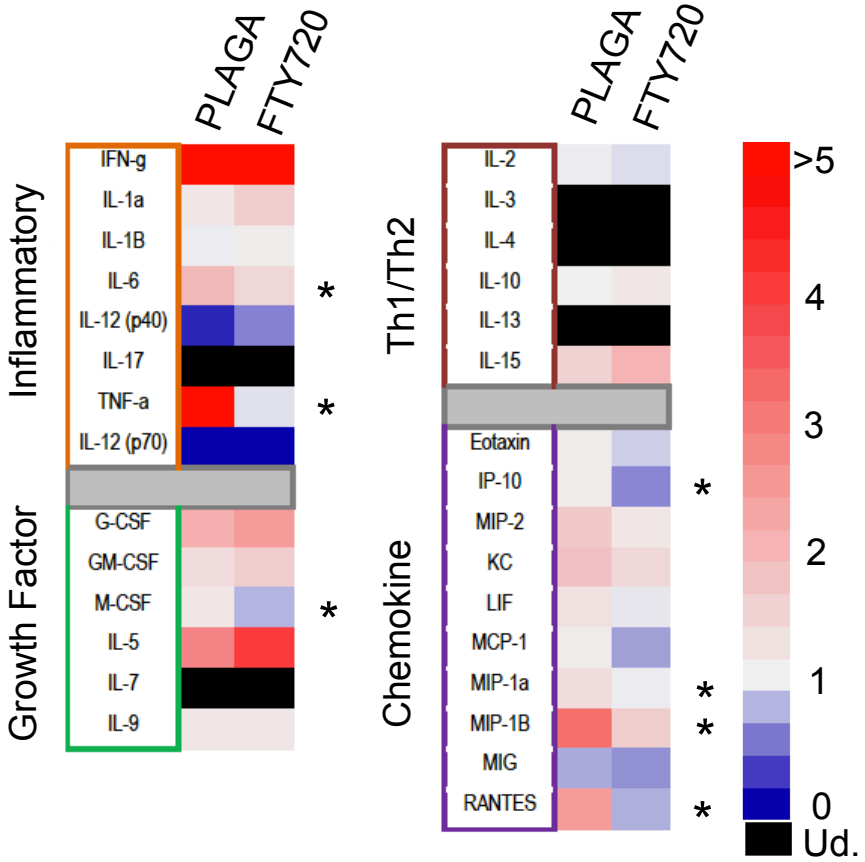

Figure A.2. FTY720 reduces inflammatory cytokine concentration in tissue. Cytokine quantification (fold increase over sham) in tissue surrounding FTY720-loaded implants shows significant reduction of inflammatory cytokines with FTY720 3 days after implantation (Ud. Is undetectable by luminex).

Additionally, anti-inflammatory and pro-regenerative cytokines (i.e. IL-5, IL-10 and GCSF) were elevated with FTY720 release (**Figure A.2**). These results suggest that local S1P receptor activation alters the concentration and balance of inflammatory and regenerative cytokines, which, as a result, may affect the recruitment of inflammatory and regenerative cells. Interestingly, FTY720 implantation reduced the MCP-1: SDF-1α ratio (10.71) relative to sham (18.55) and PLAGA-treated (18.3) peri-implant tissues after only 1 day (**Figure A.1G**).

FTY720 differentially regulates the recruitment, rolling and adhesion of distinct monocyte subsets

Geissman et al. characterized two populations of macrophages with distinct migratory roles during inflammation in mice: a $CX3CR1^{lo}CCR2^{+}Ly6C^{+}$ M1-like subset, recruited to inflamed tissues and a $CX3CR1^{hi}CCR2^{-}Ly6C^{-}$ M2-like subset recruited to non-inflamed tissues (121). As these cells transmigrate into tissues they develop distinct differentiation states, while maintaining their polarization, as macrophages. For the remainder of this paper we refer to these cells as monocytes when in circulation and macrophages when in tissue. In order to determine how these two distinct subsets of macrophages are affected by FTY720 during an inflammatory stimulus, backpacks were implanted on CX3CR1-eGFP mice (**Figure A.3A**).

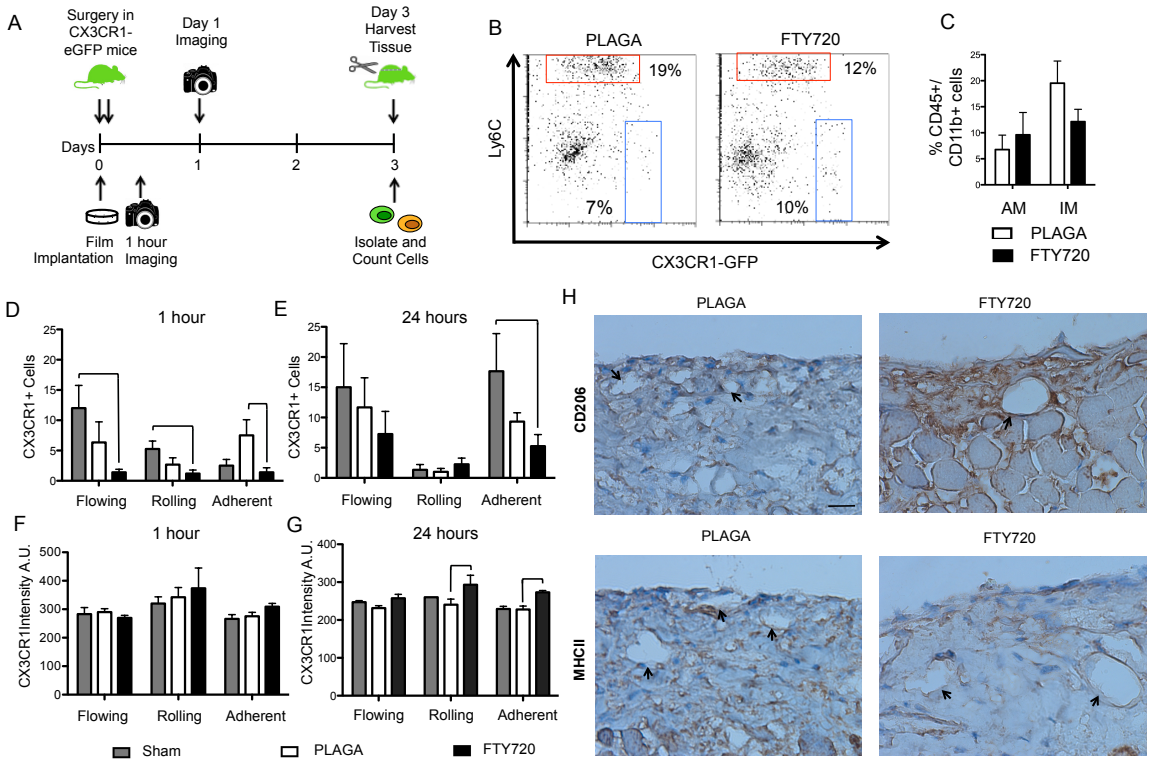

Figure A.3. FTY720 regulates monocyte rolling and adhesion and recruits AM to tissue surrounding implants. (A) Schematic for CX3CR1-eGFP mice surgeries, imaging and tissue harvest. (B-C) FTY720 released from thin films in backpack tissue decreased CD45+/CD11b+/Ly6C+/CX3CR1- IM (red box) infiltration and increased CD45+/CD11b+/Ly6C-/CX3CR1+ AM (blue box) infiltration 3 days after surgery. (D-E) FTY720-loaded polymer films decrease total number of flowing, rolling and adherent monocytes around subcutaneous implants one hour (D) and one day (E) after surgery relative to sham. (F) Average CX3CR1 expression of rolling and adherent monocytes one hour after surgery is suggestively higher with FTY720. (G) Average CX3CR1 expression of rolling and adherent monocytes in tissue one day after surgery is significantly increased with FTY720 relative to PLAGA. (H) There is a significant increase in CD206 staining, and a decrease in MHCII staining (brown staining), in vessels (arrows) directly around FTY720-loaded implants 7 days post-surgery. Blood vessel diameter also increased with FTY720 treatment. *Scale bar = 100μm.*

The two subsets of macrophages, $CD45^{+}CD11b^{+}Ly6C^{-}eGFP^{hi}$ AM and $CD45^{+}CD11b^{+}Ly6C^{+}eGFP^{lo}$ IM were easily distinguished with flow cytometry (**Figure A.4).**

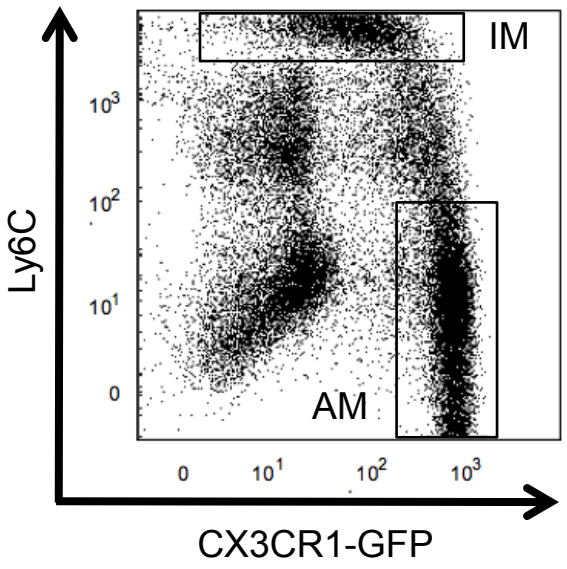

Figure A.4. Gating strategy for sorting AM and IM. Cells were stained and sorted for CD45+/CD11b+ cells and Ly6C-/CX3CR1^{hi} are AM while Ly6C+/CX3CR1^{lo} are IM.

FTY720 decreased the proportion of CD45+/CD11b+ (myeloid) cells that were IM (12%) relative to unloaded PLAGA (19%) and increased the proportion of AM (10%) relative to unloaded PLAGA (7%) in tissues around implants 3 days post-implantation (**Figure A.3B and Figure A.3C**).

To determine whether the rolling and adhesion of monocytes was altered with FTY720, intravital microscopy was used to capture one-minute videos of monocytes in the backpack of CX3CR1-eGFP mice (**Figure A.3A**). One hour after surgery, there were markedly less monocytes that were flowing (1.4 per minute), rolling (1.2) and adherent (1.4) around FTY720-loaded polymer films (**Figure A.3D**) compared to sham (12, 5.25, 2.5, respectively) and PLAGA-treated (6.33, 2.66, 7.5, respectively) tissues. The reduction of total numbers of monocytes relative to PLAGA and sham controls persisted at 24 hours post-surgery (**Figure A.3E**). Secondary analysis of the CX3CR1-eGFP

expression intensity, in arbitrary units, on recruited cells at 1 and 24 hours showed that FTY720 significantly enhanced the recruitment of CX3CR1^{hi} AM. There were no significant differences in the CX3CR1 intensity of flowing (282.6, 290, 269.7), rolling (319.8, 342.48, 373.7) or adherent (265.7, 275.6, 309.2) cells between sham, PLAGA-treated or FTY720-treated tissues, respectively, but the intensity of both rolling and adherent cells treated with FTY720 was suggestively higher 1 hour after surgery (**Figure A.3F**). By 24 hours post-surgery, the fluorescent intensity, in arbitrary units, of rolling (293.2 +/- 12.3) and firmly adherent (273 +/- 7.7) cells was significantly enhanced by FTY720 relative to sham (260 and 222.9 +/- 8.9) and unloaded PLAGA-treated (229.5 +/- 6.3 and 227.85 +/- 1.9) tissues (**Figure A.3G**). These results, taken together, suggest that local FTY720 delivery selectively recruits CX3CR1^{hi} AM that are able to firmly adhere to the endothelium before extravasation into the tissue.

S1P, the naturally occurring ligand for S1P receptors, has been shown to alter the recruitment and adhesion of inflammatory cells to endothelium (122). 7 days after implantation of S1P-loaded films in the backpack model, there was a significant reduction in the adhesion of CD11b+ inflammatory cells to the surrounding endothelium (14.5) relative to unloaded PLAGA films (33.3) (**Figure A.5A**).

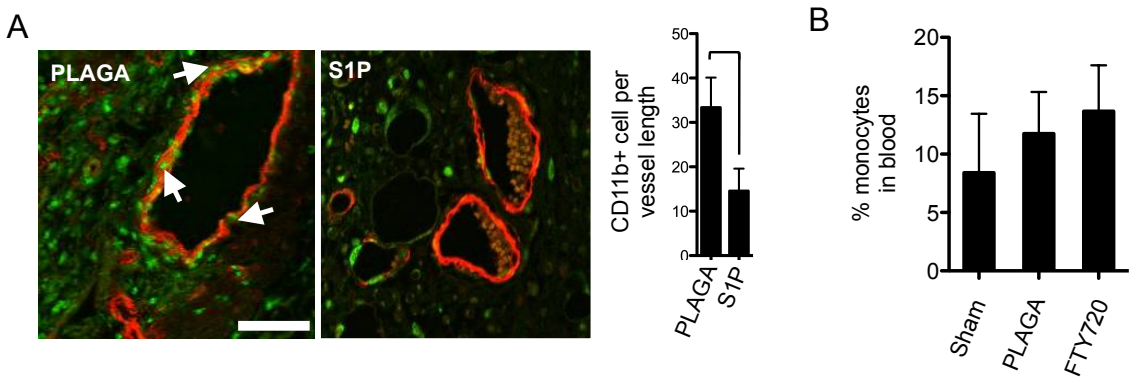

Figure A.5. S1P reduces CD11b+ cell recruitment to endothelium and local FTY720 does not mobilize monocytes into circulation (A) Reduction of CD11b+ cells lining lumen of vessels (arrows) around S1P-loaded implants. (B) FTY720 delivered locally does not mobilize monocytes into circulation. Backpacks were implanted on mice and blood was drawn 3 days after implantation to quantify percentage of monocytes. Unloaded or FTY720-loaded PLAGA did not result in a significant increase in monocytes in circulation. $P<0.05$ compared to PLAGA. *Scale bar = 100μm.*

To further characterize the inflammatory cells infiltrating tissues surrounding implants FTY720 encapsulated in nanofibers was implanted in the backpack model for 7 days before tissue was harvested for immunohistochemical staining for CD206 (an M2 marker) and MHCII (an M1 marker). Tissue surrounding unloaded implants had significant recruitment of MHCII+ cells (brown) to vessels (arrows) relative to FTY720-loaded implants (**Figure A.3H**). FTY720 delivery also enhanced the recruitment of CD206+ cells to vessels in the tissue (**Figure A.3H, brown cells**). Furthermore, blood vessels (arrows) surrounding FTY720-loaded implants were larger than those surrounding unloaded implants supporting the role of FTY720 in microvessel diameter enlargement. The local changes in macrophage content were not due to mobilization of monocytes into circulation as monocyte counts did not significantly differ with PLAGA nanofibers implantation (**Figure A.5B**).

$S1P_1$ and $S1P_3$ activation result in reduced secretion of inflammatory cytokines from macrophages and enhanced secretion of regenerative cytokines from endothelial cells.

We wished to elucidate the mechanism of FTY720-induced alteration of angiocrine signaling so we sorted and treated marrow-derived AM and IM or HUVEC with FTY720 or SEW2871 (a selective $S1P_1$ agonist) and collected the conditioned media for cytokine quantification (**Figure A.6A**).

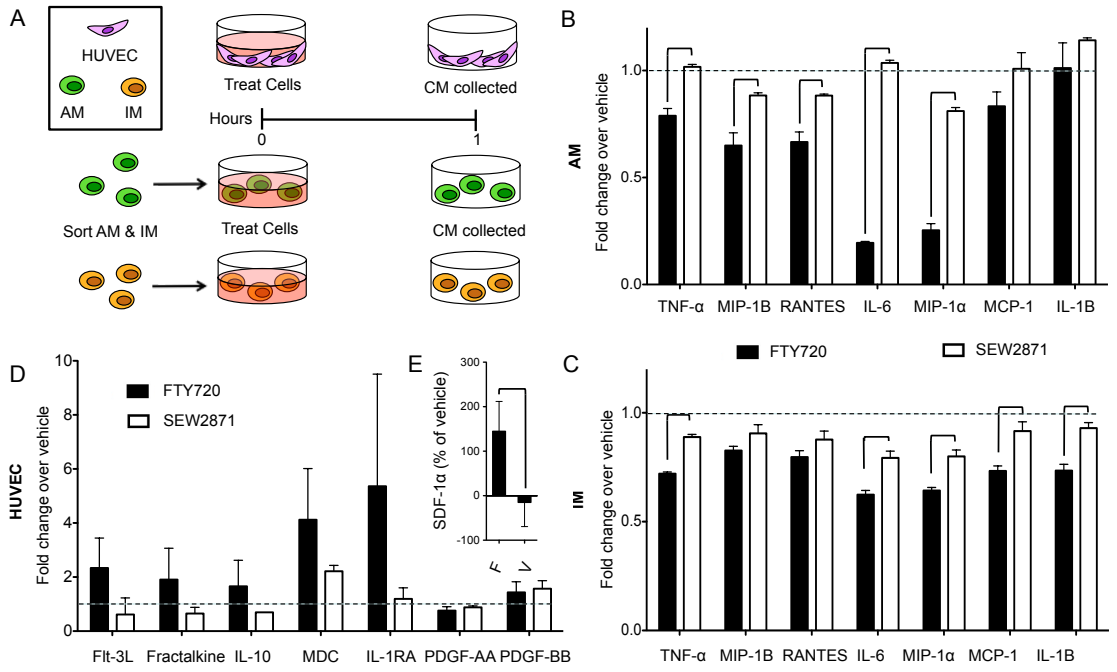

Figure A.6. $S1P_3$ activation reduces the secretion of inflammatory, and increases the secretion of regenerative cytokines from AM, IM and EC (A) Schematic of *in vitro* conditioned media harvest for cytokine assays. (B) Conditioned media from HUVEC treated with FTY720 for one hour show an increase in regenerative cytokines relative to SEW2871 and vehicle. (C) SDF-1α production from HUVEC cultured with VPC0101 was completely ablated relative to FTY720. (D-E) Inflammatory cytokine secretion is decreased in conditioned media from primary isolated marrow-derived murine AM (D) and IM (E) treated for one hour with FTY720 or SEW2871 *P<0.05 compared to SEW2871/VPC01091.*

HUVEC were treated with FTY720 or SEW2871 for 1, 6 or 24 hours to quantify differences in angiocrine cytokine secretion. Cases where SEW2871 and FTY720 elicit the same change in secretion of factors suggests a dominant role for $S1P_1$ in regulating the secretion of that cytokine; cases where FTY720 and not SEW2871 stimulated cytokine changes support a role for $S1P_3$-dominated regulation of the secretion. As early as one hour after treatment, the secretion of many pro-regenerative cytokines (Flt-3L, fractalkine, IL-10, MDC, IL-1RA) (59, 119, 123, 124) were elevated in FTY720-treated endothelial cells (**Figure A.6D**). These increases persisted throughout 24 hours of treatment (**Figure A.7C**).

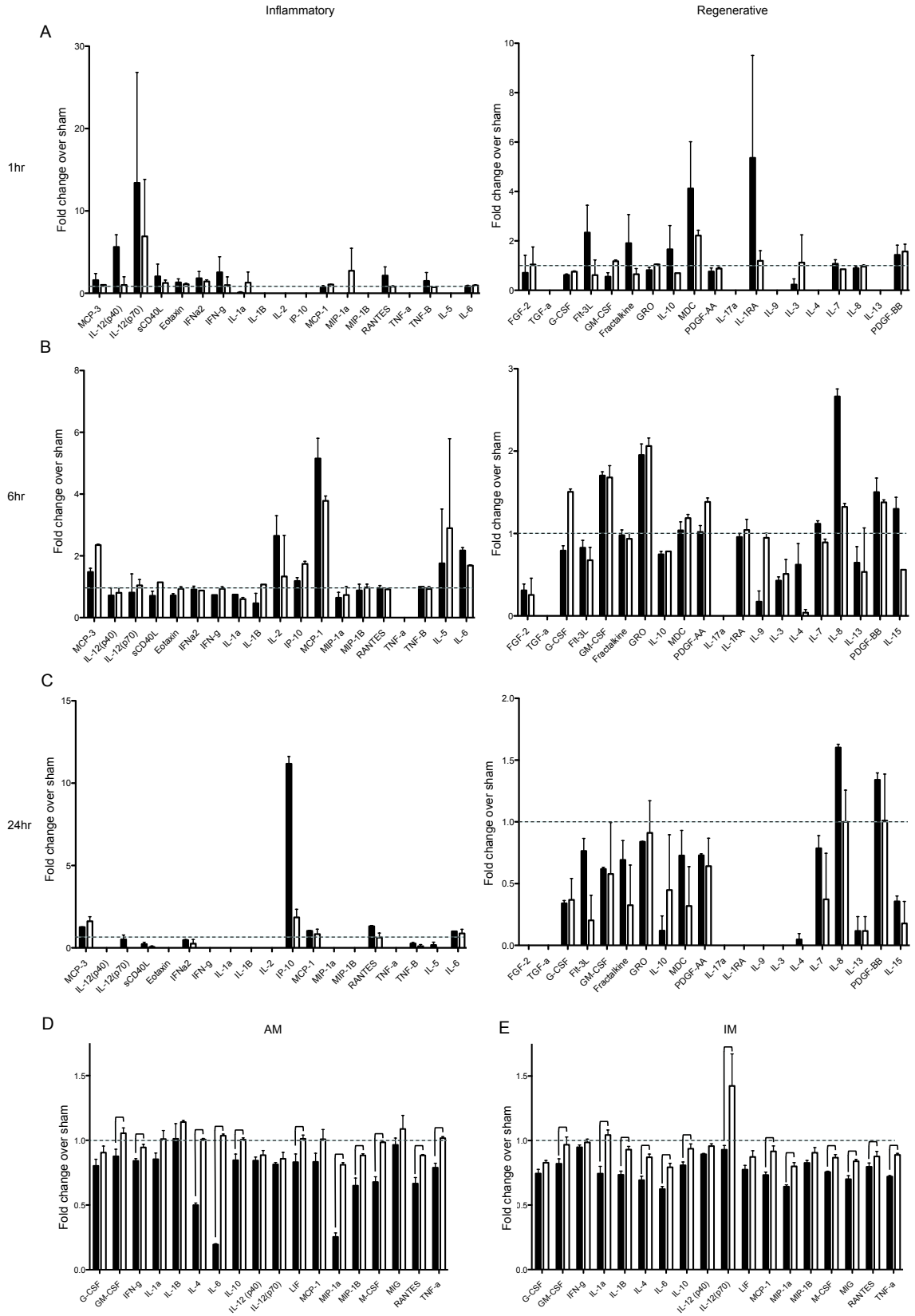
Inflammatory
Regenerative
A
1hr
B
6hr
C
24hr
Fold change over sham
MCP-3
IL-12(p40)
IL-12(p70)
sCD40L
Eotaxin
IFNa2
IFN-g
IL-1a
IL-1B
IL-2
IP-10
MCP-1
MIP-1a
MIP-1B
RANTES
TNF-a
TNF-B
IL-5
IL-6
FGF-2
TGF-a
G-CSF
Flt-3L
GM-CSF
Fractalkine
GRO
IL-10
MDC
PDGF-AA
IL-17a
IL-1RA
IL-9
IL-3
IL-4
IL-7
IL-8
IL-13
PDGF-BB
IL-15
D
AM
E
IM
G-CSF
GM-CSF
IFN-g
IL-1a
IL-1B
IL-4
IL-6
IL-10
IL-12 (p40)
IL-12(p70)
LIF
MCP-1
MIP-1a
MIP-1B
M-CSF
MIG
RANTES
TNF-a

Figure A.7. Inflammatory and Regenerative cytokine secretion from HUVEC, AM and IM treated with FTY720/SEW2871 for 1, 6 and 24 hours. (A-C) Inflammatory (left) and regenerative (right) cytokine quantification (fold increase over vehicle) in conditioned media from HUVEC treated with 1uM FTY720 or SEW2871 for 1 (A), 6 (B) and 24 (C) hours. $S1P_1$ activation promotes regenerative cytokine secretion early and maintains a balance late. $S1P_3$ activation enhances secretion of regenerative cytokines from 1 to 24 hours treatment. (D-E) Inflammatory cytokine quantification (fold increase over vehicle) in conditioned media from AM (D) and IM (E) treated with 1uM FTY720 or SEW2871 for 1 hour. $S1P_1$ and $S1P_3$ regulate the secretion of distinct cytokines from AM and IM and decrease most inflammatory cytokines relative to vehicle. Dotted line represents fold change of 1, $P<0.05$ compared to SEW2871.

To confirm the role of $S1P_3$ in the secretion of regenerative cytokines, HUVEC were cultured for 24 hours with an established $S1P_1$ agonist/$S1P_3$ antagonist, VPC01091 (122). $S1P_3$ antagonism completely abated the secretion of SDF-1α (**Figure A.6E**).

Activation of both $S1P_1$ and $S1P_3$ resulted in reduced secretion of many inflammatory cytokines 1 hour after treatment of both AM and IM (**Figure A.7D-E**). Of the seven inflammatory cytokines that were significantly decreased in tissue treated with FTY720 (**Figure A.1F**), $S1P_3$ activation on AM resulted in significant decreases in five cytokines (TNF-α, MIP-1β, RANTES, IL-6 and MIP-1α) (**Figure A.6C**) and did not change MCP-1 and IL-1β secretion. $S1P_3$ activation on IM also resulted in significant decreases in five (TNF-α, IL-6, MIP-1α, MCP-1 and IL-1β) of the seven cytokines (**Figure A.6D**) while $S1P_1$ activation significantly reduced the secretion of only MIP-1β and RANTES from IM (**Figure A.6D**). These results, taken together, show that endothelial cells and macrophages work together to push local tissue towards regeneration in the presence of FTY720 by reducing the secretion of inflammatory cytokines and increasing the secretion of regenerative cytokines.

FTY720 differentially modulates the chemotaxis of AM and IM towards SDF-1α

While both subsets of macrophages express CXCR4, the receptor that responds to SDF-1α, Ly6C+ IM gradually lose CXCR4 expression (125). Furthermore, CXCR4+ cells have been shown to potently induce angiogenesis (126-128). Locally released S1P receptor compounds are phosphorylated, taken into EC and secreted where they can then interact with cells in circulation. We wished to assess whether S1P receptor signaling could regulate the chemotaxis of monocytes towards SDF-1α through direct activation of $S1P_1$ or $S1P_3$. AM ($CD45^+CD11b^+Ly6C^-eGFP^{hi}$) and IM ($CD45^+CD11b^+Ly6C^+eGFP^{lo}$) were sorted based on their receptor expression profile from CX3CR1-eGFP mice using FACS. The two distinct cell types showed differential chemotactic responses towards SDF-1α (**Figure A.8A-B, white bars**).

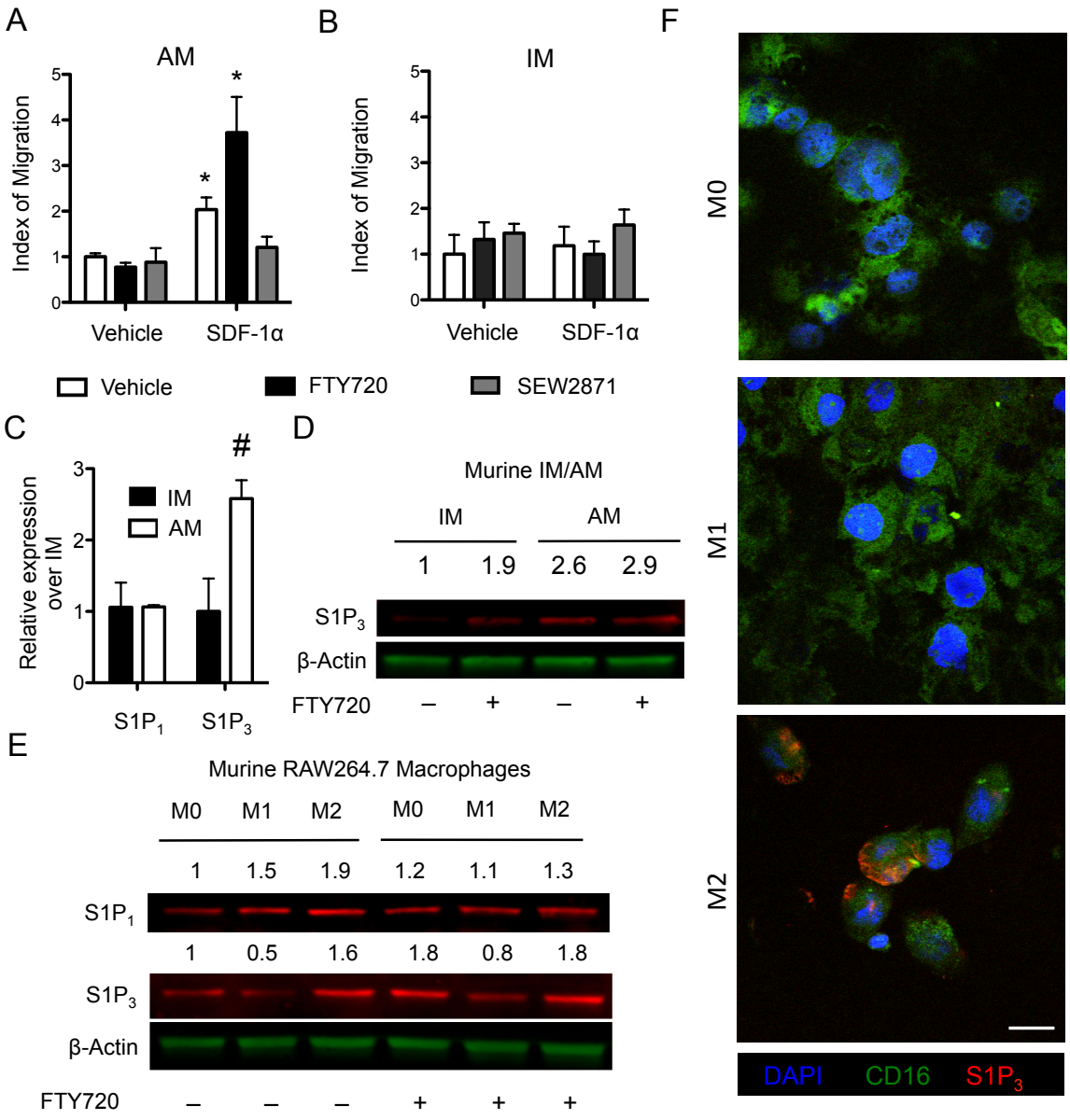

Figure A.8. $S1P_3$ activation promotes SDF-1α chemotaxis of AM and $S1P_3$ is elevated on AM A-B) FTY720, but not SEW2871, enhances chemotaxis of marrow-derived AM (A), but not IM (B) towards SDF-relative to vehicle. C) RAW264.7 macrophages were polarized to M1 and M2 phenotypes and treated with FTY720 for 1 hour. Membrane $S1P_3$ expression was higher in RAW264.7 M2 macrophages and elevated with FTY720. D) Murine IM and AM were harvested from BM and sorted and treated for one hour with FTY720. Membrane $S1P_3$ protein was higher in AM and enhanced with FTY720 treatment. E) mRNA was extracted from AM and IM and PCR was performed to measure transcription of $S1P_1$ and $S1P_3$, which was also elevated in AM. Results show a trend toward increased expression of $S1P_3$ in AM cells. F) Polarized THP-1 were stained with antibodies against $S1P_3$ (62), CD16 (59) and DAPI (blue). M2 macrophages express significantly higher levels of membrane $S1P_3$. *Dotted line*

*represents fold change of 1, *, P<0.05 compared to vehicle-vehicle. #, P = 0.09 compared to IM. Scale bar = 10μm.*

AM showed a 2.03 fold increase in migration towards SDF-1α over basal media (**Figure A.8A**), while IM showed only a 1.19-fold increase (**Figure A.8B**). Pre-treatment with FTY720 enhanced AM chemotaxis towards SDF-1α by 3.72-fold over plain media but did not affect the chemotaxis of IM towards SDF-1α (0.99 fold change over plain media). Pre-treatment with SEW2871, a $S1P_1$ specific agonist, did not enhance SDF-1α mediated chemotaxis of AM (1.21-fold increase) supporting our hypothesis that these responses are mediated through $S1P_3$ (**Figure A.8A-B**). These data show that FTY720 preferentially promotes the chemotaxis of AM towards SDF-1α in an $S1P_3$-dependent manner. Walter et al. observed a similar $S1P_3$-dependent SDF-1α mediated chemotaxis in endothelial progenitor cells (28).

$S1P_3$ expression is significantly enhanced in anti-inflammatory macrophages, relative to inflammatory macrophages, and FTY720 enhances this expression

To interrogate the mechanism involved in the distinct subtype-specific differences in SDF-1α mediated chemotaxis, we postulated that $S1P_3$ receptor expression was different between AM (M2-like) and IM (M1-like). Murine M0 RAW264.7 macrophages were polarized to M1 and M2 phenotypes by treatment with LPS+IFN-γ or IL-4, respectively. M2-polarized RAW264.7 macrophages expressed more $S1P_3$ protein (1.6 fold over M0) compared to M1-polarized cells (0.5 fold over M0) (**Figure A.8C**). Surprisingly, FTY720 enhanced the expression of $S1P_3$ in M0 (1.8 fold) and M2 (1.8 fold) macrophages but not M1 macrophages (0.8 fold). $S1P_1$ was higher in both M1 (1.5 fold) and M2 (1.9 fold) phenotypes relative to M0 but was not different or elevated with

FTY720 treatment (**Figure A.8C**). These data suggest that $S1P_3$ is either down-regulated in M1 macrophages, up-regulated in M2 macrophages, or both. We confirmed the differential expression of $S1P_3$ in BM primary isolated AM and IM. The $S1P_3$ protein expression in AM was increased 2.63-fold relative to IM. One hour FTY720 treatment resulted in a 1.91-fold increase in $S1P_3$ in IM and a 2.94 increase in $S1P_3$ in AM (**Figure A.8D**). There was no difference in mRNA expression of $S1P_1$ between AM and IM; however, in agreement with to the protein results, AM had an increasing trend of $S1P_3$ mRNA over IM with significance at an alpha level of 0.1 (**Figure A.8E**), suggesting that these differences in $S1P_3$ expression were transcriptionally regulated. To assess whether human macrophages shared these phenotypic profiles, human THP-1 macrophages were polarized to M1 and M2 phenotypes with LPS and IFN-γ, or IL-4, respectively and cells were fixed and stained with antibodies against $S1P_3$. M2 polarized macrophages express less CD16, an M1 marker, and significantly more $S1P_3$ on their surface (**Figure A.8F**). $S1P_1$ expression was not changed between M0, M1 or M2 cell types. Taken together, these results reveal $S1P_3$ as a novel marker for distinguishing anti-inflammatory or M2 macrophages from inflammatory or M1 macrophages as well as the receptor that enhances the SDF-1α chemotaxis with FTY720 treatment. This differential expression of $S1P_3$ is likely the source of the differential response to SDF-1α mediated chemotaxis after FTY720 treatment of monocytes (**Figure A.8A-B**).

FTY720-induced microvascular growth is dependent on $S1P_3$ activation on circulating and local cells

To interrogate the role of $S1P_3$ on circulatory cells (i.e. monocytes) and local cells (i.e. endothelial cells) during microvascular remodeling in the backpack model we

created $S1P_3$ bone marrow chimeras by lethally irradiating wild type mice and injecting $S1P_3^{-/-}$ (global knockout) marrow-derived cells into the tail vein (BM $S1P_3^{-/-}$) (**Figure A.9A, top**).

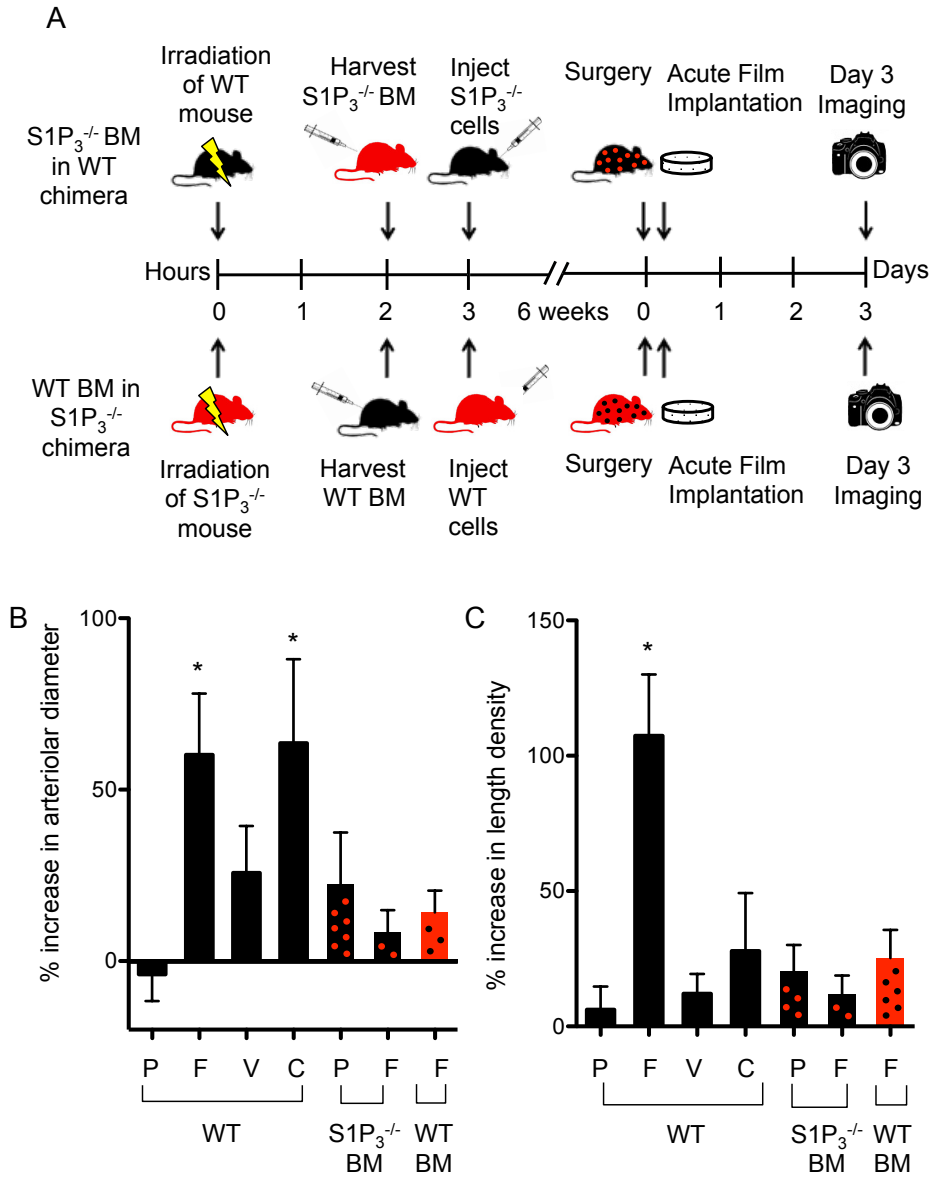

Figure A.9. FTY720 induced microvascular growth is dependent on $S1P_3$ activation on local and circulatory cells. (A) Schematic of $S1P_3^{-/-}$ BM and WT BM chimera generation. (B-C) $S1P_3$ activation is critical for maximum arteriolar diameter expansion (B) and length density (C) expansion on both marrow derived cells as well as local vascular cells. *, *P<0.05 relative to WT-PLAGA*. P: PLAGA, F: FTY720, V: VPC01091, C: Compound 26.

Selective knockout of $S1P_3$ on marrow-derived cells eliminated the vessel diameter expansion induced by acute implantation of FTY720 in the backpack. Three days after polymer implantation BM $S1P_3^{-/-}$ mice treated with FTY720 showed a significant reduction in arteriolar diameter expansion (8.35%) and length density (11.9%) relative to wild type chimeras (60.1% and 107.34%, respectively) (**Figure A.9B-C**). $S1P_3^{-/-}$ mice reconstituted with wild type marrow (Fig. 5A, bottom) did not recover this reduction in growth (8.36% and 11.9%, respectively) and mice treated locally with PLAGA eluting VPC01091 showed similar reductions in diameter expansion (27.76%) and length density (11.99%) (**Figure A.9B-C**). Surprisingly, delivery of a specific $S1P_1$ agonist, Compound 26 (C), in the backpack model resulted in significant increase in arteriolar diameter expansion (63.58%) (**Figure A.9B**) but not length density (27.8%) (**Figure A.9**C) which suggested an $S1P_1$ dependent mechanism for arteriolar remodeling. $S1P_1$ activation has already been shown to enhance the recruitment of pericytes, which enlarge small arterioles and capillaries (109). To assess the role of $S1P_1$ activation in the proliferation of pericytes, primary human microvascular pericytes were treated with 1uM FTY720 or SEW2871 and assessed longitudinally for proliferation. Both compounds enhanced the proliferation of pericytes over the course of 7 days, which supports the role of $S1P_1$ activation in pericyte proliferation/viability (**Figure A.10**).

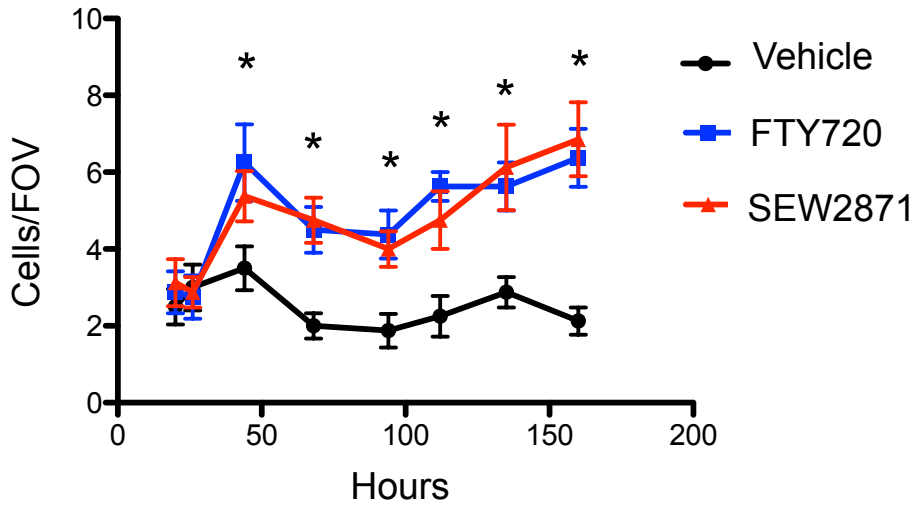

Figure A.10. $S1P_1$ activation enhances pericyte proliferation. 1uM SEW2871 and FTY720 enhance proliferation of primary isolated pericytes after 48 hours of treatment *, $P<0.05$ compared to vehicle.

While $S1P_1$ activation alone promotes arteriolar enlargement through pericyte recruitment and/or proliferation, without $S1P_3$ activation microvascular networks do not undergo significant network-wide growth and maturation of vessels. Furthermore, the "length density" metric is only enhanced with $S1P_3$ activation (**Figure A.9C**) and encompasses new vessels, and vessels that were smaller than the threshold of detection by imaging (roughly 10μm in diameter) initially and expanded above this threshold. Therefore enhanced length density due to $S1P_3$ activation also represents small capillaries that expand above 10μm: arteriogenesis. We show here that $S1P_3$ regulates both circulatory cells (monocytes) and local cells (EC) and is critical for FTY720-induced microvascular remodeling. These results, taken together, indicate that $S1P_1$ and $S1P_3$ activation contribute to maximum diameter and network expansion but $S1P_3$ is critical in the SDF-1α dependent recruitment of regenerative macrophages for arteriogenesis.

FTY720 enhances arteriogenesis of ischemic arterioles and promotes the peri-vascular localization of AM

In order to examine the spatial localization of CX3CR1^{hi} AM to vascular networks, we employed a mouse model of skeletal muscle ischemia, the spinotrapezius ligation model. Main feeder arterioles were ligated in DsRed-NG2/CX3CR1-eGFP mice promoting consequent arteriolar remodeling (**Figure A.11A**).

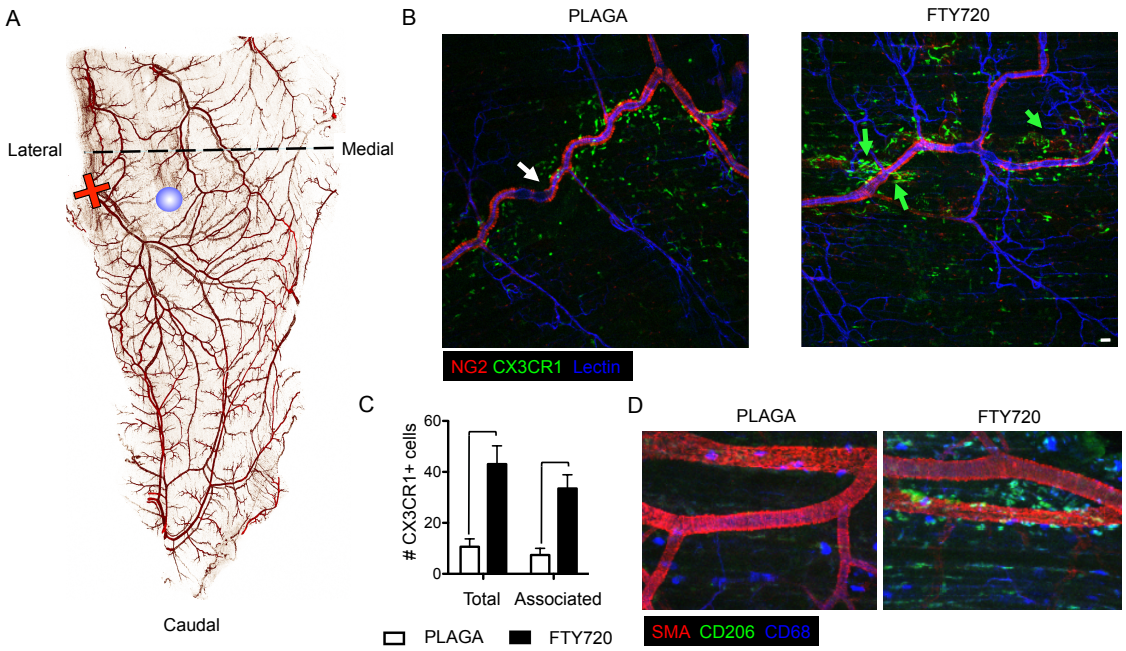

Figure A.11. FTY720 recruits AM to ischemic vessels in the spinotrapezius ligation model and enhances arteriogenesis. (A) Diagram of smooth muscle actin-stained whole-mounted spinotrapezius muscle with ligation (red cross) and film implantation (blue circle). (B) Immunohistochemistry images of the spinotrapezius vasculature surrounding an unloaded PLAGA film (left) or FTY720-loaded film (right) (10x magnification) obtained 7 days after ligation and implantation in a DsRed-NG2 CX3CR1-eGFP mouse. Left: Blue is perfused lectin of endothelium and red NG2-expressing perivascular cells illustrate remodeling vasculature. CX3CR1-GFP+ cells can be seen in the interstitial space proximal to the "remodeling" artery (white arrow) induced by ligation. Right: Encapsulation and delivery of FTY720 results in CX3CR1-GFP+ cell recruitment (green arrows) together with increased sprouting and remodeling of microvascular networks. (C) FTY720 significantly increased overall CX3CR1+ cell content as well as CX3CR1+ cells directly associated with remodeling vessels. (D)

Further analysis of remodeling arterioles revealed significant CD206+ cell recruitment with FTY720. *P<0.05 Scale bars = 50μm.*

These mice express DsRed on pericytes and eGFP on monocytes. Quantitative analysis of microvascular remodeling in peri-implant blood vessels from whole muscle showed that sustained local delivery of FTY720 enhanced classic signs of arteriogenesis, including increased tortuosity and collateralization of branching microvascular networks. FTY720-loaded scaffolds enhanced the growth of lectin-positive capillaries from remodeling arterioles relative to unloaded PLAGA scaffolds (**Figure A.11B**). The tortuosity of vessels surrounding FTY720 loaded PLAGA thin films was significantly greater than that surrounding unloaded PLAGA films (1.133 vs. 1.078) (**Figure A.12**).

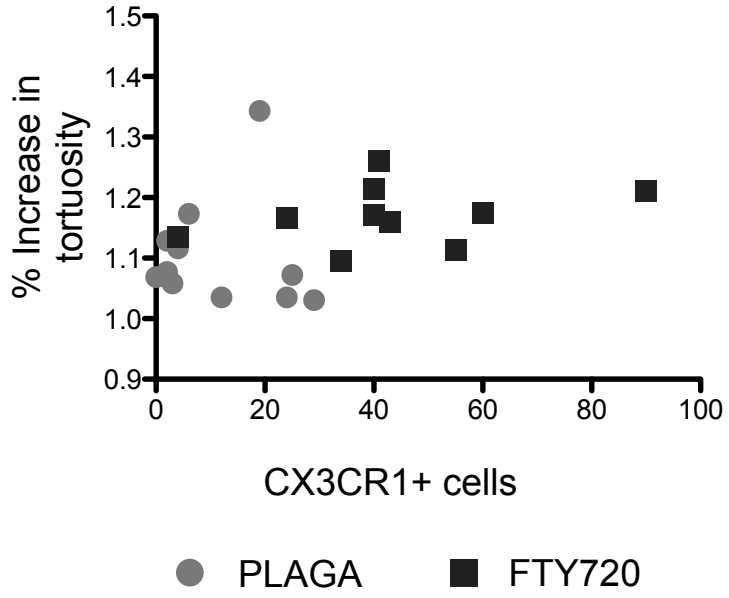

Figure A.12. Tortuosity of ischemic vessels correlated with CX3CR1+ cell recruitment with FTY720. Enhanced tortuosity (actual vessel length divided by end-to-end length) of vessels was observed in the remodeling watershed of FTY720-treated muscles along with higher CX3CR1+ content. Tortuosity was positively correlated with CX3CR1+ cell content in watershed. FTY720 significantly enhanced tortuosity (average = 1.17) relative to unloaded PLAGA (average = 1.1).

Small increases in tortuosity can significantly enhance the surface area for oxygen and nutrient transport, which is critical for regeneration in ischemic tissue. Significantly more CX3CR1-eGFP^{hi} cells were observed within one cell length away from vessels around FTY720-releasing implants (43.1 vs. 10.7) relative to unloaded PLAGA implants. Closer examination of vessel networks revealed significantly more AM directly associated with remodeling vessels downstream of arterial ligation, per field of view, in FTY720 treated tissues (33.5 vs. 7.4) relative to unloaded PLAGA implants (**Figure A.11B-C**). Interestingly, the tortuosity of vessels in the remodeling watersheds was positively correlated with CX3CR1-eGFP^{hi} cell association and both were elevated with FTY720 treatment (**Figure A.12**). We wished to further characterize the phenotype of the CX3CR1+ cells recruited to remodeling vessels in the spinotrapezius and stained for CD68, a pan-macrophage marker, and CD206, an M2 macrophage marker. Paralleling FTY720-dependent recruitment of CD206+ macrophages in inflamed tissue (**Figure A.3H**), muscles treated with FTY720 resulted in a significant recruitment of CD206+ cells to the perivascular space around remodeling vessels (**Figure A.11D**). These results strongly suggest that local delivery of the $S1P_1/S1P_3$ agonist, FTY720, promotes phenotypically selective localization of endogenous host anti-inflammatory cells that enhance vascularization and recovery in response to injury.

Discussion

Activation of EC after injury triggers programs that release angiocrine cytokines which accelerate tissue repair through the recruitment of inflammatory cells (129). For example, IL-4, propagates TH2 (anti-inflammatory) immune responses by stimulating the

proliferation of AM and S1P receptor signaling has been shown to skew immune responses towards a TH2-cell response (102). Together, the recruitment and polarization of cells by locally produced angiocrine factors can concentrate regenerative cells and enhance tissue repair, vascular remodeling and implant integration. The results presented here reveal that local $S1P_3$ activation can enhance tissue regeneration through the recruitment of $CD45^+CD11b^+Ly6C^-eGFP^{hi}$ AM during tissue injury and ischemia (**Figure A.13**).

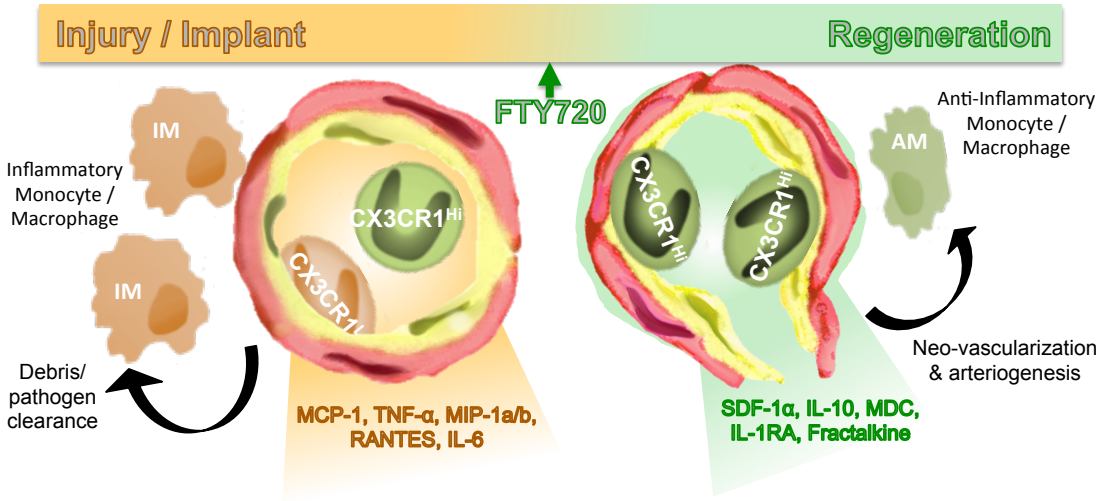

Figure A.13. FTY720 promotes the generation of a regenerative module after injury and implantation. Microvascular injury and biomaterial implant leads to the production of pro-inflammatory cytokines and chemokines (e.g. MCP-1) from local and recruited cells. This enhances the recruitment of CX3CR1 low IM (orange cells) which clear debris and pathogens in the inflamed tissue (left). FTY720, through $S1P_3$ agonism, enhances the production of pro-regenerative chemokines (e.g. SDF-1α) by endothelial cells and the chemotaxis of CX3CR1 high AM (green cells) resulting in the recruitment of AM which contribute to neo-vascularization and arteriogenesis (right).

Other groups have shown that different subsets of macrophages contribute to wound healing and microvascular remodeling when recruited to tissues (130, 131). During acute inflammation in the backpack, a model of wound healing and inflammation, FTY720 (a potent $S1P_{1/3}$ agonist) released from PLAGA films significantly enhanced

microvascular growth 3 and 7 days post-surgery. When FTY720-loaded films were implanted 7 days post-surgery, after for significant inflammatory cell recruitment, the microvascular growth responses there was substantial microvascular growth relative to PLAGA (**Figure A.1D, right and Figure A.1E, right**) suggesting that FTY720 acts on cells recruited days after insult.

Though PLAGA is biocompatible, as it degrades it releases products that are ultimately engulfed by tissue-resident macrophages, eliciting an inflammatory response (132). In characterizing the polymer films we noted a significant decrease in hydrophobicity of the polymer, which is to be expected based on the amphipathic structure of the FTY720 molecule (**Figure A.14A-B**).

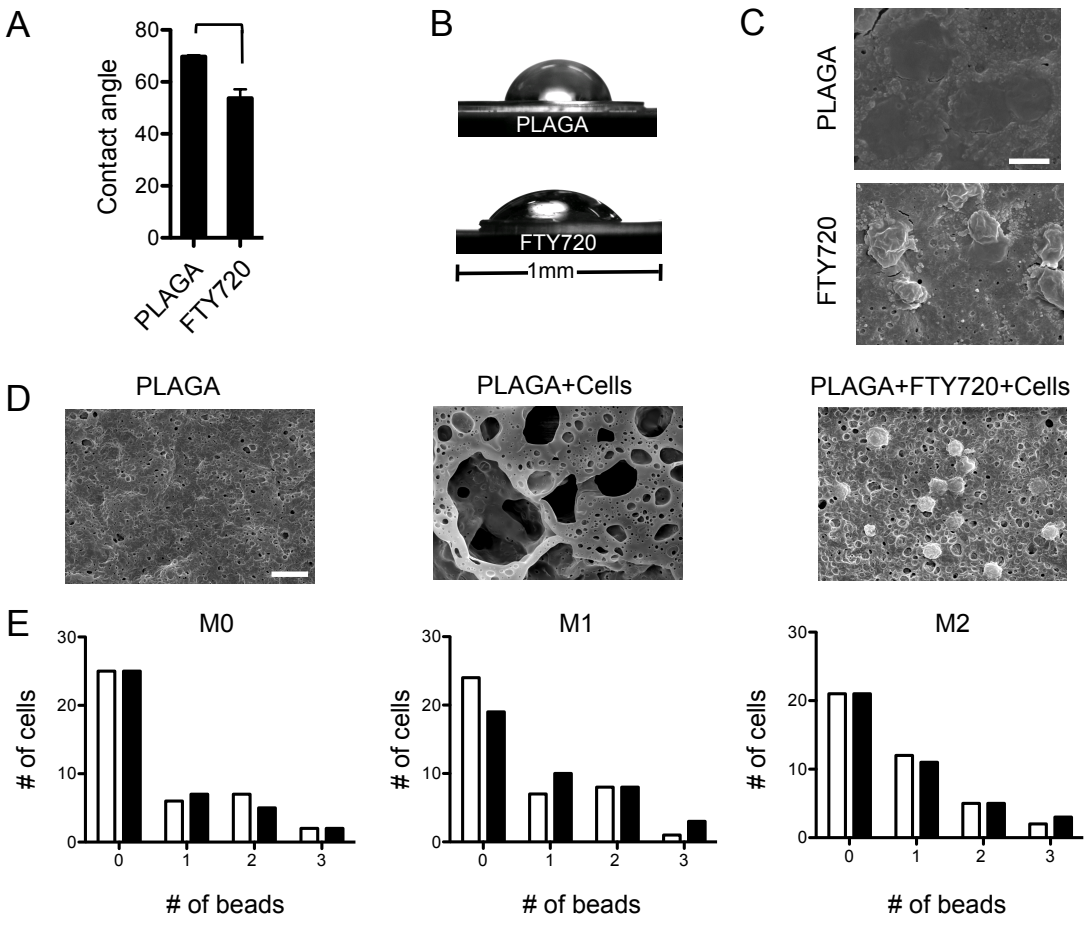

Figure A.14. FTY720 reduces the hydrophobicity of PLAGA and monocyte spreading but not phagocytosis. A-B) FTY720 lowers the contact angle of water on, and increases hydrophilicity of, PLAGA films. C) LPS stimulated WEHI monocytes 7 days after being seeded on unloaded (top) PLAGA polymer films are more spread out than those seeded on FTY720-loaded (bottom) films. This implied that FTY720 mediates an effect on cell morphology. D) The PLAGA-unloaded polymer with cells exhibited increased porosity compared to the PLAGA-FTY720 polymer with cells. This suggested an increased phagocytosis or interaction of the cells with the polymer. E) FTY720 does not alter the phagocytosis of M0, M1 or M2 macrophages. *P<0.05 compared to PLAGA*.

Interestingly, increased hydrophilicity decreased cell spreading and adhesion to the polymer surface, which implied that FTY720 mediates an effect on cell morphology (**Figure A.14C**). Due to the difference in cell morphology on the polymer surface, we further investigated the morphology of the polymer after 14 days of culture. The

PLAGA-unloaded polymer with cells exhibited increased porosity compared to the PLAGA-FTY720 polymer with cells (**Figure A.14D**). In order to determine the effect of FTY720 on phagocytic activity, we used polarized macrophages of M0, M1 and M2 types in a fluorescent bead phagocytosis assay where cells were incubated with beads for 4 hours and the number of internalized beads was quantified. There were no significant changes in bead phagocytosis with FTY720 co-treatment in any of the polarized cell types (**Figure A.14E**). Taken together, these data indicate that the increase in porosity of the cells/PLAGA-unloaded polymer is more likely due to increase contact morphology of the inflammatory monocytes with the film than an increase in phagocytosis.

Subsequent to biomaterial implantation inflammatory cytokines are secreted by EC to recruit monocytes. There was a significant reduction in many pro-inflammatory cytokines in tissues treated with FTY720-loaded PLAGA films (**Figure A.1F and Figure A.2**). While S1P has already been shown to regulate monocyte adhesion to EC through the expression of adhesion molecules (133, 134) its role in the production of chemotactic molecules has not been assessed to this point. We focused on two specific chemokines, MCP-1 and SDF-1α, which are known to recruit inflammatory cells and regenerative cells, respectively, *in vivo.* MCP-1 secretion peaked early in wound healing followed by SDF-1α secretion (**Figure A.1B**). Interestingly, peak SDF-1α expression also corresponded with the time point where maximal enhancements in microvascular remodeling were observed with FTY720 (**Figure A.1D-E**). In agreement with the reduction of many other inflammatory cytokines, tissue surrounding FTY720-loaded implants had a lower MCP-1:SDF-1α ratio (**Figure A.1G**). Marrow-derived AM and IM and HUVEC were treated with FTY720 or SEW2871 to determine the contributors to

S1P receptor-specific changes in cytokine secretion. While activation of both $S1P_1$ and $S1P_3$ resulted in a reduction in the secretion of inflammatory cytokines from AM and IM, $S1P_3$ activation consistently reduced the secretion of more inflammatory cytokines (**Figure A.6B-C, and Figure A.7D-E**). $S1P_3$ activation on HUVEC resulted in an increase in the secretion of regenerative cytokines (**Figure A.6D and Figure A.7A-C**). Furthermore, conditioned media from HUVEC treated with FTY720 contained a significantly higher amount of SDF-1α relative to VPC01091, an established $S1P_3$ antagonist, which completely abated the secretion of SDF-1α from HUVEC (**Figure A.6E**). These results show that $S1P_3$, and to a lesser extent $S1P_1$, activation alters the angiocrine secretome by reducing the secretion of inflammatory cytokines from macrophages and increasing the secretion of regenerative cytokines from endothelial cells.

SDF-1α is a more potent chemoattractant for AM, than IM, and FTY720 further enhanced chemotaxis in an $S1P_3$-dependent fashion (**Figure A.8A-B**). Keul et al. showed that the recruitment of monocytes that contributed to atherosclerosis was dependent on $S1P_3$ (32). Furthermore, van der Pouw et al. recently performed a comprehensive genome analysis between classically and alternatively activated macrophages and found that $S1P_3$ was one of the top 40 genes most differentially regulated between the two subsets (135). We assessed the expression of membrane $S1P_3$ in murine and human monocytes and macrophages and found that $S1P_3$ was significantly elevated in anti-inflammatory (M2) macrophages relative to inflammatory (M1) macrophages. FTY720 enhanced this expression (**Figure A.8C-D and Figure A.8F**). This difference in $S1P_3$ expression was transcriptionally regulated as $S1P_3$ mRNA from primary isolated murine AM was

significantly elevated (**Figure A.8E**). This differential expression is likely responsible for the differential SDF-1α mediated chemotaxis between the two subtypes.

Local $S1P_3$ activation results in the recruitment of CX3CR1+, CD206+ macrophages to vessels surrounding polymer implant (**Figure A.3B-C and Figure A.3H**) Monocyte extravasation in an activated tissue follows three steps: flowing, rolling and firm adhesion, governed by a host of different molecules (122). Fong et al. discovered a mechanism of monocyte rolling and firm adhesion mediated by fractalkine and its receptor, CX3CR1 (136). FTY720 significantly reduced the number of flowing, rolling and adhering CX3CR1+ monocytes and macrophages, relative to sham and PLAGA groups, between 1 hour and 24 hours post-implantation (**Figure A.3D-E**). However, the rolling and adherent cells around FTY720-loaded implants one day post-implantation expressed significantly higher levels of CX3CR1 confirming that FTY720 specifically recruits highly CX3CR1 expressing AM relative to IM (**Figure A.3G**). These results, taken together, support a multi-factorial role for FTY720 in the recruitment of AM. FTY720 directly enhances the secretion of SDF-1α from EC and the chemotaxis of AM towards SDF-1α resulting in a lower proportion of $CD45^+CD11b^+Ly6C^+eGFP^{lo}$ IM and a higher proportion of $CD45^+CD11b^+Ly6C^-eGFP^{hi}$ AM in injured tissue (**Figure A.3C**).

In addition to EC and AM, pericytes participate in many events during inflammation (137) and vascular remodeling (138). Others have already noted that $S1P_1$ activation enhances the recruitment of pericytes to developing or remodeling vessels and that these cells are involved in the arteriogenic process through proliferation and differentiation processes (109, 139). Recent evidence by Stark *et al.* identifies interactions between arterial pericytes and CX3CR1+ monocytes during inflammation

(137), which may suggest that pericytes play multiple roles in regulation of vascular and inflammatory modulation. The current literature does not describe a role for S1P receptors in the interaction between monocytes and pericytes, however, we can not rule out a role of vascular mural cells in angiocrine type signaling. To further examine the roles of $S1P_1$ and $S1P_3$ in pericytes we examined the proliferation of human microvascular pericyte cultures. Agonism of either $S1P_1$ & $S1P_3$ (FTY720) or $S1P_1$ alone (SEW2871) induces statistically significant increases in cell number over 7 days *in vitro* (**Figure A.10**). It is important to note that while our data implies that $S1P_1$ activation alone, with Compound 26, is sufficient in promoting significant arteriolar diameter expansion (**Figure A.9B**) wild type mice have endogenous S1P that has the potential of activating functional $S1P_3$. When $S1P_3$ is antagonized in the presence of $S1P_1$ activation, as with $S1P_3^{-/-}$ BM chimeras treated with FTY720, significant arteriolar diameter expansion is not observed (Fig. 5B). Our results show that $S1P_3$ activation on monocytes recruited from circulation as well as local EC is critical in order for microvascular networks to undergo robust growth and expansion (**Figure A.9B-C**).

Others have found that macrophages recruited to blood vessels can play roles in vessel support and stabilization in a "chaperoning" manner (140) and several studies have shown that skeletal muscle ischemia results in local up-regulation in SDF-1α (32,33); the spatial localization of recruited AM was assessed around remodeling vessels. As expected, in vessels surrounding FTY720-loaded PLAGA scaffolds in ischemic muscle there was a significant increase in cells expressing high levels of CX3CR1. This was accompanied by an increase in capillary expansion (**Figure A.11B-C**). Upon closer observation these cells adopted a peri-vascular location and were in direct contact with

vessels, especially at the arteriolar bases of new collaterals (**Figure A.11B**). Additional staining revealed that CD68+/CD206+ cells (M2 macrophages) were significantly recruited to remodeling vessels with FTY720 treatment and not unloaded PLAGA (**Figure A.11D**). In addition to this, tortuosity, a classic sign of arteriogenesis, was significantly increased in vessels surrounding FTY720-loaded implants (**Figure A.12**).

These findings provide novel and exciting insight into the mechanism of macrophage-supported implant arteriogenesis during ischemia and wound healing. $S1P_3$ plays a critical, non-redundant, role in conditioning local tissues with angiocrine factors like SDF-1α and preferentially recruiting AM (**Figure A.13**). These cells are able to extravasate into inflamed tissue and contribute to arteriogenesis, which has the potential to promote tissue regeneration and enhance biomaterial implant integration and functionality. These data also provide support for the use of FTY720, and other $S1P_3$-activating compounds for the therapeutic induction of arteriogenesis. In this regard, it is notable that FTY720 is now approved in the United States for use as an immunomodulatory agent for multiple sclerosis.

APPENDIX B

List of primers

Gene Name	Left primer	Right primer
SPTLC1	tggaagagagcactgggtct	gctacctccttgatggtgga
KDSR	ccaccagacacagacacacc	ccgagagcatgtacccatct
SPHK1	ggcgtcatgcatctgttcta	caaacacacctttcccatcc
SPHK2	ggctgtccttcaacctcatc	cagtcagggcgatctaggag
SGPP1	aggaagtggtgctggaattg	gcaggctaaaggaatggtga
SGPP2	tcctcttggttcgtcagctt	cacaaaggttgtagcgcaga
SGPL1	cttgatgcacttcggtgaga	gttccacccctagcagtca
LPPR1, LPPR2	tgcaagccaaactacaccag	tcgactgctcttcgtcttga
LPPR3	gaacaagatcccgaaggaca	gtagggcatggagagagtgc
CERS1	cagtgacgtgcagcttgagt	ctggtggcatacaggacctt
CERS2	tcagcattgcctctgatgtc	ccagcaggtaatcggaagag
CERS3	ggatcacgatggactcgtct	ttgccttgtggaatgtttga
CERS4	tggagctgggggactgatta	cctgccaaaaccactcgttg
CERS5	gttctgggacatccgacagt	caatggtgaccaagtgatgc
CERS6	ggtttcgacaaagacgcaat	agcaatgcctcgtattccac
ASAH1	tctacgccacccttttcgtg	gactaaggcgacgcaactcc
ACER3	ctggtacatcgccgagttct	accaggatcccattcctacc
DEGS1	gagctgatggcgtcgatgta	gacctgtgccacggtattga
SGMS1	tagttggcacgctgtacctg	gtgttagcatgaccgtgtgg
SGMS2	aggagcttagccctccactc	aacagaatctgcgtcccact
SMPDL3B	ctataccagcaatgcgctga	gccttgttttgcgtcttctc
SMPD4	ggttcgtccagcagaaactc	aaagcccacaaacaacttgg
ENPP7	aagaagggaggctggagaag	gtgctccccattgttgaact
CERK	gggcacccctcaattgtgta	cagcatgaggaacggtgtct
DGKZ	gtctctaaggtgacactcggg	cgacgcttagacgacaggag
KSR1	atggatccccacagatggta	cagattctgtcctccgaagc
PRKCA	cctaaaggctgaggttgctg	atttagtgtggagcggatgg
PRKCB	tgaaggggaggatgaagatg	taaggggctggatctcttt
ENPP2	atggattacagccaccaagc	atccattaattgccccacaa
PP1A	actatgtggacaggggcaag	caggcagttgaagcagtcag
PP2A	ccacacagttccagacatgg	actgtggccaccaagttttc
SMPD2	catggtgactggttcagtgg	tctgccttcttggatgtgtg
SMPD1	ctgactctcgggttctctgg	aggttgatggcggtgaatag
PPAP2C	agttcttcctggtggccttt	cctcctccttcagacagtgc
PPAP2B	tcgagacaagcaccatcaag	accgcgacttcttcaggtaa
PPAP2A	tcaactgcagcgatggttac	gcccacataaatggatacgg
LPPR5	gccctgtgtaagcccaatta	agtctggttcccttggcttt
PLA2G4A	tggctctgtgtgatcaggag	gagccagaaagaccagcaac
PARP1	ggtggatgggttctctgagc	acccccttgcacgtacttctg
PARP2	gaagctgacagtggcacaaa	tgtccggattagtggaggag

PARP3	agggccctgagaagaagaag	tggttcagggtgcagttgta
PARP4	gggcactgttggtgtctttt	ctgccttccatggtgctaat
MMP9	gagaccggtgagctggatag	tacacgcgagtgaaggtgag
MMP12	atgcagcacttcttgggtct	tcacggttcatgtcaggtgt
CCL2	ccccagtcacctgctgttat	tggaatcctgaacccacttc
M1P-1	gcttgttgctgtccttggat	gagtgaacacgggatgcttt
CCL5	cgctgtcatcctcattgcta	acacacttggcggttctttc
ITGA3	cccaactacaggcgaaacat	gcatccgcaaaggtaaagag
ITGAM	gggaagtggcaaggaatgta	ctgcgtgtgctgttctttgt
ITGA4	atcggagctccacaagaaga	gcagaatcagaccgaaaagc
ITGAL	agagtccaggcttctgtcca	tacaggatggggatgatggt
ICAM1	ggctggagctgtttgagaac	aggagtcgttgccataggtg
B3gnt5	ctggcttgggaagatcaaag	cacgatgaacacgaccaatc
UGCG	ctttgctgccaccttagagc	cttcggcaatgtactgagca
HES4	tggacgccctcagaaaagag	ttcacctccgccagacactc
CDKN1C	tttagagcccaaagagcccc	accagtgtaccttctcgtgc
ADA	gacccgctcatcttcaagtc	ggtcgagaagctccctcttt
C1QB	ccccagggataaaaggagag	ttttctgggtggccttgtag
C1QA	ccaggaagaaccgtaccaga	ccttgttggtggtgtcacag
SH2D1B	gcgagtcgataccaggagtc	cccctgatttggtttttcaa
MTSS1	cccgtcatctcagatcccta	agtcatgctccgtggtctct
RHOC	acagcagggcaggaagacta	ttcatcttggccagctctct
CKB	catatcaagctgcccaacct	accagctccacctctgagaa
S100A12	aggagcttgcaaacaccatc	ctttgtgggtgtggtaatgg
C19orf59	agagccatcctgagcctgta	tctcttcgcatgcttgtacg
PADI4	gaaatccacaggttcctcca	caccccggtgaggtagagta
ALOX5AP	gcgtttgctggactgatgta	gagatggtggtggagatcgt
PROK2	ctatgggcaaactgggagac	agacatgggcaagtgtgatg
MOSC1	tggtgacgtggaactgaaaa	acacagggtctcccactttg
VCAN	cagggaacctggtgaagaaa	cttccacagtgggtggtctt
CD14	ctgcaacttctccgaacctc	ccagtagctgagcaggaacc
QPCT	ccctcaatcccactgctaaa	tcttgtctaaggcacgagca
S1PR1	ccacaacgggagcaataact	cagaatgacgatggagagca
S1PR2	tggaaaaccttctggtgctc	caggaggctgaagacagagg
S1PR3	tggtcatctgcagcttcatc	gaacatactgccctccctga
S1PR4	agccttctgcccctctactc	gatcatcagcaccgtcttca
S1PR5	gcatctactgccaggtacgc	agcaacagcagcaggaagag
CSF1	cccagtgtcatcctggtctt	gcagttccacctgtctgtca
CSF2	atgtgaatgccatccaggag	agggcagtgctgcttgtagt
IFNG	tgaccagagcatccaaaaga	ctcttcgacctcgaaacagc
IL1B	cgatgcacctgtacgatcac	tctttcaacacgcaggacag
IL4	actgcttccccctctgttct	gtccttctcatggtggctgt
IL10	agaacagctgcacccacttc	gcatcacctcctccaggtaa
TGFB1	gggactatccacctgcaaga	cctccttggcgtagtagtcg
CXCR4	ggtggtctatgttggcgtct	tggagtgtgacagcttggag
CX3CR1	gccttcaccatggatcagtt	gacactcttgggcttcttgc

CD14	ctgcaacttctccgaacctc	ccagtagctgagcaggaacc
MRC1	acggactgggttgctatcac	ttccacctgctccataaacc
CXCL12	gccgattcttcgaaagccatta	ctaggctttgcccaggttga
CTSK	gggtcagtgtggttcctgtt	cccacatatgggtaggcatc
CTSS	tctctcagtgcccagaacct	gccacagcttctttcaggac
CTSL1	gtggacatccctaagcagga	tttcaaatccgtagccaacc
CTSL2	tccgtgagcctctgtttctt	ctagccatgaagccaccatt
CTSV	tccgtgagcctctgtttctt	ctagccatgaagccaccatt

APPENDIX C

List of cytokines

Cytokine	Abbreviation
Epidermal growth factor	EGF
Eotaxin	
Fibroblast growth factor 2	FGF-2
Fms-related tyrosine kinase 3 ligand	Flt-3L
Fractalkine	
Granulocyte colony stimulating factor	G-CSF
Granulocyte macrophage colony stimulating factor	GM-CSF
Growth-related oncogene	GRO
Interferon α2	IFNα2
Interferon-γ	IFN-γ
Interleukin 1-α	IL-1α
Interleukin 1-β	IL-1β
Interleukin 1 receptor antagonist A	IL-1RA
Interleukin 2	IL-2
Interleukin 3	IL-3
Interleukin 4	IL-4
Interleukin 5	IL- 5
Interleukin 6	IL-6
Interleukin 7	IL-7
Interleukin 8	IL-8
Interleukin 9	IL-9
Interleukin 10	IL-10
Interleukin 12	IL-12 - p40
Interleukin 12	IL-12 - p70
Interleukin 13	IL-13
Interleukin 15	IL- 15
Interleukin 17	IL-17
Interleukin 17a	IL-17a
Interferon-inducible protein 10	IP-10
Keratinocyte chemoattractant	KC
Leukemia inhibitory factor	LIF
Macrophage colony stimulating factor	M-CSF
Macrophage derived chemokine	MDC
Macrophage inflammatory protein 1α	MIP-1α
Macrophage inflammatory protein 1β	MIP-1β
Macrophage inflammatory protein 2	MIP-2
Monocyte chemoattractant protein 1	MCP-1
Monocyte chemoattractant protein 3	MCP-3
Monokine induced by gamma interferon	MIG
Platelet derived growth factor AA	PDGF-AA

Platelet derived growth factor BB	PDGF-BB
Regulated on activation, normal T-cell expressed and secreted	RANTES
Tumor necrosis factor α	TNF-α
Tumor necrosis factor β	TNF-β
Transforming growth factor α	TGF-α
Soluble cluster of differentiation 40 ligand	sCD40L
Stromal derived factor 1α	SDF-1α
Vascular endothelial growth factor	VEGF

REFERENCES

1. Connes P, Verlhac S, & Bernaudin F (2013) Advances in understanding the pathogenesis of cerebrovascular vasculopathy in sickle cell anaemia. *British journal of haematology* 161(4):484-498.

2. Barrett O, Jr., Saunders DE, Jr., McFarland DE, & Humphries JO (1984) Myocardial infarction in sickle cell anemia. *American journal of hematology* 16(2):139-147.

3. Wahl S & Quirolo KC (2009) Current issues in blood transfusion for sickle cell disease. *Current opinion in pediatrics* 21(1):15-21.

4. Jacob E & American Pain S (2001) Pain management in sickle cell disease. *Pain management nursing : official journal of the American Society of Pain Management Nurses* 2(4):121-131.

5. Ohanian J & Ohanian V (2001) Sphingolipids in mammalian cell signalling. *Cellular and molecular life sciences : CMLS* 58(14):2053-2068.

6. Rosen H, Gonzalez-Cabrera PJ, Sanna MG, & Brown S (2009) Sphingosine 1-phosphate receptor signaling. *Annual review of biochemistry* 78:743-768.

7. Dinkla S*, et al.* (2012) Functional consequences of sphingomyelinase-induced changes in erythrocyte membrane structure. *Cell death & disease* 3:e410.

8. Trajkovic K*, et al.* (2008) Ceramide triggers budding of exosome vesicles into multivesicular endosomes. *Science* 319(5867):1244-1247.

9. Pettus BJ, Chalfant CE, & Hannun YA (2004) Sphingolipids in inflammation: roles and implications. *Current molecular medicine* 4(4):405-418.

10. Balreira A, Lacerda L, Miranda CS, & Arosa FA (2005) Evidence for a link between sphingolipid metabolism and expression of CD1d and MHC-class II: monocytes from Gaucher disease patients as a model. *British journal of haematology* 129(5):667-676.

11. Chatterjee S (1998) Sphingolipids in atherosclerosis and vascular biology. *Arteriosclerosis, thrombosis, and vascular biology* 18(10):1523-1533.

12. Fuggle P, Shand PA, Gill LJ, & Davies SC (1996) Pain, quality of life, and coping in sickle cell disease. *Archives of disease in childhood* 75(3):199-203.

13. Yale SH, Nagib N, & Guthrie T (2000) Approach to the vaso-occlusive crisis in adults with sickle cell disease. *American family physician* 61(5):1349-1356, 1363-1344.

14. Belcher JD, Marker PH, Weber JP, Hebbel RP, & Vercellotti GM (2000) Activated monocytes in sickle cell disease: potential role in the activation of vascular endothelium and vaso-occlusion. *Blood* 96(7):2451-2459.

15. Segel GB, Halterman MW, & Lichtman MA (2011) The paradox of the neutrophil's role in tissue injury. *Journal of leukocyte biology* 89(3):359-372.

16. Sebastiano V*, et al.* (2011) In situ genetic correction of the sickle cell anemia mutation in human induced pluripotent stem cells using engineered zinc finger nucleases. *Stem cells* 29(11):1717-1726.

17. Zou J, Mali P, Huang X, Dowey SN, & Cheng L (2011) Site-specific gene correction of a point mutation in human iPS cells derived from an adult patient with sickle cell disease. *Blood* 118(17):4599-4608.

18. Shander A, Cappellini MD, & Goodnough LT (2009) Iron overload and toxicity: the hidden risk of multiple blood transfusions. *Vox sanguinis* 97(3):185-197.

19. Teng C*, et al.* (2008) Serine palmitoyltransferase, a key enzyme for de novo synthesis of sphingolipids, is essential for male gametophyte development in Arabidopsis. *Plant physiology* 146(3):1322-1332.

20. Jenkins RW, Canals D, & Hannun YA (2009) Roles and regulation of secretory and lysosomal acid sphingomyelinase. *Cellular signalling* 21(6):836-846.

21. Wong ML*, et al.* (2000) Acute systemic inflammation up-regulates secretory sphingomyelinase in vivo: a possible link between inflammatory cytokines and atherogenesis. *Proceedings of the National Academy of Sciences of the United States of America* 97(15):8681-8686.

22. Marathe S*, et al.* (1998) Human vascular endothelial cells are a rich and regulatable source of secretory sphingomyelinase. Implications for early atherogenesis and ceramide-mediated cell signaling. *The Journal of biological chemistry* 273(7):4081-4088.

23. Sakata A*, et al.* (2007) Acid sphingomyelinase inhibition suppresses lipopolysaccharide-mediated release of inflammatory cytokines from macrophages and protects against disease pathology in dextran sulphate sodium-induced colitis in mice. *Immunology* 122(1):54-64.

24. Weigert A*, et al.* (2010) Cleavage of sphingosine kinase 2 by caspase-1 provokes its release from apoptotic cells. *Blood* 115(17):3531-3540.

25. Hannun YA & Luberto C (2000) Ceramide in the eukaryotic stress response. *Trends in cell biology* 10(2):73-80.

26. Olivera A, Allende ML, & Proia RL (2013) Shaping the landscape: metabolic regulation of S1P gradients. *Biochimica et biophysica acta* 1831(1):193-202.

27. Golan K*, et al.* (2012) S1P promotes murine progenitor cell egress and mobilization via S1P1-mediated ROS signaling and SDF-1 release. *Blood* 119(11):2478-2488.

28. Walter DH*, et al.* (2007) Sphingosine-1-phosphate stimulates the functional capacity of progenitor cells by activation of the CXCR4-dependent signaling pathway via the S1P3 receptor. *Arteriosclerosis, thrombosis, and vascular biology* 27(2):275-282.

29. Massberg S*, et al.* (2007) Immunosurveillance by hematopoietic progenitor cells trafficking through blood, lymph, and peripheral tissues. *Cell* 131(5):994-1008.

30. Ishii M, Kikuta J, Shimazu Y, Meier-Schellersheim M, & Germain RN (2010) Chemorepulsion by blood S1P regulates osteoclast precursor mobilization and bone remodeling in vivo. *The Journal of experimental medicine* 207(13):2793-2798.

31. Tani M, Ito M, & Igarashi Y (2007) Ceramide/sphingosine/sphingosine 1-phosphate metabolism on the cell surface and in the extracellular space. *Cellular signalling* 19(2):229-237.

32. Keul P*, et al.* (2011) Sphingosine-1-phosphate receptor 3 promotes recruitment of monocyte/macrophages in inflammation and atherosclerosis. *Circulation research* 108(3):314-323.

33. Fueller M, Wang DA, Tigyi G, & Siess W (2003) Activation of human monocytic cells by lysophosphatidic acid and sphingosine-1-phosphate. *Cellular signalling* 15(4):367-375.

34. Weis T, Volker W, Holtwick R, Al Chahaf M, & Schmidt A (2010) Sphingosine 1-phosphate (S1P) induces expression of E-selectin and adhesion of monocytes via

intracellular signalling pathways in vascular endothelial cells. *European journal of cell biology* 89(10):733-741.

35. Safaya S, Steinberg MH, & Klings ES (2012) Monocytes from sickle cell disease patients induce differential pulmonary endothelial gene expression via activation of NF-kappaB signaling pathway. *Molecular immunology* 50(1-2):117-123.

36. Mohandas N & Gallagher PG (2008) Red cell membrane: past, present, and future. *Blood* 112(10):3939-3948.

37. Zennadi R*, et al.* (2012) Erythrocyte plasma membrane-bound ERK1/2 activation promotes ICAM-4-mediated sickle red cell adhesion to endothelium. *Blood* 119(5):1217-1227.

38. Lopez DJ*, et al.* (2012) Accumulated bending energy elicits neutral sphingomyelinase activity in human red blood cells. *Biophysical journal* 102(9):2077-2085.

39. Allan D, Limbrick AR, Thomas P, & Westerman MP (1982) Release of spectrin-free spicules on reoxygenation of sickled erythrocytes. *Nature* 295(5850):612-613.

40. Tantawy AA, Adly AA, Ismail EA, Habeeb NM, & Farouk A (2012) Circulating platelet and erythrocyte microparticles in young children and adolescents with sickle cell disease: Relation to cardiovascular complications. *Platelets*.

41. Shet AS*, et al.* (2003) Sickle blood contains tissue factor-positive microparticles derived from endothelial cells and monocytes. *Blood* 102(7):2678-2683.

42. Mause SF & Weber C (2010) Microparticles: protagonists of a novel communication network for intercellular information exchange. *Circulation research* 107(9):1047-1057.

43. Camus SM*, et al.* (2012) Erythrocyte microparticles can induce kidney vaso-occlusions in a murine model of sickle cell disease. *Blood* 120(25):5050-5058.

44. Bardelli C*, et al.* (2012) Autocrine activation of human monocyte/macrophages by monocyte-derived microparticles and modulation by PPARgamma ligands. *British journal of pharmacology* 165(3):716-728.

45. Barry OP, Pratico D, Savani RC, & FitzGerald GA (1998) Modulation of monocyte-endothelial cell interactions by platelet microparticles. *The Journal of clinical investigation* 102(1):136-144.

46. Rautou PE*, et al.* (2011) Microparticles from human atherosclerotic plaques promote endothelial ICAM-1-dependent monocyte adhesion and transendothelial migration. *Circulation research* 108(3):335-343.

47. Vasina EM*, et al.* (2013) Aging- and activation-induced platelet microparticles suppress apoptosis in monocytic cells and differentially signal to proinflammatory mediator release. *American journal of blood research* 3(2):107-123.

48. Gladwin MT & Sachdev V (2012) Cardiovascular abnormalities in sickle cell disease. *Journal of the American College of Cardiology* 59(13):1123-1133.

49. Awojoodu AO*, et al.* (2013) Sphingosine 1-phosphate receptor 3 regulates recruitment of anti-inflammatory monocytes to microvessels during implant arteriogenesis. *P Natl Acad Sci USA* 110(34):13785-13790.

50. Cuschieri J, Bulger E, Billgrin J, Garcia I, & Maier RV (2007) Acid sphingomyelinase is required for lipid Raft TLR4 complex formation. *Surgical infections* 8(1):91-106.

51. Manwani D & Frenette PS (2013) Vaso-occlusion in sickle cell disease: pathophysiology and novel targeted therapies. *Blood* 122(24):3892-3898.

52. Zolla L & D'Alessandro A (2013) An efficient apparatus for rapid deoxygenation of erythrocyte concentrates for alternative banking strategies. *Journal of blood transfusion* 2013:896537.

53. Shaner RL*, et al.* (2009) Quantitative analysis of sphingolipids for lipidomics using triple quadrupole and quadrupole linear ion trap mass spectrometers. *Journal of lipid research* 50(8):1692-1707.

54. Kaul DK, Fabry ME, Windisch P, Baez S, & Nagel RL (1983) Erythrocytes in Sickle-Cell-Anemia Are Heterogeneous in Their Rheological and Hemodynamic Characteristics. *J Clin Invest* 72(1):22-31.

55. Xu R, Sun W, Jin J, Obeid LM, & Mao C (2010) Role of alkaline ceramidases in the generation of sphingosine and its phosphate in erythrocytes. *FASEB journal : official publication of the Federation of American Societies for Experimental Biology* 24(7):2507-2515.

56. Hanel P, Andreani P, & Graler MH (2007) Erythrocytes store and release sphingosine 1-phosphate in blood. *Faseb J* 21(4):1202-1209.

57. Shet AS (2008) Characterizing blood microparticles: technical aspects and challenges. *Vascular health and risk management* 4(4):769-774.

58. Pathare A*, et al.* (2004) Cytokine profile of sickle cell disease in Oman. *American journal of hematology* 77(4):323-328.

59. Greaves DR*, et al.* (2001) Linked chromosome 16q13 chemokines, macrophage-derived chemokine, fractalkine, and thymus- and activation-regulated chemokine, are

expressed in human atherosclerotic lesions. *Arteriosclerosis, thrombosis, and vascular biology* 21(6):923-929.

60. Hebbel RP, Schwartz RS, & Mohandas N (1985) The adhesive sickle erythrocyte: cause and consequence of abnormal interactions with endothelium, monocytes/macrophages and model membranes. *Clinics in haematology* 14(1):141-161.

61. Zennadi R, Chien A, Xu K, Batchvarova M, & Telen MJ (2008) Sickle red cells induce adhesion of lymphocytes and monocytes to endothelium. *Blood* 112(8):3474-3483.

62. Sabaa N*, et al.* (2008) Endothelin receptor antagonism prevents hypoxia-induced mortality and morbidity in a mouse model of sickle-cell disease. *The Journal of clinical investigation* 118(5):1924-1933.

63. Vince RV, Chrismas B, Midgley AW, McNaughton LR, & Madden LA (2009) Hypoxia mediated release of endothelial microparticles and increased association of S100A12 with circulating neutrophils. *Oxidative medicine and cellular longevity* 2(1):2-6.

64. Urbina P, Flores-Diaz M, Alape-Giron A, Alonso A, & Goni FM (2011) Effects of bilayer composition and physical properties on the phospholipase C and sphingomyelinase activities of Clostridium perfringens alpha-toxin. *Biochimica et biophysica acta* 1808(1):279-286.

65. Opreanu M*, et al.* (2011) The unconventional role of acid sphingomyelinase in regulation of retinal microangiopathy in diabetic human and animal models. *Diabetes* 60(9):2370-2378.

66. Bhatia R, *et al.* (2004) Ceramide triggers Weibel-Palade body exocytosis. *Circulation research* 95(3):319-324.

67. Becker KA, *et al.* (2010) Acid sphingomyelinase inhibitors normalize pulmonary ceramide and inflammation in cystic fibrosis. *American journal of respiratory cell and molecular biology* 42(6):716-724.

68. Keegan PM, Surapaneni S, & Platt MO (2012) Sickle cell disease activates peripheral blood mononuclear cells to induce cathepsins k and v activity in endothelial cells. *Anemia* 2012:201781.

69. Harvey KA, Welch Z, Sliva D, & Siddiqui RA (2010) Role of Rho kinase in sphingosine 1-phosphate-mediated endothelial and smooth muscle cell migration and differentiation. *Molecular and cellular biochemistry* 342(1-2):7-19.

70. Yogi A, *et al.* (2011) Sphingosine-1-phosphate-induced inflammation involves receptor tyrosine kinase transactivation in vascular cells: upregulation in hypertension. *Hypertension* 57(4):809-818.

71. Fontana V, *et al.* (2008) Increased procoagulant cell-derived microparticles (C-MP) in splenectomized patients with ITP. *Thrombosis research* 122(5):599-603.

72. Truman JP, *et al.* (2012) Differential regulation of acid sphingomyelinase in macrophages stimulated with oxidized low-density lipoprotein (LDL) and oxidized LDL immune complexes: role in phagocytosis and cytokine release. *Immunology* 136(1):30-45.

73. Jilani K, *et al.* (2013) Fluoxetine induced suicidal erythrocyte death. *Toxins* 5(7):1230-1243.

74. Ozdogu H*, et al.* (2007) The apoptosis of blood polymorphonuclear leukocytes in sickle cell disease. *Cytom Part B-Clin Cy* 72B(4):276-280.

75. Watson AD (2006) Thematic review series: systems biology approaches to metabolic and cardiovascular disorders. Lipidomics: a global approach to lipid analysis in biological systems. *Journal of lipid research* 47(10):2101-2111.

76. Didangelos A, Stegemann C, & Mayr M (2012) The -omics era: proteomics and lipidomics in vascular research. *Atherosclerosis* 221(1):12-17.

77. Ingram VM (1956) A specific chemical difference between the globins of normal human and sickle-cell anaemia haemoglobin. *Nature* 178(4537):792-794.

78. Petremand J & Widmann C (2008) Lipid metabolism: sphingolipids- from membrane constituents to signaling molecules that control cell-to-cell communications. *Current opinion in lipidology* 19(6):620-621.

79. Wasserstein MP*, et al.* (2006) Acid sphingomyelinase deficiency: prevalence and characterization of an intermediate phenotype of Niemann-Pick disease. *The Journal of pediatrics* 149(4):554-559.

80. Vanier MT (2010) Niemann-Pick disease type C. *Orphanet journal of rare diseases* 5:16.

81. Kolter T & Sandhoff K (2006) Sphingolipid metabolism diseases. *Biochimica et biophysica acta* 1758(12):2057-2079.

82. Zhang Y*, et al.* (2014) Elevated sphingosine-1-phosphate promotes sickling and sickle cell disease progression. *The Journal of clinical investigation* 124(7):3274.

83. Awojoodu AO*, et al.* (2014) Acid sphingomyelinase is activated in sickle cell erythrocytes and contributes to inflammatory microparticle generation in sickle cell disease. *Blood*.

84. Hannun YA, Luberto C, & Argraves KM (2001) Enzymes of sphingolipid metabolism: from modular to integrative signaling. *Biochemistry* 40(16):4893-4903.

85. Cowart LA*, et al.* (2010) Revealing a signaling role of phytosphingosine-1-phosphate in yeast. *Molecular systems biology* 6:349.

86. Ozbayraktar FB & Ulgen KO (2010) Drug target identification in sphingolipid metabolism by computational systems biology tools: metabolic control analysis and metabolic pathway analysis. *Journal of biomedical informatics* 43(4):537-549.

87. Gupta S, Maurya MR, Merrill AH, Jr., Glass CK, & Subramaniam S (2011) Integration of lipidomics and transcriptomics data towards a systems biology model of sphingolipid metabolism. *BMC systems biology* 5:26.

88. Orth JD, Thiele I, & Palsson BO (2010) What is flux balance analysis? *Nature biotechnology* 28(3):245-248.

89. Zhang Y*, et al.* (2014) Elevated sphingosine-1-phosphate promotes sickling and sickle cell disease progression. *The Journal of clinical investigation* 124(6):2750-2761.

90. Pownall HJ & Massey JB (1982) Mechanism of association of human plasma apolipoproteins with dimyristoylphosphatidylcholine: effect of lipid clusters on reaction rates. *Biophysical journal* 37(1):177-179.

91. Connes P*, et al.* (2013) Decreased Hematocrit-To-Viscosity Ratio and Increased Lactate Dehydrogenase Level in Patients with Sickle Cell Anemia and Recurrent Leg Ulcers. *Plos One* 8(11).

92. Osawa Y*, et al.* (2005) Roles for C16-ceramide and sphingosine 1-phosphate in regulating hepatocyte apoptosis in response to tumor necrosis factor-alpha. *The Journal of biological chemistry* 280(30):27879-27887.

93. Seumois G*, et al.* (2007) De novo C16- and C24-ceramide generation contributes to spontaneous neutrophil apoptosis. *Journal of leukocyte biology* 81(6):1477-1486.

94. Liu SC*, et al.* (1996) Red cell membrane remodeling in sickle cell anemia. Sequestration of membrane lipids and proteins in Heinz bodies. *The Journal of clinical investigation* 97(1):29-36.

95. Wagner GM, Schwartz RS, Chiu DT, & Lubin BH (1985) Membrane phospholipid organization and vesiculation of erythrocytes in sickle cell anaemia. *Clinics in haematology* 14(1):183-200.

96. Awojoodu AO*, et al.* (2013) Sphingosine 1-phosphate receptor 3 regulates recruitment of anti-inflammatory monocytes to microvessels during implant arteriogenesis. *Proceedings of the National Academy of Sciences of the United States of America* 110(34):13785-13790.

97. Tantawy AA, Adly AA, Ismail EA, Habeeb NM, & Farouk A (2013) Circulating platelet and erythrocyte microparticles in young children and adolescents with sickle cell disease: Relation to cardiovascular complications. *Platelets* 24(8):605-614.

98. Grosch S, Schiffmann S, & Geisslinger G (2012) Chain length-specific properties of ceramides. *Prog Lipid Res* 51(1):50-62.

99. Hanel P, Andreani P, & Graler MH (2007) Erythrocytes store and release sphingosine 1-phosphate in blood. *FASEB journal : official publication of the Federation of American Societies for Experimental Biology* 21(4):1202-1209.

100. Canellini G*, et al.* (2012) Red blood cell microparticles and blood group antigens: an analysis by flow cytometry. *Blood transfusion = Trasfusione del sangue* 10 Suppl 2:s39-45.

101. Westerman MP, Cole ER, & Wu K (1984) The effect of spicules obtained from sickle red cells on clotting activity. *British journal of haematology* 56(4):557-562.

102. Weigert A*, et al.* (2007) Tumor cell apoptosis polarizes macrophages role of sphingosine-1-phosphate. *Molecular biology of the cell* 18(10):3810-3819.

103. Rollins BJ, Yoshimura T, Leonard EJ, & Pober JS (1990) Cytokine-activated human endothelial cells synthesize and secrete a monocyte chemoattractant, MCP-1/JE. *The American journal of pathology* 136(6):1229-1233.

104. Yun HJ & Jo DY (2003) Production of stromal cell-derived factor-1 (SDF-1)and expression of CXCR4 in human bone marrow endothelial cells. *Journal of Korean medical science* 18(5):679-685.

105. Kryczek I, Wei S, Keller E, Liu R, & Zou W (2007) Stroma-derived factor (SDF-1/CXCL12) and human tumor pathogenesis. *American journal of physiology. Cell physiology* 292(3):C987-995.

106. Namiki A*, et al.* (1995) Hypoxia induces vascular endothelial growth factor in cultured human endothelial cells. *The Journal of biological chemistry* 270(52):31189-31195.

107. Idzko M*, et al.* (2002) Sphingosine 1-phosphate induces chemotaxis of immature and modulates cytokine-release in mature human dendritic cells for emergence of Th2 immune responses. *FASEB journal : official publication of the Federation of American Societies for Experimental Biology* 16(6):625-627.

108. Cinamon G*, et al.* (2004) Sphingosine 1-phosphate receptor 1 promotes B cell localization in the splenic marginal zone. *Nature immunology* 5(7):713-720.

109. Takuwa Y*, et al.* (2010) Roles of sphingosine-1-phosphate signaling in angiogenesis. *World journal of biological chemistry* 1(10):298-306.

110. Sefcik LS*, et al.* (2011) Selective activation of sphingosine 1-phosphate receptors 1 and 3 promotes local microvascular network growth. *Tissue engineering. Part A* 17(5-6):617-629.

111. Mosser DM & Edwards JP (2008) Exploring the full spectrum of macrophage activation. *Nature reviews. Immunology* 8(12):958-969.

112. Sakurai E, Anand A, Ambati BK, van Rooijen N, & Ambati J (2003) Macrophage depletion inhibits experimental choroidal neovascularization. *Investigative ophthalmology & visual science* 44(8):3578-3585.

113. Moldovan NI, Goldschmidt-Clermont PJ, Parker-Thornburg J, Shapiro SD, & Kolattukudy PE (2000) Contribution of monocytes/macrophages to compensatory neovascularization: the drilling of metalloelastase-positive tunnels in ischemic myocardium. *Circulation research* 87(5):378-384.

114. Moldovan NI (2002) Role of monocytes and macrophages in adult angiogenesis: a light at the tunnel's end. *Journal of hematotherapy & stem cell research* 11(2):179-194.

115. Takeda Y*, et al.* (2011) Macrophage skewing by Phd2 haplodeficiency prevents ischaemia by inducing arteriogenesis. *Nature* 479(7371):122-126.

116. Weisser SB, McLarren KW, Kuroda E, & Sly LM (2013) Generation and characterization of murine alternatively activated macrophages. *Methods Mol Biol* 946:225-239.

117. Gordon S & Taylor PR (2005) Monocyte and macrophage heterogeneity. *Nature reviews. Immunology* 5(12):953-964.

118. Jenkins SJ*, et al.* (2011) Local macrophage proliferation, rather than recruitment from the blood, is a signature of TH2 inflammation. *Science* 332(6035):1284-1288.

119. Mantovani A*, et al.* (2004) The chemokine system in diverse forms of macrophage activation and polarization. *Trends in immunology* 25(12):677-686.

120. Sefcik LS, Petrie Aronin CE, Wieghaus KA, & Botchwey EA (2008) Sustained release of sphingosine 1-phosphate for therapeutic arteriogenesis and bone tissue engineering. *Biomaterials* 29(19):2869-2877.

121. Geissmann F, Jung S, & Littman DR (2003) Blood monocytes consist of two principal subsets with distinct migratory properties. *Immunity* 19(1):71-82.

122. Muller WA & Randolph GJ (1999) Migration of leukocytes across endothelium and beyond: molecules involved in the transmigration and fate of monocytes. *Journal of leukocyte biology* 66(5):698-704.

123. Retzlaff S*, et al.* (2002) Interleukin 8 and Flt3 ligand as markers of advanced disease in primary gastrointestinal non-Hodgkin's lymphoma. *Oncology reports* 9(3):525-527.

124. Ruitenberg MJ*, et al.* (2008) CX3CL1/fractalkine regulates branching and migration of monocyte-derived cells in the mouse olfactory epithelium. *Journal of neuroimmunology* 205(1-2):80-85.

125. Wang Y*, et al.* (2009) CCR2 and CXCR4 regulate peripheral blood monocyte pharmacodynamics and link to efficacy in experimental autoimmune encephalomyelitis. *J Inflamm (Lond)* 6:32.

126. Shantsila E, Tapp LD, Wrigley BJ, Montoro-Garcia S, & Lip GY (2013) CXCR4 positive and angiogenic monocytes in myocardial infarction. *Thrombosis and haemostasis* 109(2):255-262.

127. Jin DK*, et al.* (2006) Cytokine-mediated deployment of SDF-1 induces revascularization through recruitment of CXCR4+ hemangiocytes. *Nature medicine* 12(5):557-567.

128. Hur J*, et al.* (2013) Highly angiogenic CXCR4(+)CD31(+) monocyte subset derived from 3D culture of human peripheral blood. *Biomaterials* 34(8):1929-1941.

129. Butler JM, Kobayashi H, & Rafii S (2010) Instructive role of the vascular niche in promoting tumour growth and tissue repair by angiocrine factors. *Nature reviews. Cancer* 10(2):138-146.

130. Willenborg S*, et al.* (2012) CCR2 recruits an inflammatory macrophage subpopulation critical for angiogenesis in tissue repair. *Blood* 120(3):613-625.

131. Linde N*, et al.* (2012) Vascular endothelial growth factor-induced skin carcinogenesis depends on recruitment and alternative activation of macrophages. *The Journal of pathology* 227(1):17-28.

132. Prior S*, et al.* (2002) In vitro phagocytosis and monocyte-macrophage activation with poly(lactide) and poly(lactide-co-glycolide) microspheres. *European journal of pharmaceutical sciences : official journal of the European Federation for Pharmaceutical Sciences* 15(2):197-207.

133. Whetzel AM*, et al.* (2006) Sphingosine-1 phosphate prevents monocyte/endothelial interactions in type 1 diabetic NOD mice through activation of the S1P1 receptor. *Circulation research* 99(7):731-739.

134. Bolick DT*, et al.* (2005) Sphingosine-1-phosphate prevents tumor necrosis factor-{alpha}-mediated monocyte adhesion to aortic endothelium in mice. *Arteriosclerosis, thrombosis, and vascular biology* 25(5):976-981.

135. van der Pouw Kraan TC, van der Laan AM, Piek JJ, & Horrevoets AJ (2012) Surfing the data tsunami, a bioinformatic dissection of the proangiogenic monocyte. *Vascular pharmacology* 56(5-6):297-305.

136. Fong AM*, et al.* (1998) Fractalkine and CX3CR1 mediate a novel mechanism of leukocyte capture, firm adhesion, and activation under physiologic flow. *The Journal of experimental medicine* 188(8):1413-1419.

137. Stark K*, et al.* (2013) Capillary and arteriolar pericytes attract innate leukocytes exiting through venules and 'instruct' them with pattern-recognition and motility programs. *Nature immunology* 14(1):41-51.

138. Jain RK (2003) Molecular regulation of vessel maturation. *Nature medicine* 9(6):685-693.

139. Paik JH*, et al.* (2004) Sphingosine 1-phosphate receptor regulation of N-cadherin mediates vascular stabilization. *Genes & development* 18(19):2392-2403.

140. Fantin A*, et al.* (2010) Tissue macrophages act as cellular chaperones for vascular anastomosis downstream of VEGF-mediated endothelial tip cell induction. *Blood* 116(5):829-840.

VITA

ANTHONY O. AWOJOODU

Anthony O. Awojoodu was born in Gaithersburg, Maryland. He attended public schools in Montgomery County, Maryland and received a B.S. in Bioengineering, *Summa Cum Laude,* from the University of Maryland, College Park, MD in 2009. Anthony started graduate school at the University of Virginia in the fall of 2009 and received a M.S. in Biomedical Engineering in 2011 before coming to Georgia Tech to pursue a doctorate in Biomedical Engineering. When he is not working on research, Mr. Awojoodu enjoys sports, food, salsa and hanging out with his friends, family and dogs, Malcolm and Coco.